TECHNISCHE UNIVERSITÄT MÜNCHEN

Lehrstuhl II des Instituts für Organische Chemie und Biochemie
und Institute for Advanced Study at the Department Chemie

Impact of the Integrin αvβ3 Transmembrane Domain Sequence and the Cytoplasmic Contacts on Cell/Matrix Adhesiveness and Integrin-mediated Cell Signalling

Martina Müller

Vollständiger Abdruck der von der Fakultät für Chemie der Technischen Universität München zur Erlangung des akademischen Grades eines

Doktors der Naturwissenschaften (Dr. rer. nat.)

genehmigten Dissertation.

Vorsitzender: Univ.-Prof. Dr. St. J. Glaser
Prüfer der Dissertation:
1. Univ.-Prof. Dr. Dr. h.c. H. Kessler
2. apl. Prof. Dr. U. Reuning

Die Dissertation wurde am 12.10.2011 bei der Technischen Universität München eingereicht und durch die Fakultät für Chemie am 05.12.2011 angenommen.

Meinen Eltern

Abbreviations

Ab	Antibody
AFM	Atomic force microscopy
Amino acids	One letter code
APS	Ammonium persulfate
Bad	Bcl-2-associated death promoter
Bcl-2	B-cell leucemia 2 protein
bp	Base pairs
BSA	Bovine serum albumin
Ca^{2+}	Calcium
CDF	Cummulative distribution function
CLSM	Confocal laser-scanning microscopy
CoIP	Coimmunoprecipitation
c-myc	Cellular homologue avian myelocytomatosis virus oncogene
c-Src	Cellular homologue rous sarcoma oncogene
DAPI	4',6-diamidino-2-phenylindole
DMEM	Dulbecco's modified eagle medium
DMSO	Dimethylsulfoxide
DNA	Deoxyribonucleic acid
dNTP	Deoxyribonucleic triphosphate
ECM	Extracellular matrix
EDTA	Ethylendiamintetraacetic acid
EGFR	Epidermal growth factor receptor
ELISA	Enzyme-linked immunosorbent assay
$Erk^{1/2}$	Extracellular signal regulated kinases 1/2 (MAPK)
FACS	Fluorescence-activated cell sorting
FAK	Focal adhesion kinase
FCS	Foetal calf serum
FLIM	Fluorescence lifetime imaging microscopy
FN	Fibronectin
FRET	Fluorescence/Förster resonance energy transfer
GAM	Growth arrest medium

GAPDH	Glyceraldehyde 3-phosphate dehydrogenase
GpA	Glycophorin A
Grb2	Growth factor receptor-bound protein 2
HEPES	(4-(2-hydroxyethyl)- 1-piperazineethanesulfonic acid
IgG	Immunoglobulin G
IP	Immunoprecipitation
h	Hour
ICC	Immunocytochemistry
kDa	Kilo Dalton
mAb	Monoclonal antibody
MAPK	Mitogen-activated protein kinase
Mg^{2+}	Magnesium
mM	Milli Molar
Mn^{2+}	Manganese
MTT	3-(4,5-Dimethylthiazol-2-yl)-2,5-diphenyltetrazolium bromide
MLCK	Myosin light chain kinase
nm	Nanometer
NF-κB	Nuclear factor κB
OD	Optical density
ON	Over night
p	Phosphate group
PBS	Phosphate-buffered saline
PCR	Polymerase chain reaction
PFA	Paraformaldehyde
PI3K	Phosphatidylinositol 3-kinase
PKB/Akt	Protein kinase B/cellular homologue AKT8 virus oncogene
PL	Poly-L-lysine
pN	Pico Newton
RGD	Arginine-glycine-aspartate tripeptide
RT	Room temperature
S.D.	Standard deviation
SDS	Sodium dodecyl sulfate
SDS-PAGE	Sodium dodecyl sulfate polyacrylamide gel electrophoresis

TBS	Tris-buffered saline
TMD	Transmembrane domain
Tris	Tris-(hydroxymethyl)-aminomethan
VEGFR	Vascular endothelial growth factor receptor
VN	Vitronectin
v/v	Volume/volume
WB	Western blot
WT	Wild type
w/v	Weight/volume

1 Abstract

Integrins are a family of cell adhesion receptors, which transduce signals bidirectionally across the cell membrane. By binding to various extracellular matrix (ECM) ligands, they play an important role in cell adhesion and, consequently, in cellular motility. Integrins consist of two non-covalently linked subunits, the α- and β-chain, forming a heterodimeric receptor, which has a large extracellular domain, containing the ligand binding site, two single pass transmembrane domains (TMD) and a small cytoplasmic tail. Even a lot is known about the integrin's function and signal transduction, the exact molecular mechanism underlying integrin activation remains elusive. Crystal structures of the cancer- and angiogenesis-related integrin αvβ3 as well as of the platelet integrin αIIbβ3 did so far not provide full information about the conformational changes during activation. Nevertheless, mutational studies as well as cryoelectron microscopical images suggested that association and dissociation of the integrin TMD and the cytoplasmic tails, as well as receptor elongation, seem to play an important role in integrin activation. Considering these data, a three state model of integrin activation was proposed. Here, upon activation and signalling, the integrin conformation is altered from a resting, bent state to an extended high-affinity conformation with an open TMD and an exposed extracellular ligand binding site. However, until now, not much is known about how single TMD associate and regulate receptors in the cell membrane. Yet, molecular dynamics simulation indicated that integrins, in their energetically favoured conformation after insight-out activation, might adopt a similar TMD conformation as the well studied homodimeric, transmembrane protein glycophorin A (GpA). In the present work, the impact of the integrin TMD sequence on integrin activation and signalling was studied. For this, the complete integrin αvβ3 TMD was exchanged by the TMD of GpA (TMD-GpA). Moreover, a control mutation that prevents TMD association (TMD-GpA-I) was introduced. The integrin αvβ3 chimeras as well as the integrin wild type were stably transfected into an ovarian cancer cell test system. The present work demonstrated that an integrin αvβ3 with a clasped TMD (TMD-GpA), which represents a "primed" intermediate integrin conformation, is fully capable of ligand binding but restrained in intracellular signal transduction. However, mutation of the integrin TMD that results in an open conformation (TMD-GpA-I) is accompanied by constitutive activation of the receptor. Thus, we were able to decouple the integrin-mediated cellular adhesive capacity from signalling. These results suggest that

integrins are allosterically fine-tuned through their TMD. Moreover, the results give a hint that the proposed integrin intermediate conformation (TMD-GpA) exists during activation. The second part of the work dealt with the integrin αvβ3 cytoplasmic salt bridge. The cytoplasmic integrin contacts play an important role in stabilising the low-affinity integrin conformation. Disruption of a membrane-proximal cytoplasmic salt bridge and its impact on integrin activation has not been shown for the integrin αvβ3 before. In the present work, disruption of the integrin cytoplasmic salt bridge, accomplished by introduction of charge reversal mutations, led to constitutive integrin αvβ3 activation and signalling in a cellular test system. Thus, we propose that the interchain salt bridge in the integrin αvβ3 cytoplasmic domains is instrumental for the regulation of adhesive strength and signal transduction of integrin αvβ3.

Since αv-integrins are upregulated during angiogenesis and cancer progression, the receptors became an interesting therapeutic target. However, functional blocking of αv-integrins with a monoclonal antibody and a small molecule drug so far lacks therapeutic efficacy. Thus, profound knowledge of the mechanism and conformational rearrangements underlying integrin receptor activation is inevitable for proper targeting of integrins.

2 Introduction

2.1 Cellular adhesion, a fundamental process in multicellular organisms

For the maintenance of multicellular life-forms, adhesion to the extracellular matrix (ECM) and coherence between neighbouring cells is one of the most important criteria. In addition to connective cell-cell junctions, which provide a linkage between the cells, cells simultaneously attach to the surrounding connective tissue, the ECM, by forming cell-matrix-adhesive contacts. There are different variants of these cell/ECM linkages. Focal complexes are small adhesions, found in membrane protrusions of spreading and migrating cells (Truong et al. 2009). Focal adhesion sites encompass large dynamic protein complexes anchoring the actin cytoskeleton mechanically to the ECM. Furthermore, proteolytically active adhesions termed “podosomes” or “invadopodia” are formed by invasive cancer cells and some other non-transformed cell types like osteoclasts and macrophages (Zamir et al. 2001). Newly formed focal adhesions, which are built in the leading edge and disassembled in the rear end of migrating cells, enable them to move along the underlying growth substrate. Common to all these structures is the local connection between ECM proteins outside and the actin cytoskeleton within the cell (Truong et al. 2009). This is provided by the formation of a dynamic protein complex that implies cell adhesion molecules and adaptor proteins, which generate a link to the cytoskeleton. The main group of transmembrane cell adhesion and signalling receptors that mediate connection to the ECM as well as cell/cell contacts is the superfamily of integrins (Hynes 2002).

Cellular adhesion as well as the ability of cells to migrate and invade the surrounding tissue are crucial processes during development, wound healing, and angiogenesis, the formation of new vessels. Aberrant cellular migration, invasion into the surrounding tissue, and angiogenesis also play crucial roles in pathological conditions like the formation of solid tumours and metastases. Transformed cancer cells are highly proliferative and the growing primary tumour needs to be supplied with blood by newly formed vessels. Tumour cells invade the surrounding tissue and some are able to metastasize in a haematogenous or lymphatic fashion into other body compartments. Because of the fact that cellular adhesion to the ECM, migratory capacity of cells arising thereof, and angiogenesis are dependent on integrins and

their (up)regulation, the receptors became in recent years new targets in cancer treatment.

Although many studies focussed on the issue of cellular adhesion mediated by integrins, as well as on the role of the integrins during cancer progression, the functional mechanisms of integrin activation and signalling are still not fully resolved yet. Hence, in the present study, we aimed at gaining further insight into the mechanisms and conformational regulation underlying integrin activation and signalling.

2.2 The integrin receptor superfamily

Integrins represent the main family of cell adhesion and signalling receptors, present in all different cell types of metazoa. No homologues are detected in prokaryotes, plants, or fungi (Whittaker et al. 2002). These adhesion receptors were first described in different publications in the middle 1980s and summarised under the name integrin in 1986 by the group around Richard Hynes (Tamkun et al. 1986). The term “integrin” was chosen to avoid the confusing multiplicity of names used, until then, for the independently discovered receptors. It describes the receptors’ integral membrane nature as well as their role in the integrity of both, the ECM and the cytoskeleton (Tamkun et al. 1986).

Integrins are type I, single pass transmembrane proteins. They pass signals bidirectionally across cell membranes and also mediate cellular adhesion to other cells or the surrounding ECM glycoproteins such as collagen, fibronectin (FN) and vitronectin (VN) (Hynes 2002). The heterodimeric integrin receptor is composed of two non-covalently linked subunits, the α- (120-160 kDa) and the β- (90-119 kDa) integrin chain. Each subunit consists of a large extracellular domain (N-terminus), forming together the ligand binding site between the head groups, a transmembrane domain (TMD) and a relatively short cytoplasmic tail (C-terminus) of about 40-70 amino acids, connecting the integrin with the actin cytoskeleton (Fig. 1).

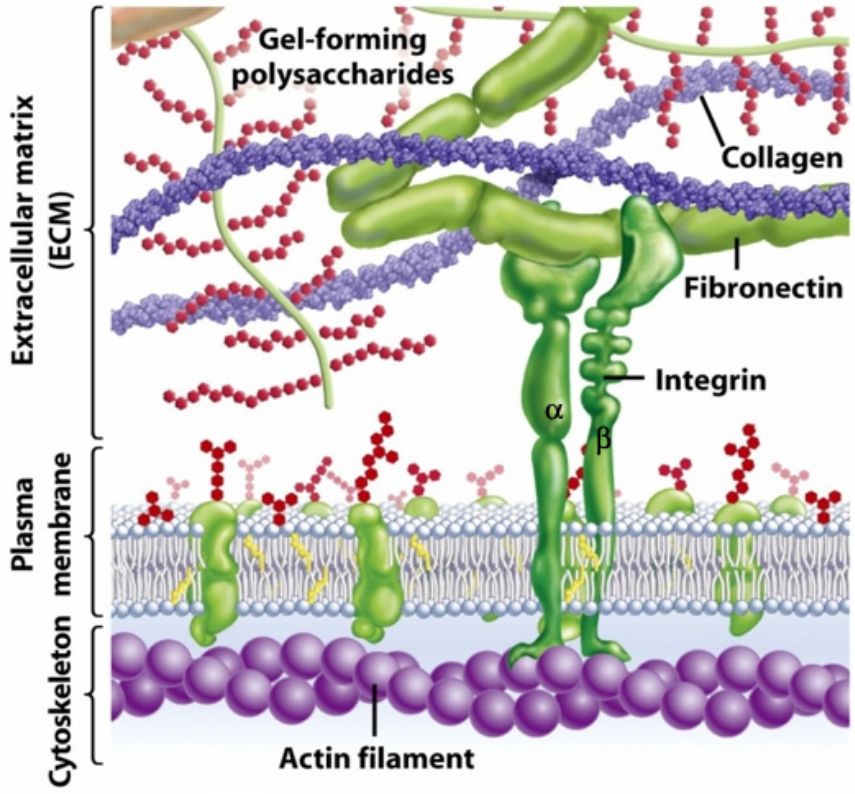

Fig.1 Scheme of an integrin in its cellular microenvironment

Integrins are type I transmembrane proteins with an extracellular N-terminal part. The heterodimeric receptor is composed of an α- and a β-subunit, which are non-covalently linked. The large extracellular domain binds to ECM proteins such as VN, FN, and collagen, respectively. Upon integrin activation, the small cytoplasmic tail of the β-subunit connects the receptor with components of the cytoskeleton.

In mammals, 18 α- and 8 β-subunits have been identified, which are able to form 24 distinct integrin heterodimers through different combinations (Hynes 2002) (Fig. 2). The genes encoding the different subunits are found on various chromosomes. Based on sequence alignments, functional properties, or expression patterns, different integrin subfamilies were defined: the arginine-glycine-aspartate (RGD) receptors, the collagen receptors, the laminin-binding integrins, and the leukocyte integrins (Hynes 2002) (Fig. 2). The relevance of the RGD-motif as a recognition site for cell attachment was first described by Ruoslahti and co-workers (Pierschbacher et al. 1984). A large number of adhesive ECM proteins, blood, and cell surface proteins contain this binding motif and nearly half of the known integrins, including the αv-integrins, recognise this sequence in certain ECM proteins (Ruoslahti 1996).

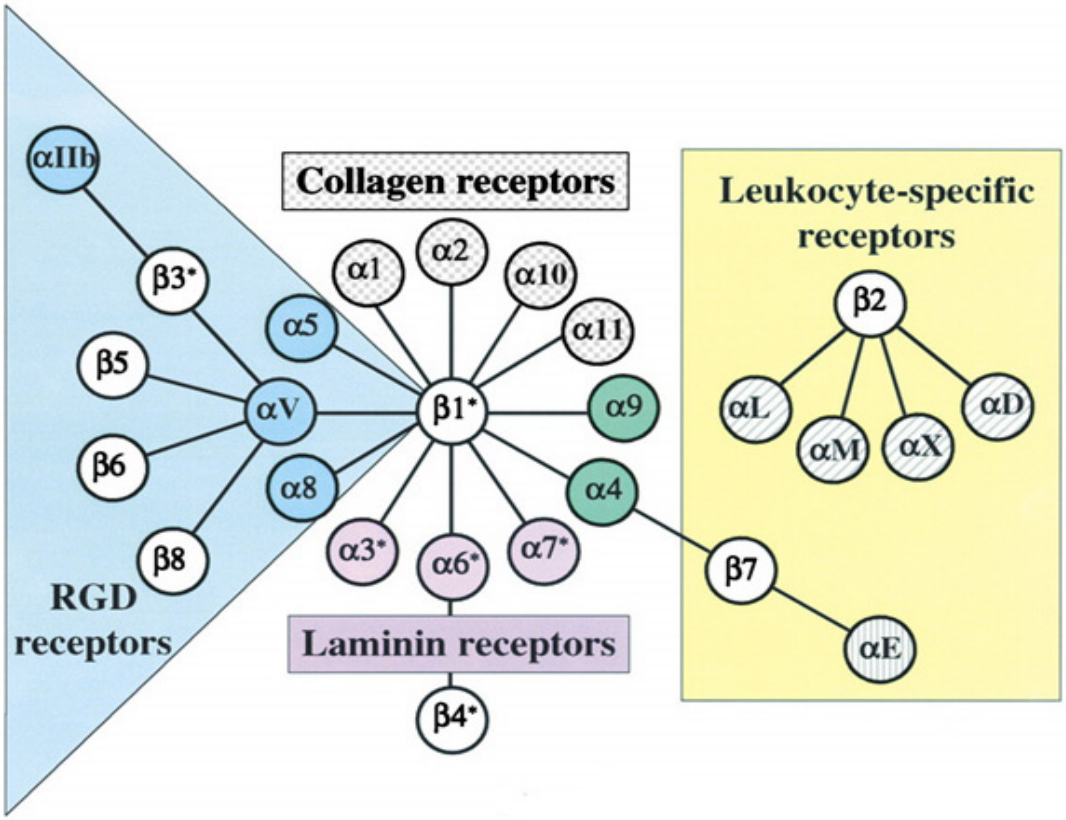

Fig. 2 Heterodimeric associations of 18 α- and 8 β-integrin subunits

The heterodimeric integrin receptor superfamily consists of 24 members, formed by different subunit combination. The integrin superfamily can be divided in several subfamilies based on evolutionary relationships and emerging ligand specificity (see colouring of α-subunits) and, in case of the β2 subunit restriction leukocytes (Hynes 2002). α-subunits that belong to the collagen receptors (grey), the laminin receptors (purple) or the RGD receptors (blue) are found throughout the metazoa. Restricted to chordates are α-subunits α4 and α9 (green) and subunits β2-β8. Asterisks denote alternatively spliced cytoplasmic domains (Figure modified from Hynes 2002).

2.3 Bidirectional transmembrane signalling- a key feature of integrins

A key feature all integrins have in common is their ability of bidirectional signal transduction across the cellular plasma membrane (Humphries 1996; Hynes 2002; Arnaout et al. 2005). Both signalling events, inside-out and outside-in, are in most cases closely linked. Integrin affinities towards their ECM ligands are regulated by intracellular signal transduction, resulting in integrin activation through inside-out signalling (Hynes 2002). Therefore, integrin inside-out activation is important for anchorage-dependent cellular properties, such as cell adhesion and migration (Shattil et al. 2010). During inside-out signalling, binding of intracellular, cytoskeletal proteins, like talin or kindlin, leads to drastic conformational changes within the

integrin from a “bent” resting state to an activated state with elongated extracellular domains (Adair et al. 2002; Takagi et al. 2002a). The structural changes are described in detail in chapter 2.8. Through this conformational alteration, the receptor’s affinity to ECM proteins is upregulated, resulting in enhanced adhesive capacity and cell migration. On the contrary, integrins also behave like “traditional” signalling receptors in transmitting signals into the cell by outside-in signalling (Hynes 2002) (Fig. 3). As a result of ligation by an ECM ligand, integrins provide a transmembrane mechanical link from the extracellular contacts to the cytoskeleton inside the cell (Hynes 2002). This triggers outside-in signalling, which leads to activation of intracellular signalling cascades (detailed description see also chapter 2.11). Alterations of the intracellular signalling cascades modulate many aspects of cell behaviour, including proliferation, motility, survival/apoptosis (the programmed cell death), and gene expression (Hynes 2002).

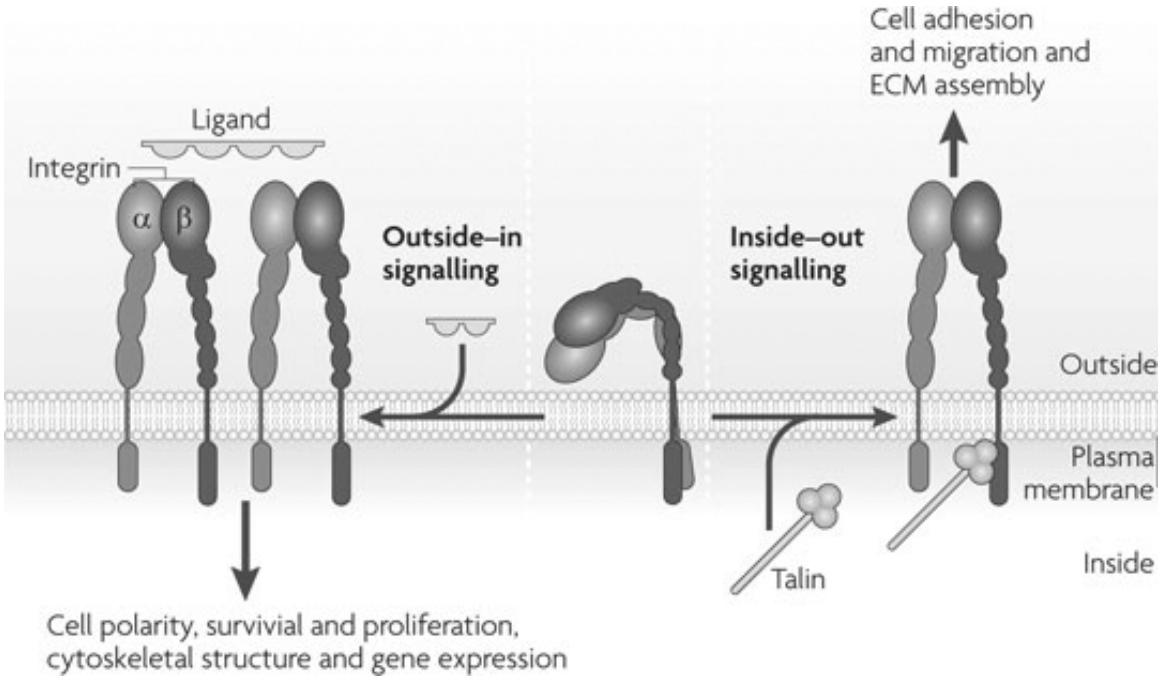

Fig. 3 Bidirectional integrin signalling

Binding of intracellular activators to the integrin β-cytoplasmic tail leads to changes in the integrin conformation from a resting state to an activated state and results in inside-out activation. By subsequent binding of the integrin extracellular domain to ECM ligands, integrins provide a transmembrane mechanical link from the extracellular contacts to the cytoskeleton. This leads to integrin-triggered intracellular signalling, termed outside-in signalling. Alterations of the intracellular signalling cascades then result in changes of cell proliferation, motility, survival, and gene expression (Figure modified from Shattil et al. 2010).

2.4 The integrin αvβ3

The main focus of the present work was laid on one member of the integrin superfamily, integrin αvβ3, formerly known as the VN-receptor because of its preferred binding to this ECM protein (Pytela et al. 1985; Hapke et al. 2003). The following descriptions regarding integrin structure and signalling mostly refer to integrin αvβ3, but may also be considered generally because of close relations between the different members of the integrin family.

Integrin αvβ3 is widely expressed in diverse cell types among them endothelial cells, vascular smooth muscle cells, monocytes, platelets, leukocytes, and cancer cells (Murphy et al. 1994; Hapke et al. 2003). As a result of its binding to ECM proteins, integrin αvβ3 mediates cellular adhesion and cell migration. As both processes contribute to the invasion of endothelial cells into the surrounding tissue, integrin αvβ3 is involved in the formation of new blood vessels, a process termed angiogenesis.

Integrin αvβ3 was first described by Pytela et al. in 1985 (Pytela et al. 1985). In this early work, it was shown that the FN- and VN-receptors each recognise the RGD-tripeptide. This peptide was originally identified as the sequence within FN that mediates cell attachment, but it has also been found in the ECM protein VN and numerous other proteins (D'Souza et al. 1991). However, it has been proven that the name VN-receptor is too restrictive for integrin αvβ3 because other integrins also bind VN and integrin αvβ3 binds other ligands, even though to a lesser extent (Hynes 1992). Among the variety of ECM proteins, integrin αvβ3 is capable of binding, are FN, fibrinogen, laminin, von-Willebrand-factor, and osteopontin (Humphries et al. 2006). The specific interaction between integrins and the RGD-containing ECM proteins may be mediated by a second specific binding site within ECM proteins. Even more likely, integrin receptors are able to recognise distinct conformations of RGD-sequences arising of varying protein folding and sequences adjacent to the RGD-motif.

Despite the other ECM proteins, bound by integrin αvβ3, VN is the main ligand of integrin αvβ3. VN is a 75 kDa glycoprotein encoded by the VTN gene and found in human blood predominantly as a monomer and in the ECM as a multimer. The protein consists of an N-terminal somatomedin-B domain, an adjacent RGD-motif, a central domain with hemopexin homology and a C-terminal domain (Fig. 4). As an αv-integrin ligand VN is involved in cell adhesion and spreading and it also plays a

role in regulation of coagulation, fibrinolysis, complement activation, and haemostasis (Preissner et al. 1998). Generally, low VN levels are detectable in most normal tissues; however, elevated levels are predominantly observed in tumour tissue and injured tissues. For example, VN was found to be strongly accumulated in the ECM around breast cancer cell clusters, compared to normal breast tissue (Aaboe et al. 2003). VN is also expressed in highly differentiated ovarian carcinomas but not in most of less differentiated tumours (Carreiras et al. 1996; Liapis et al. 1997). Moreover, a recent study showed that integrin αvβ3 itself is involved in the regulation of the direct synthesis of VN by human ovarian cancer cells. Thus, upregulation of integrin αvβ3 in these cells induces expression of VN and contributes to remodelling of the tumour environment, in favour of tumour progression (Reuning 2011).

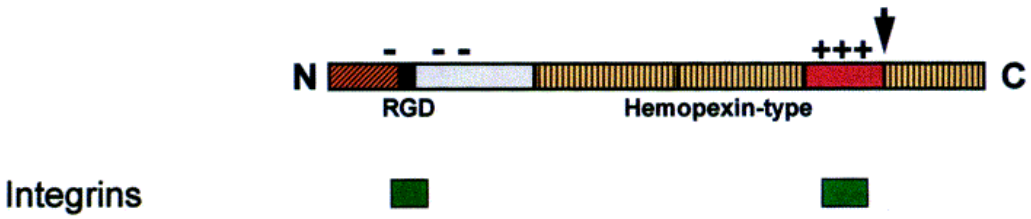

Fig. 4 Scheme of the structure and ligand binding domains of VN

The domain organisation of human VN is depicted, indicating the somatomedin-B (SMB) region at the acidic (−−−) N-terminus, followed by the major integrin binding site (RGD), hemopexin-like repeats, and the glycosaminoglycan-binding site at the (+++) C-terminus. The arrow points to the position of an endogenous protease cleavage site. Positions of integrin binding sites in VN are highlighted by green coloured bars (Figure modified from Preissner et al. 1998).

2.5 Role of integrin αvβ3 in angiogenesis and cancer progression

Integrin αvβ3 is overexpressed in a wide variety of highly malignant tumours, including melanoma, glioblastoma, ovarian cancer and breast cancer. A large proportion of normal ovarian epithelium and highly differentiated ovarian tumours express the two integrin subunits, αv and β3, as well as the ligand VN (Carreiras 1996). Additionally, it was found that integrin αvβ3 is expressed to a higher extent in invasive ovarian carcinoma compared to those ovarian tumours with low malignant potential (Liapis et al. 1997). High expression levels of integrin αvβ3 and its main ligand VN have also been shown to enhance the metastatic potential in breast cancer cell lines (Wong et al. 1998; Desgrosellier et al. 2010). Indeed, the expression of integrin αvβ3 is significantly higher in breast cancer tumours of patients with

metastasis than in those without metastasis (Gasparini et al. 1998). For several reasons, integrin αvβ3 contributes to and regulates diverse processes, important for tumour progression such as angiogenesis, cell proliferation, migration, and invasion. First, integrins provide the connection of cells with the surrounding ECM, which is essential for both, migration and invasion. Second, they regulate remodelling of the ECM through control of adjacent proteases. This enhances the invasive capacity of the tumour. For example, integrin αvβ3 interacts with molecules of proteolytic cascades like the urokinase-receptor (uPAR) and ADAM15, which alters their binding preference towards specific ECM proteins (Reuning et al. 2003; Beck et al. 2005). Both receptors, uPAR and integrin αvβ3, bind VN and considerable evidence suggests that integrins are signalling co-receptors of uPAR (Smith et al. 2010). This interaction has been shown to alter the integrin's adhesive function as well as integrin-mediated intracellular signalling cascades (Reuning et al. 2003). The matrix metalloprotease ADAM15 is a natural binding partner of integrin αvβ3. It binds and functionally blocks integrins via its disintegrin motif. Consequently, ADAM15 has the potency to loosen tumour cell adhesion to the underlying matrix and therefore regulates tumour cell migration and invasion. Moreover, integrins crosstalk with growth factor receptors. This promotes intracellular signalling, hence triggers tumour growth and progression (Desgrosellier et al. 2010). It was shown that the epidermal growth factor receptor (EGFR) expression level is upregulated depending on integrin αvβ3-induced signalling (Lössner et al. 2008). Integrin αvβ3 and EGFR form complexes at the cellular adhesion sites, which have an impact on signalling cascades. This crosstalk may activate ligand-independent EGFR downstream signalling (Cabodi et al. 2004). Third, angiogenesis, thus provision of the growing tumour with blood, is regulated by crosstalk between integrin αvβ3, its connection to ECM proteins, and the vascular endothelial growth factor receptor (VEGFR) (Somanath et al. 2009). Studies showed that integrin αvβ3 and VEGFR-2 are able to form complexes and that phosphorylation of VEGFR-2 is enhanced when endothelial cells are plated onto ECM proteins like VN. This led to the assumption that integrin αvβ3 is involved in increased angiogenesis mediated by VEGFR-2 (Somanath et al. 2009).

Additionally to these ligation-dependent events, recent studies indicate that integrin αvβ3 plays a crucial and contradictory role in tumour cell survival that does not necessarily imply occupation and activation by ligands (Desgrosellier et al. 2009). Under normal conditions, unligated integrins play a role in modulating apoptosis.

Here, ligated integrins transduce survival signals and unligated integrins can promote pro-apoptotic cascades. The balance of these signals is based on the ability of cells to interact with the surrounding ECM. After complete loss of normal cell-matrix adhesion, cell death is initiated via integrins through a process termed anoikis, which is a special form of programmed cell death with respect to anchorage-dependent cells (Desgrosellier et al. 2010). However, integrin αvβ3 also participates in tumour progression by enhancing anchorage-independent cell growth, a hallmark of transformed cells. This requires integrin αvβ3 controlled activation of the intracellular tyrosine kinase cellular homologue rous sarcoma oncogene (c-Src) and is independent of cell adhesion or activation of the important integrin-interacting signalling molecule focal adhesion kinase (FAK) (Desgrosellier et al. 2009). The anchorage-independent signalling events mediated by integrin αvβ3 contribute to tumour cell survival. Consequently, metastatic tumour cells may escape from anoikis and invade other organs.

Since the integrin αvβ3 plays an important role in cancer progression and angiogenesis we chose it as a model protein. Understanding of the complex process of integrin activation and molecular/conformational rearrangements contributing to integrin-triggered signal transduction are necessary to target integrins properly.

2.6 Integrin αvβ3 as a therapeutic target

Because of its role in angiogenesis and cancer progression, from the early 1990s on, integrin αvβ3 has been an attractive target in the development of new cancer therapeutics (Brooks et al. 1994). Two integrin αvβ3 binding antagonists have made their way to clinical trials in the oncological field. One of them is the monoclonal antibody (mAb) Etaracizumab (synonym: Vitaxin, Abegrin), a humanised version of the anti-angiogenic mAb LM609 directed to integrin αvβ3 (Wu et al. 1998). This function blocking antibody showed considerable anti-angiogenic effects in preclinical models (Brooks et al. 1995). Currently, Etaracizumab is being tested in many in vitro/ in vivo studies as well as in clinical phase I/II trials of different cancer types like melanoma, glioblastoma, and breast carcinoma. The benefit of its effect is, however still elusive. It seems that the observed in-vitro effects are not reproducible under physiological or pathophysiological conditions and that patients' benefit is rather small (Hersey et al. 2010).

The other integrin αvβ3 antagonist is a small molecule drug. Cilengitide (cyclo-[RGDfN(Me)V]) is a high affinity cyclic pentapeptide, which was developed by Horst Kessler from the Technische Universität München in cooperation with the Merck KGaA (Goodman et al. 2002). To date, it is the most promising αv-integrin targeting substance. It blocks endothelial cell adhesion mediated by RGD-binding integrins αvβ3 and αvβ5. Cilengitide functions as a ligand mimetic through attaching to the integrins' RGD binding site, thus suppressing angiogenesis by inducing anoikis. So far, it has been shown that Cilengitide, in combination with chemotherapeutics, has a synergistic efficacy in prolonging the overall survival of patients afflicted with recurrent glioblastoma (Reardon et al. 2008). However, recently other studies have shown that Cilengitide may not only exert an antagonistic effect by blocking αv-integrins but also works as an integrin activating agonistic peptide. There is evidence that Cilengitide activates surface integrin αvβ3, which results in phosphorylation and thus activation of the signalling kinases c-Src and FAK (Alghisi et al. 2009). An explanation for Cilengitide-mediated integrin activation might be dose-dependence. Reynolds and co-workers (Reynolds et al. 2009) reported that in mouse models low (nanomolar) concentrations of RGD-mimetic αvβ3/αvβ5 inhibitors can paradoxically stimulate tumour growth and tumour angiogenesis. They also showed that low concentrations of the inhibitors promote VEGF-mediated angiogenesis by altering integrin αvβ3 and VEGFR-2 trafficking. Consequently, the pro-angiogenic effects of low concentrations of RGD-mimetic αvβ3/αvβ5 integrin inhibitors could compromise their efficacy as anticancer agents. This will have major implications for the use of RGD-mimetic compounds in humans.

2.7 The integrin structure

In order to mediate specific cellular signals "inside-out" and "outside-in" between components of the cytoskeleton and the ECM, the integrin receptor requires a special and flexible structure, passing through the cell membrane. The integrin α- and β-subunits are each composed of large N-terminal extracellular domains, single-pass TMD and usually short C-terminal cytoplasmic tails. The integrin ligand-binding head, formed by both subunits, is followed in each subunit by legs, which are elongated in the transmembrane-cytoplasmic domains. The αv-leg is composed of an upper thigh domain and a lower calf module, consisting of two large β-sandwich domains, calf-1

and -2. The β3-leg consists of an upper leg segment comprising a plexin-semaphorin-integrin (PSI)-, an immunoglobulin (Ig)-like hybrid-, and integrin EGF-like 1 (IE1) domain, followed by a lower leg segment made up of three EGF-like domains and the β-tail (Fig. 5B). Ligand specificity is provided by the integrin ligand binding pocket. It comprises a seven-bladed β-propeller domain of the αv-subunit and a βA- or I-like domain of the β3-subunit, which together form the ligand binding site (Springer 1997). In case of αv- and αIIb-integrins this is the RGD-binding site (Humphries et al. 2006). Three closely linked metal ion binding sites in the βA/I-domain are especially important for ligand binding. These are referred to as the metal ion-dependent adhesion site (MIDAS), a site adjacent to the metal ion-dependent adhesion site (ADMIDAS), and the ligand-induced metal-binding site (LIMBS). Divalent cations can bind to these sites, whereupon Mn^{2+} and Mg^{2+} ions have an activating effect (Vallar et al. 1999; Takagi et al. 2002a). The role of Ca^{2+} ions remains unclear. However, it has an inhibiting effect on ligand binding of the β3A domain (Pesho et al. 2006).

Different studies focussed on the elusive integrin αvβ3 steric structure. Crystal structures of the entire crystallised integrin αvβ3 ectodomain, in absence or presence of cyclic pentapeptide ligand RGDfV, were solved (Xiong et al. 2001; Xiong et al. 2002). They revealed an inactive bent integrin conformation. Furthermore, these studies showed that ligand binding is accompanied by structural rearrangements of the integrin (Fig. 5B). Additionally, they provided a first atomic view how the integrin αvβ3 binding pocket interacts with an RGD peptide. Yet, complete structural information on the remaining α/β transmembrane-cytoplasmic residues was still missing (Xiong et al. 2009). In other approaches, cryoelectron microscopy confirmed that the inactivated receptor is strongly bent and that it undergoes conformational changes during activation (Adair et al. 2002; Takagi et al. 2002a) (Fig. 5A). More recently, the complete crystal structure of the αIIbβ3 integrin ectodomain plus an α/β-TMD fragment was solved (Xiong et al. 2009). It revealed a hydrodynamically more compact integrin than without the TMD, reflecting a conformational coupling between the lower leg and head domains that regulates integrin activation (Xiong et al. 2009).

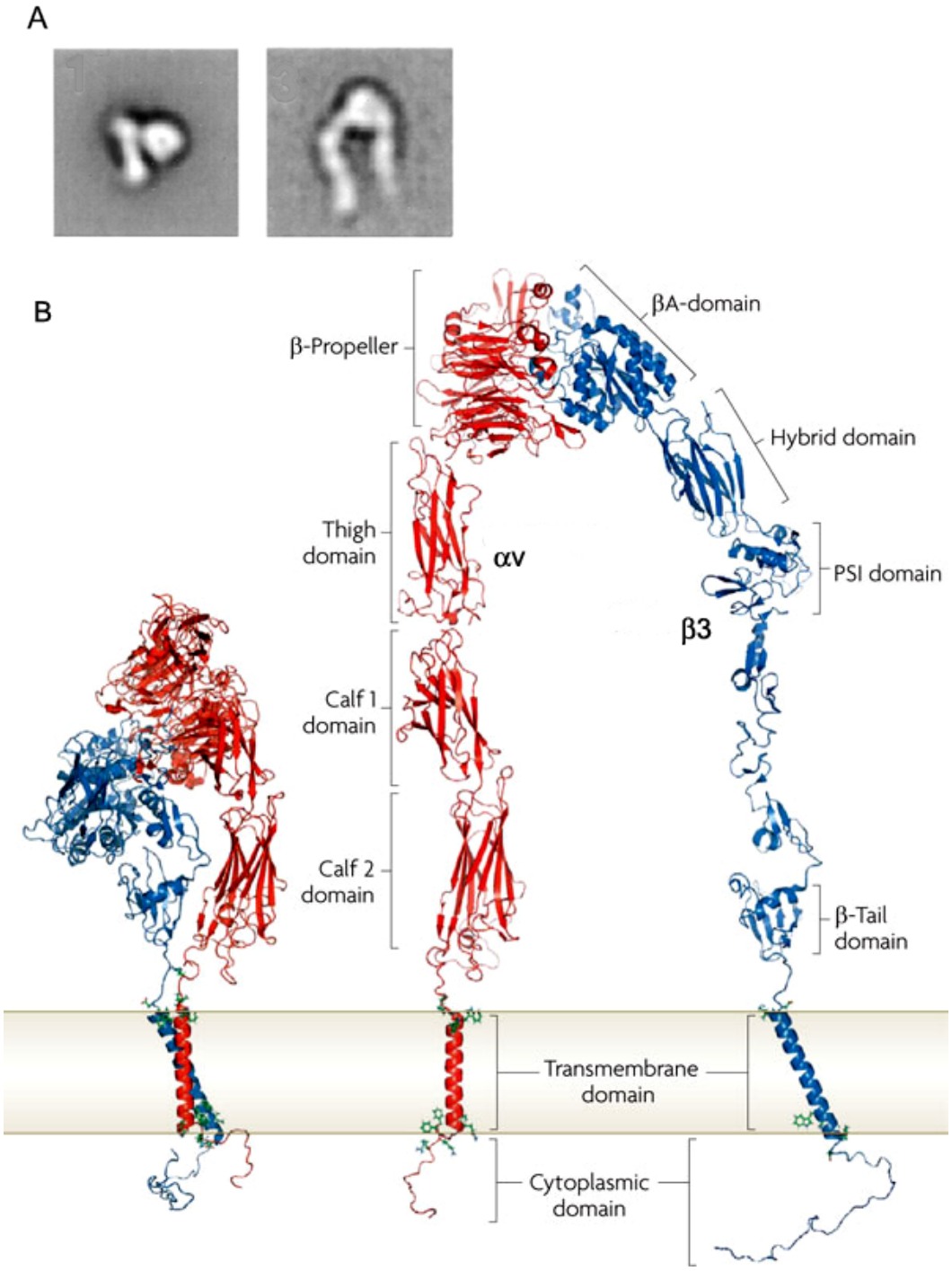

Fig. 5 The integrin αvβ3 structure

The figure shows a cryoelectron microscopical image and a cartoon model of the integrin αvβ3 structure. **A)** A cryoelectron microscopical image of the integrin αvβ3 is depicted. On the left side, the clasped, inactive integrin is depicted. The right picture shows an unclasped, extended integrin, which was activated by 1 mM Mn^{2+} and 60 µM cyclo-RGDfV peptide (Figure modified from Takagi et al. 2002a). **B)** On the left, a cartoon model depicts the bent integrin conformation, observed in crystal structures (Xiong et al. 2001; Takagi et al. 2002a; Zhu et al. 2008; Xiong et al. 2009). On the right, the integrin is unfolded and permits insight into the different domains. The N-terminal ends of both subunits (β-propeller of the αv- and βA/I-domain of the β3-subunit) assemble by non-covalent interaction to form the integrin head, which provides a ligand binding site (Figure modified from Shattil et al. 2010).

2.8 Conformational changes during integrin activation

The conformation of the integrin extracellular domains and its affinity for ligand binding are dynamically regulated in the process of integrin activation. The “bent” integrin conformation was, in mutational and electron microscopical studies, found to be the physiologically relevant, low-affinity conformation (Takagi et al. 2002a; Xiong et al. 2009). Integrins are activated (inside-out) by binding to intracellular proteins like talin or kindlin (Moser et al. 2009). It has been shown that binding of talin to the cytoplasmic tail of the integrin β3-subunit is essential for integrin inside-out activation (Calderwood et al. 1999; Tadokoro et al. 2003). Recently, in-vitro assays revealed that talin binding is sufficient to activate and extend membrane embedded integrin αIIbβ3 without the presence of a ligand. Moreover, the talin head domain can activate a kindlin binding-defective integrin mutant in cells (Ye et al. 2010). Binding of talin then leads to changes within the integrin conformation from the “bent” resting state to an activated state (Fig. 6). The dramatic conformational changes occurring in integrin αIIbβ3 during activation were revealed by electron cryomicroscopy (Adair et al. 2002; Takagi et al. 2002a). Integrin activation results in a less compact conformation with a different arrangement of the leg domains (Takagi et al. 2002a; Xiong et al. 2009). The main conformational changes include: 1) integrin extension and 2) a subunit separation in the transmembrane-cytoplasmic domains (Hantgan et al. 1999). Separation of the TMD of the α- and β-subunit during inside-out and outside-in signalling was additionally demonstrated by fluorescence resonance energy transfer (FRET). In the same approach, it was also shown that separation of the cytoplasmic tails is essential for TMD separation and the resulting conformational changes (Luo et al. 2007). Based on these findings, a “switch blade”/ three state model of integrin activation was proposed. Here, upon activation the integrin legs extend (Adair et al. 2002; Luo et al. 2007; Zhu et al. 2008), the legs/ TMD separate and the headpieces either remain in the closed conformation, as when bent, or opening of the βA/hybrid hinge provokes a change to high ligand binding affinity (Takagi et al. 2002b; Xiao et al. 2004) (Fig. 6). Conformational changes of the integrin to high ligand binding affinity then triggers increased adhesiveness in the extracellular domain (inside-out) towards ECM ligands. Ligand binding by integrin extracellular domains then triggers signal transduction to the cytoplasm in outside-in direction. By this, intracellular signalling cascades that affect cellular growth, differentiation, migration, and apoptosis are regulated (Kim et al. 2003).

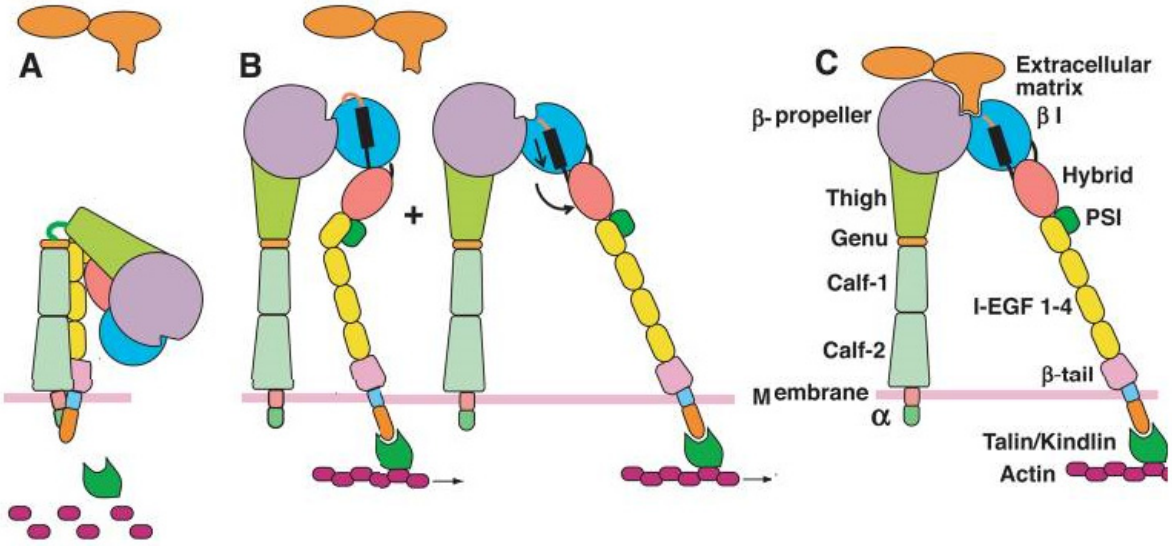

Fig.6 Model of integrin activation

The figure depicts the three state model of integrin activation. **A)** In the inactive bent conformation, the integrin ligand binding pocket is hidden, thus integrins have low affinity for ligands. **B)** Binding of talin or kindlin (green) to the β-subunit leads to disruption of the cytoplasmic domains. The unclasping causes integrin extension and results in an engagement with the actin cytoskeleton. Both, the open headpiece, with an exposed ligand binding site, as well as the closed headpiece conformation are present. **C)** Binding to an immobilised ECM ligand greatly increases the lateral force, thus the high-affinity, open headpiece conformation is favoured. Upon ligand binding, signals are then transduced to the cytoplasm (Figure modified from Zhu et al. 2008).

In contrast to the “switch blade”/three state model, another study suggested a “deadbolt” model of integrin activation. It was accomplished by fluorescence lifetime imaging microscopy (FLIM) of integrin αvβ3 in viable cells. These measurements revealed that changes in the apparent distance between the integrin head and the plasma membrane were minimal in inactive, Mn^{2+}-activated, constitutively active, or FN-bound full-length integrin. Thus, integrin activation here occurred in the absence of integrin leg extension (Xiong et al. 2009). Since the legs remain bent in the “deadbolt”- and become extended in the “switch blade” model, both are often presented as incongruent. However, in both paradigms, the conformation displaying bent legs and a closed headpiece hinge angle represents “low-affinity” and activation necessitates disruption of headpiece-tailpiece contacts (Puklin-Faucher et al. 2006).

2.9 The integrin transmembrane domains

2.9.1 Impact of integrin TMD on integrin activation and integrin-mediated signalling

The central feature of integrin receptors is their capacity to rapidly change their adhesive function as a result of alteration in their ligand binding affinity. Modulation of inside-out and outside-in signalling occurs via conformational changes of the integrin TMD (Luo et al. 2007; Shattil et al. 2010). Dimerisation or lateral association of helical TMD within lipid bilayers is a key event during the folding of membrane proteins (Psachoulia et al. 2010). Direct interaction between the integrin α- and β-TMD was demonstrated by several approaches. An in vitro model system (Schneider et al. 2004a), as well as an affinity capture assay using mini integrins, which exclusively encompass the TMD and the cytoplasmic domain, revealed preferential heterodimeric association of the αIIb- and the β3-integrin TMD (Kim et al. 2009). Mutational studies and molecular modelling suggested that interaction between the TMD of an α- and β-integrin subunit are important in maintaining an inactive, low-affinity state and that activation requires alteration of these interactions (Luo et al. 2004; Gottschalk 2005; Partridge et al. 2005). Moreover, it was demonstrated by FRET that the TMD separate, following integrin ligand binding (Kim et al. 2003). Constraining the αv- and β3-TMD separation by experimental introducing intersubunit disulfide bonds between the integrin extracellular domains blocked integrin activation from inside the cell (Luo et al. 2004). In a similar approach, it has been shown that a disulfide bond between the integrin TMD resulted in an integrin that bound ligand, mediated adhesion, and adopted an extended conformation after ligand binding. However, the TMD-bonded integrin exhibited a profound defect in adhesion-induced outside-in signalling (Zhu et al. 2007).

Computational modelling and recent NMR approaches disclosed that the helical packing within the TMD interface of both integrin subunits adopts a distinct right-handed coiled-coil conformation (Gottschalk et al. 2002; Yang et al. 2009). Within this tightly packed conformation, the TMD and membrane-proximal parts of the cytoplasmic tails mainly associate through two structural elements: 1) a $G^{972}xxxG^{976}$ motif of the αIIb-subunit (similar in αv) interacting with $S^{699}xxxA^{703}$ of the β3-subunit, respectively, and 2) a highly conserved $G^{991}FFKR^{995}$ motif of the α-subunit. In the

latter, R^{995} forms a potential salt bridge together with a β-aspartate (D^{723}) (Weljie et al. 2002; Lau et al. 2009; Zhu et al. 2009) (Fig. 7).

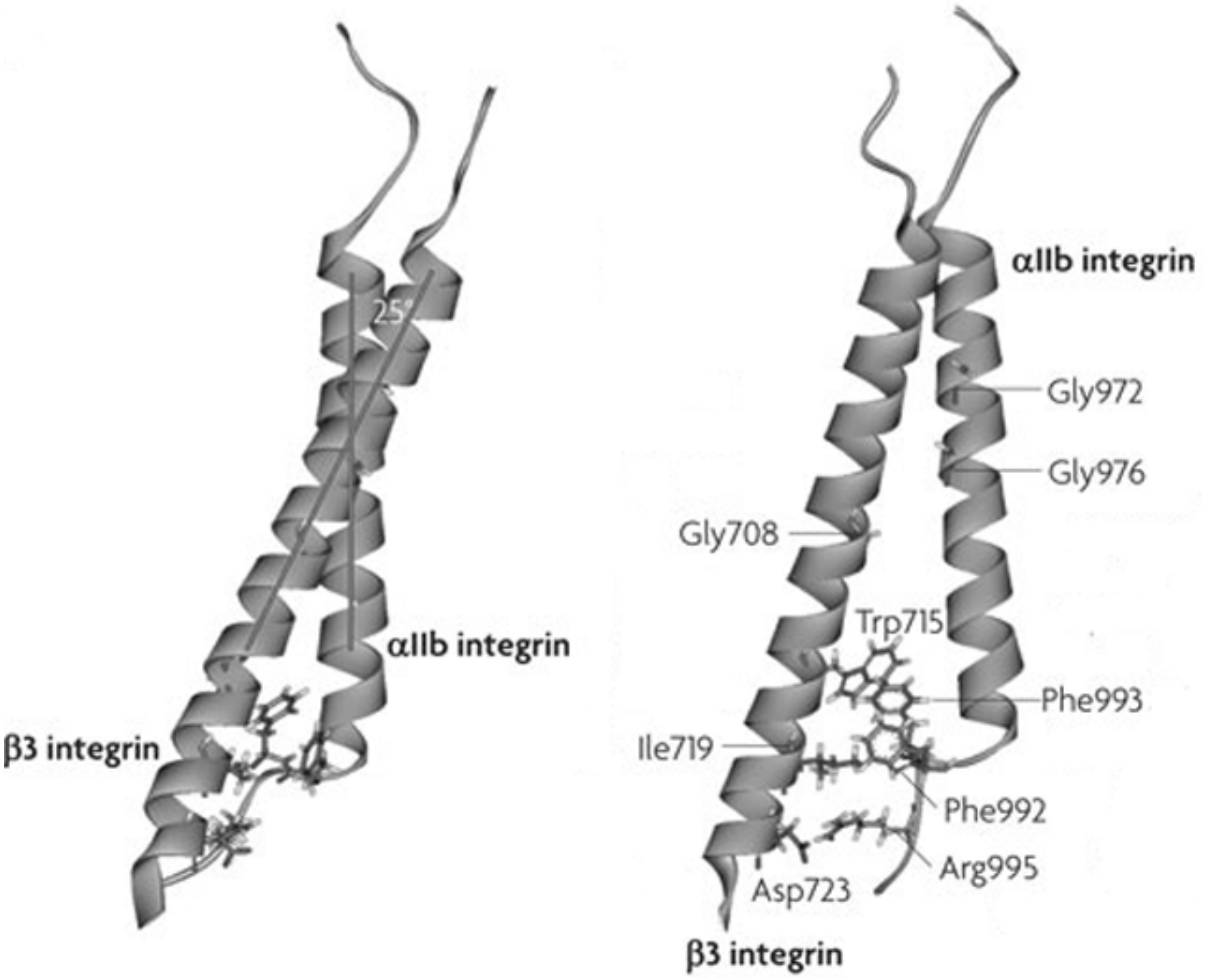

Fig.7 Structure of the integrin transmembrane complex and the small cytoplasmic tails (using the example of integrin αIIbβ3)

The TMD of αIIb- and β3-integrin subunits adopt right-handed, α-helical, coiled-coil conformations with a predicted crossing angle of 25° (left). Rotating the model (left) by 90° (right) reveals the GxxxG binding motif (αIIb G972-G976; β3 S699-A703) and a potential salt bridge (αIIb R995; β3 D723), which mediate the main interaction of the TMD and the cytoplasmic tails (Figure modified from Shattil et al. 2010).

2.9.2 Similarity of integrin TMD with the TMD of glycophorin A

Binding of intracellular proteins to the integrin cytoplasmic tails leads to a transition from the “bent” low-affinity state to a primed state with high ligand binding affinity.

Required for this adjustment is a kinetically favoured movement of the TMD that leads to conformational changes in the integrin ectodomains. On the basis of independent global searches of helix-helix interactions of 16 different integrin subunits, Gottschalk and co-workers (Gottschalk et al. 2002) predicted TMD helix conformations by molecular dynamics simulation. This computational molecular modelling revealed that the high-affinity state with the lowest energy conformation of integrins showed close similarity to the TMD helical structure of glycophorin A (GpA). GpA is a member of the glycophorin family (Chasis et al. 1992). Glycophorins are transmembrane, homodimeric, heavily glycosylated sialoglycoproteins, located on the membrane of erythrocytes. The GpA α-helical TMD dimer represents a paradigm for helix-helix packing in transmembrane proteins, mediated by a $G^{79}xxxG^{83}$ sequence motif (Psachoulia et al. 2010).

The structural similarity of the integrin TMD and the GpA TMD is also reflected by a certain sequence similarity. A multiple sequence alignment of the TMD of the α- and β-subunits of different integrins showed that the amino acid residues corresponding to the crucial G residues of the central $G^{79}xxxG^{83}$ dimerisation motif of GpA are small residues such as G, A, or S. These small, neutral and in case of A non-polar residues do not exert steric interference within the tightly packed, coiled-coil TMD and are often seen as a replacement for G in packing motifs of transmembrane domains (Russ et al. 2000). In a later work, Gottschalk and co-workers showed that the GpA-like association of the β-subunit is not located in the interface of the integrin resting state. Therefore, it might not be involved in the TMD interactions of the resting state, as opposed to the GxxxG-like binding motif of the α-subunit (Gottschalk 2005). Contradictory, the results of a study accomplished by Schneider and Engelmann (Schneider et al. 2004a) underlined a propensity of the integrin TMD to form a dimer with the GxxxG-like motif in both helical interfaces. Based on integration of the structural model and the data gained by Schneider and Engelman, a “primed” transient GpA-like integrin TMD structure was postulated (Gottschalk 2005). In this model, binding of intracellular ligands to the integrin β-cytoplasmic tail initially disturbs the cytoplasmic interactions and removes the constraint imposed on the TMD. The latter then in turn relax, and adopt their lowest energetic conformation by forming a GpA-like structure. Such a transient integrin TMD conformational change from the resting state to a GpA-like conformation would then facilitate the extracellular conformational change necessary for raising integrin binding-affinity towards ECM ligands (Gottschalk 2005).

2.10 The integrin cytoplasmic tails and their role in integrin activation and signalling

For the mechanism of integrin activation and the arising cell signalling events thereof, not only the integrin TMD are of great importance, but also the cytoplasmic tails play a substantial role. Integrin activation requires disruption of the cytoplasmic tails (Lu et al. 2001; Takagi et al. 2001; Tadokoro et al. 2003), which provides a linkage between the integrin and cytoskeletal proteins. This mechanism depends on the configuration and flexibility of the cytoplasmic tails. Compared to the large ectodomains of the integrin receptor, the cytoplasmic tails are, with a length of 34 amino acid residues (αv) and 46 amino acid residues (β3), very short. NMR resolution experiments provided insight into the structural features of the C-terminal integrin parts. The α-helical structure of the αv-TMD is elongated in the first amino acids of the cytoplasmic tail (Yang et al. 2009). The residual αv-chain, following adjacent to Gly^{991} is rich in acidic residues and largely unstructured (Vinogradova et al. 2004; Yang et al. 2009). The α-helical structure of the β3-TMD is elongated in the C-terminal ends until amino acid residue A^{737}. However, the structure is also lost beside one short helical turn (P^{745}-A^{750}) (Yang et al. 2009). Between two amino acid residues of the conserved sequences of the αv-(GFFKR) and β3-(KLLITIHD) integrin subunits, a salt bridge exists (αv R^{995}; β3 D^{723}) (Hughes et al. 1996; Vinogradova et al. 2002; Lau et al. 2009) (Fig. 8). This non-covalent subunit interaction is a combination of hydrogen bonding and electrostatic interactions. Generally, a salt bridge can be defined as an interaction between two groups of opposite charge (e.g. amino group and carboxylate ion) in which at least one pair of heavy atoms is within hydrogen bonding distance (Donald et al. 2010). Salt bridges are known to contribute to protein stability (Sindelar et al. 1998). Indeed, functional studies have demonstrated the important role of the integrin cytoplasmic salt bridge in maintaining the receptor in a resting state (Hughes et al. 1996; Vinogradova et al. 2002; Ma et al. 2006; Imai et al. 2008; Kim et al. 2009; Lau et al. 2009). By mutational disruption of the salt bridge within integrin αIIbβ3, the integrin becomes activated which leads to constitutive outside-in signalling (Hughes et al. 1996). The importance of cytoplasmic domain separation was also shown by FRET. Here, cyan and yellow fluorescent-protein, respectively, were fused to the integrin αL and β2 cytoplasmic domains. Measuring of living cells revealed that in the resting integrin state these domains were close to each other, but underwent significant spatial separation upon either intracellular activation (inside-out

signalling) or ligand binding (outside-in signalling) (Kim et al. 2003). Under physiological conditions, disruption of the integrin cytoplasmic tail interaction is due to binding of the cytoskeletal protein talin (Vinogradova et al. 2002). The N-terminal talin head domain binds to the NPxY motif (N^{744}-Y^{747}) of the β3-integrin tail (Calderwood et al. 1999) (Fig. 8), indirectly linking the integrin to the cytoskeleton.

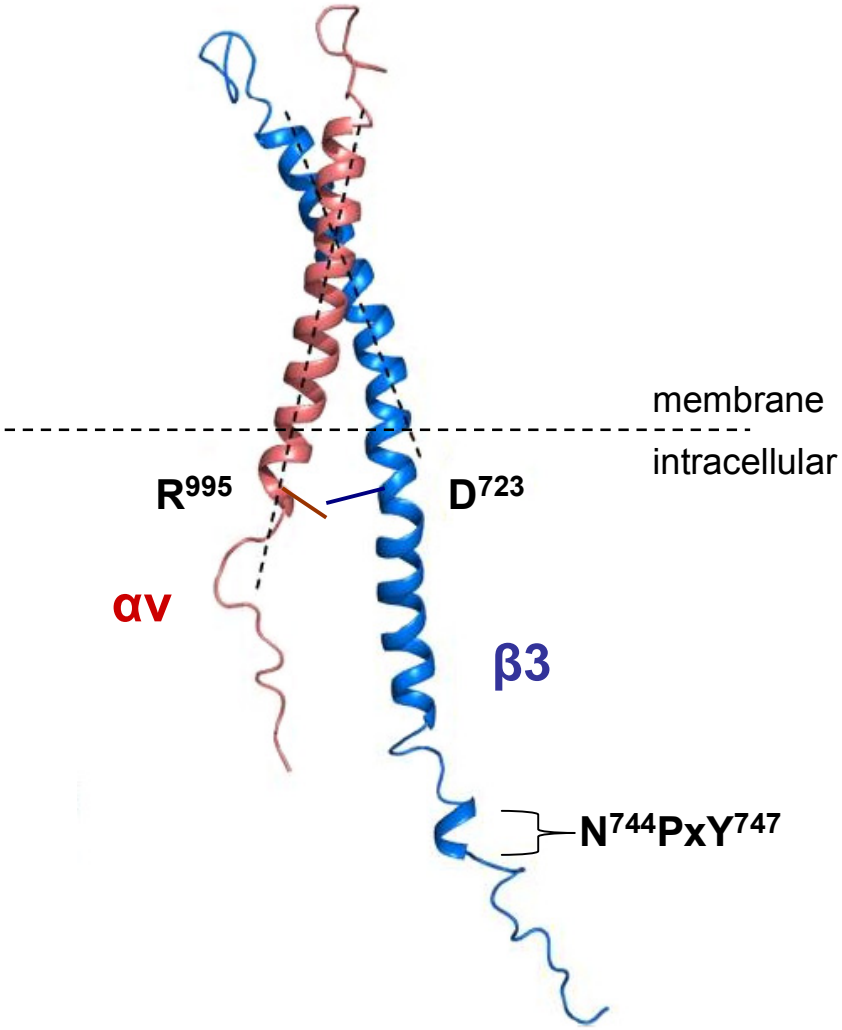

Fig. 8 Structure of integrin αvβ3 cytoplasmic tails

The structure of the αv- (red) and β3- (blue) TMD and cytoplasmic tails is depicted. The α-helix of both subunits is elongated in the C-terminal ends. After this, both cytoplasmic tails become highly unstructured. An electrostatic interaction between the αv (R^{995})- and β3 (D^{723})-tail keeps the integrin in the low-affinity "bent" conformation (Hughes et al. 1996; Lau et al. 2009). Under physiological conditions disruption of this salt bridge, by binding of talin to the NPxY motif of the β-subunit, activates the integrin receptor (Vinogradova et al. 2002) (Figure modified from Yang et al. 2009).

2.11 Integrin-triggered intracellular signalling pathways

The formation of new integrin-ECM bonds, arising molecular rearrangements thereof, and activation of the receptor triggers a variety of intracellular signalling cascades. This controls gene expression, cell survival, proliferation, and migration (Giancotti et al. 1999). Under the formation of focal adhesions, integrins are linked to talin and indirectly linked to proteins like paxillin, α-actinin, tensin, and vinculin (Desgrosellier et al. 2010) (Fig. 9). These linkages contribute to the reorganisation of the actin cytoskeleton, which is essential for cell motility (Cabodi et al. 2010). Additionally, although integrins lack kinase activity, by clustering, they can activate and recruit kinases (Desgrosellier et al. 2010). Generally, kinase activation is induced by chemical addition of phosphate groups (phosphorylation), which results in a changed enzyme activity and/or association with other proteins (Burnett et al. 1954).

2.11.1 The focal adhesion kinase

A key molecule in transducing integrin-related signalling is the non-receptor tyrosine kinase FAK. FAK is expressed in most tissues and cell types and is evolutionary conserved in mammalian species (Devor et al. 1993). Upon integrin-mediated binding of ECM proteins, FAK is auto-phosphorylated (Schlaepfer et al. 1994). The amino-terminal FERM (four-point-one, ezrin, radixin, and moesin) domain of FAK plays a critical role in FAK activation through an intramolecular interaction with the kinase domain of FAK. When FAK is in its inactive state, direct contact between the FERM domain and kinase domain blocks access to its catalytic cleft. This blocks its activation loop as well as the key auto-phosphorylation site Y397. In contrast, in the active state, the FERM domain is displaced by an activating protein like the integrin β-cytoplasmic domain, allowing rapid auto-phosphorylation of Y397. This exposes a docking site for Src family kinases, phosphatidylinositol 3-kinase (PI3K) and growth factor receptor-bound protein 7 (Grb7). Binding of these effector kinases activates a cascade of phosphorylation events and new protein-protein interactions, which constitute several signalling pathways (Zhao et al. 2009) (Fig. 9).

2.11.2 Signalling via kinase cellular sarcoma

Phosphorylation of FAK (Y397) and subsequent c-Src binding is crucial for signal transduction that results in cell migration (Cary et al. 1998). One downstream event of the FAK/Src complex formation is the association with Crk-associated substrate ($p130^{Cas}$), an adaptor protein (Fig. 9). At sites of focal adhesion, the mechanical stretching of cells, forces $p130^{Cas}$ to undergo a conformational change. This change promotes phosphorylation of $p130^{Cas}$ by Src family or FAK kinases (Geiger 2006). The Src/FAK/$p130^{Cas}$ complex targets downstream pathways which promote cell motility (Cary et al. 1998). Moreover, there is evidence that integrin-mediated Src signalling contributes to anchorage-independent cell growth (Desgrosellier et al. 2009). It was found that integrin αvβ3 promotes c-Src-dependent, but FAK-independent phosphorylation of $p130^{Cas}$ in non-adherent cells (Desgrosellier et al. 2009).

2.11.3 Activation of the mitogen-activated protein kinase pathway

Upon integrin-mediated binding of ECM proteins FAK is auto-phosphorylated which exposes a docking site for Src family kinases. In turn, the formation of a FAK/Src complex allows Src to phosphorylate FAK at position Y925. This creates a binding site for growth factor receptor-bound protein 2 (Grb2), leading to activation of the rat-sarcoma (RAS) – extracellular-signal-regulated-kinase (erk) signalling pathway (Schlaepfer et al. 1994; Zhao et al. 2009) (Fig. 9). Activation of this pathway results in phosphorylation of the mitogen-activated protein kinase (MAPK) $p44/42^{erk1/2}$ (Short et al. 1998). Subsequent $p44/42^{erk1/2}$ regulation of E-twenty six (ETS) transcription factors is required for cell cycle progression and cell proliferation (Short et al. 1998; Zhao et al. 2009) (Fig. 9). Furthermore, anchorage-dependent activation of $p44/42^{erk1/2}$, which is induced by integrin-mediated cell adhesion, plays an important role in regulating cell motility (Giancotti et al. 1999; Howe et al. 2002). Stimulation of $p44/42^{erk1/2}$ activates the myosin light chain kinase (MLCK) (Klemke et al. 1997). The active MLCK then phosphorylates myosin and thus enables the myosin crossbridge to bind to the cellular actin filament and allow contractions (Nguyen et al. 1999).

2.11.4 Activation of the protein kinase B/Akt pathway

Integrin-mediated FAK activation enhances cell survival via triggering several mechanisms such as the increased expression of B-cell leukemia-2 (Bcl-2; member of Bcl-2 family), activation of the phosphatidylinositol 3-kinase (PI3K) pathway or nuclear factor κB (NF-κB) signalling (Desgrosellier et al. 2010). PI3K then activates the protein kinase B/cellular homologue AKT8 virus oncogene (PKB/Akt) by phosphorylation of S473 in the hydrophobic motif of the regulatory domain of PKB/Akt. The PI3K/Akt pathway has been shown to be mandatory for various cellular activities, remarkably cellular proliferation and survival (Lawlor et al. 2001) (Fig. 9). The activated seronine-threonine kinase PKB/Akt stimulates cell cycle progression. Moreover, it inhibits apoptosis, at least in part, by phosphorylating and thereby inactivating two pro-apoptotic proteins, Bcl-2-associated death promoter (Bad; member of Bcl-2 family) and caspase-9 (Giancotti et al. 1999) (Fig. 9).

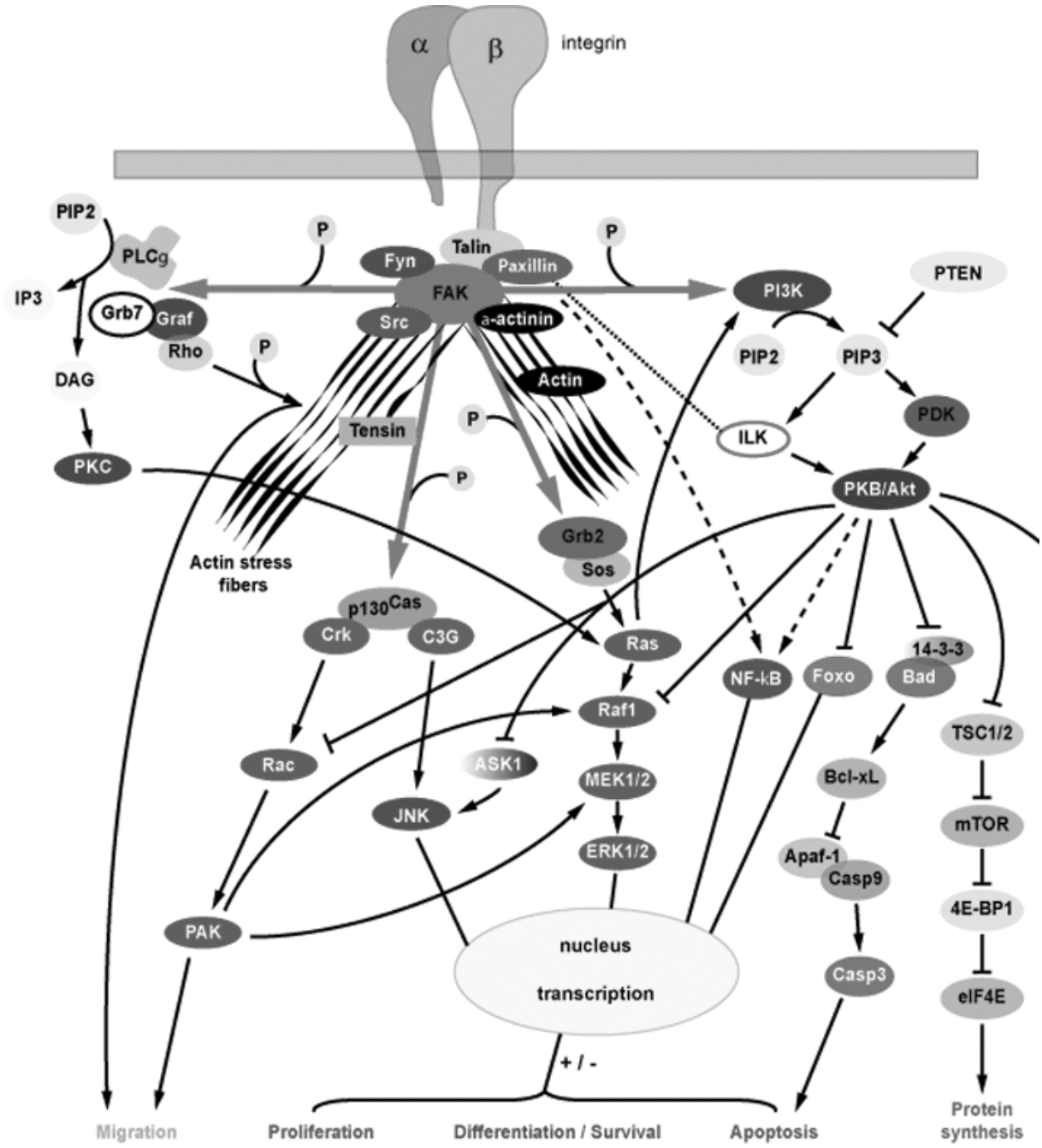

Fig. 9 Intracellular signalling cascades activated by integrins at focal contacts

The major intracellular signalling pathways activated by integrin engagement in adhesion complexes are depicted. The key element in all these pathways is FAK. This kinase is activated through auto-phosphorylation at Y397 and thereby allows binding of Src family kinases for further phosphorylation and full activation. Phosphorylation of FAK also controls its subsequent interactions with other proteins (i.e. Grb2, Grb7, PI3K), which in turn trigger cascades of events, e.g. the MAPK/ erk$^{1/2}$ and PI3K/Akt pathway, that lead to changes in cell proliferation, migration or survival (Figure modified from http://www2.unil.ch/cepo_research/introduction.html).

2.12 Integrin clustering and their ability to act as mechanosensors

At sites of focal contacts, it was found that individual integrins are differently organised and that they accumulate when cells are exposed to the respective integrin ligand (Dejana et al. 1988). This hetero-oligomer formation is called integrin clustering (Li et al. 2003). The process is inevitable for complete integrin-induced activation of intracellular signalling (Miyamoto et al. 1995). It was proposed that integrin clustering is induced by TMD-homodimerisation of α- and β-subunits (Li et al. 2003; Schneider et al. 2003). However, the corresponding assays were conducted in artificial experimental systems such as micelles and bacterial membranes. A recent study, with living mammalian cells, revealed that integrin clustering is more likely regulated by bringing integrins physically close together at sites of focal adhesion. To this end, cysteine mutagenesis and heterodimeric disulfide scanning were used to identify the integrin αIIb- and β3-TMD interactions in the cell membrane. Integrins clustered on the cell surface after adhering to immobilised fibrinogen, but the αIIb- and β3-TMD did not form any homomeric association (Wang et al. 2010). Clustering may also be induced because full-length talin has multiple integrin-binding sites (Ye et al. 2010). The process of integrin clustering is important for triggering outside-in signalling through increased “avidity”, the combined strength of multiple receptor-ligand bond interactions, of the integrin (Kucik 2002). It is also essential for the transition of mechanical forces, mediated by adhesion based intracellular structures, like focal complexes and focal adhesions (Puklin-Faucher et al. 2009). It has been proposed that integrin extension, or at least extension to the high affinity state with an open headpiece, requires force applied by the cytoskeleton to the cytoplasmic tails of the integrin (Zhu et al. 2008). During the processes of cellular adhesion and migration, pulling forces arise at sites of focal adhesion, creating tension that is passed from the actin cytoskeleton to the integrins, which are anchored by adaptor proteins. Recent computer simulation of integrin dynamics predicted that the ligand-bound integrin αvβ3 transitions into a high-affinity open headpiece state within nanoseconds, if force is applied to the ligand-headpiece complex (Puklin-Faucher et al. 2006). In other words, once the integrin binds a ligand, the ligand will resist the pulling force arising of the cytoskeletal linkage, increase the lateral tensile force, and thereby stabilise the high-affinity state (Zhu et al. 2008). Other studies also provided experimental support for this force-enhanced integrin function. It was demonstrated that application of force switches the relaxed integrin-state to a new tensioned state,

which expressed increased bond strength towards its ligand (Friedland et al. 2009). Bonds that undergo tension-strengthening are called "catch-bonds" and can function as a molecular clutch that is engaged under tension and will release when tension is released (Friedland et al. 2009; Kong et al. 2009).

3 Aims of the study

A central and still unresolved issue in integrin biology is the molecular mechanism underlying bidirectional signal transduction across cell membranes. A plethora of cell biological and biochemical data indicate that different conformational states of integrin transmembrane and cytoplasmic domains control the capacity and affinity of integrins to bind ECM ligands and thus trigger the formation of focal adhesions (Yang et al. 2009). In the present study, cellular model systems expressing different integrin αvβ3 mutants were created. With these, 1) the impact of a clasped/unclasped integrin αvβ3 TMD as well as 2) the influence of integrin cytoplasmic salt bridge formation on cellular adhesion and integrin-mediated signal transduction were analysed.

1) The integrin TMD

The integrin TMD of both subunits, αv and β3, were exchanged by the TMD of the well studied homodimeric, transmembrane human erythrocyte protein GpA (TMD-GpA).

With this cellular model system, the following scientific questions were addressed:

- How does an exchange of the integrin αvβ3 TMD by the TMD of GpA influence integrin-triggered intracellular signalling?
- What influence has a clasped/unclasped integrin αvβ3 TMD on cellular adhesion, proliferation and migration?
- Does an integrin TMD intermediate state, resembling the conformation of the GpA TMD, exist during integrin activation?

2) The integrin cytoplasmic salt bridge

Mutations were introduced in the salt bridge forming amino acids of both integrin subunits, αv and β3, respectively, which led to charge reversal exchanges (αv R995D; β3 D723R).

With this cellular model system, the following scientific questions were addressed:

- To what extent is a disrupted integrin αvβ3 cytoplasmic salt bridge influencing integrin-triggered intracellular signalling?
- How does abrogation of the integrin αvβ3 cytoplasmic salt bridge formation affect cellular adhesion, proliferation and migration?

4 Material

4.1 Eucaryotic cell line

For the following experiments, the human ovarian cancer cell line OV-MZ-6 was used. The origin and cultivation of human ovarian OV-MZ-6 cancer cells has been described previously (Möbus et al. 1992). It was originally isolated from the ascites of a patient afflicted with a serous papillary cystadenocarcinoma (FIGO IV). A cell clone, OV-MZ-6 #8, expressing low endogenous levels of integrin αvβ3, was used for transfection with wild type and mutated integrin αv- and β3-subunits, which were cloned into vector pCDNA 3.1/myc-His.

4.2 Bacteria

XL-1 blue *e.coli*	Stratagene Agilent Technologies, Santa Clara, CA, USA
SURE *e.coli*	Stratagene Agilent Technologies, Santa Clara, CA, USA

4.3 Growth media for pro- and eucaryotic cells

<u>Growth medium for human ovarian cancer cell line OV-MZ-6:</u>

Dulbecco's Modified Eagle Medium (D-MEM)	500 ml
supplemented with:	
HEPES	10 mM
Arginine	550 mM
Asparagine	272 mM
Foetal calf serum (FCS)	10% (v/v)

Selection of stably transfected cell clones occurred under antibiotic selection pressure by usage of Geneticin G418 (1 g/l).

Medium for cell cryoconservation:

FCS	90% (v/v)
Dimethylsulfoxide (DMSO)	10% (v/v)

Cell splitting solution:

Ethylenediaminetetraacetic acid (EDTA) in phosphate-buffered saline (PBS)	0.05% (v/v)

Growth medium for Bacteria:

Lysogeny broth (LB)-medium	1.0 % (w/v) Bactotrypton 0.5 % (w/v) Yeast extract 0.5 % (w/v) NaCl
LB-agar	1.5 % (w/v) Agar
Ampicillin	0.1 mg/ml
Cryoconservation (glycerol stocks)	50% LB-medium 50% glycerol

4.4 Expression plasmid

pcDNA 3.1/myc-His	Invitrogen, Karlsruhe, Germany

Full length integrin αv- and β3-cDNA were kindly provided by Ian Hart and cloned into vector pCDNA3.1/myc-His by Sandra Hapke.

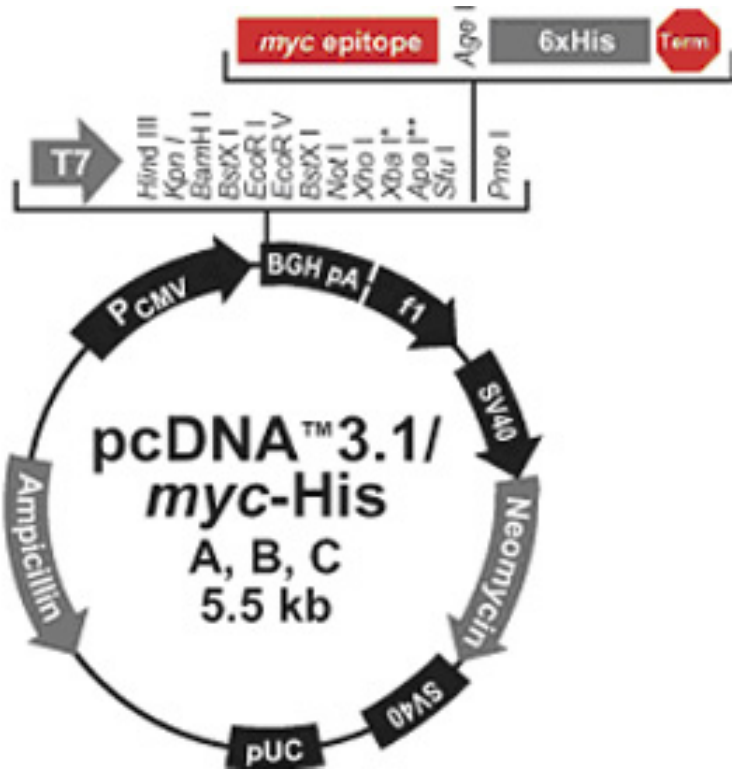

Fig. 10 Plasmid map of pcDNA 3.1/myc-His

The integrin αv-subunit was cloned into the BamHI and the EcoRI restriction sites; the β3-subunit was cloned into the EcoRV and the XbaI restriction sites.

DNA-Sequences of the αv- and β3-integrin subunit:

- restriction sites are marked in “blue”
- start-codon is marked in “green”
- part encoding the TMD is marked in “red”
- part encoding the salt bridge forming amino acid is marked in “yellow”

Sequence of αv-chain (3150 bp):

Bam HI

GGATTCcttcggcgatggcttttccgccgcggcgacggctgcgcctcggtccccgcggcctcccgcttcttctct
cgggactcctgctacctctgtgccgcgccttcaacctagacgtggacagtcctgccgagtactctggccccgagg
gaagttacttcggcttcgccgtggatttcttcgtgcccagcgcgtcttcccggatgtttcttctcgtgggagctc
ccaaagcaaacaccacccagcctgggattgtggaaggagggcaggtcctcaaatgtgactggtcttctacccgcc
ggtgccagccaattgaatttgatgcaacaggcaatagagattatgccaaggatgatccattggaatttaagtccc
atcagtggtttggagcatctgtgaggtcgaaacaggataaaattttggcctgtgccccattgtaccattggagaa
ctgagatgaaacaggagcgagagcctgttggaacatgctttcttcaagatggaacaaagactgttgagtatgctc
catgtagatcacaagatattgatgctgatggacagggattttgtcaaggaggattcagcattgattttactaaag
ctgacagagtacttcttggtggtcctggtagcttttattggcaaggtcagcttatttcggatcaagtggcagaaa
tcgtatctaaatacgaccccaatgtttacagcatcaagtataataaccaattagcaactcggactgcacaagcta
tttttgatgacagctatttgggttattctgtggctgtcggagatttcaatggtgatggcatagatgactttgttt
caggagttccaagagcagcaaggactttgggaatggtttatatttatgatgggaagaacatgtcctccttataca
attttactggcgagcagatggctgcatatttcggattttctgtagctgccactgacattaatggagatgattatg
cagatgtgtttattggagcacctctcttcatggatcgtggctctgatggcaaactccaagaggtggggcaggtct
cagtgtctctacagagagcttcaggagacttccagacgacaaagctgaatggatttgaggtctttgcacggtttg
gcagtgccatagctcctttgggagatctggaccaggatggtttcaatgatattgcaattgctgctccatatgggg
gtgaagataaaaaaggaattgtttatatcttcaatggaagatcaacaggcttgaacgcagtcccatctcaaatcc
ttgaagggcagtgggctgctcgaagcatgccaccaagctttggctattcaatgaaaggagccacagatatagaca
aaaatggatatccagacttaattgtaggagcttttggtgtagatcgagctatcttatacagggccagaccagtta
tcactgtaaatgctggtcttgaagtgtaccctagcattttaaatcaagacaataaaacctgctcactgcctggaa
cagctctcaaagtttcctgttttaatgttaggttctgcttaaaggcagatggcaaaggagtacttcccaggaaac
ttaatttccaggtggaacttcttttggataaactcaagcaaaagggagcaattcgacgagcactgtttctctaca
gcaggtccccaagtcactccaagaacatgactatttcaaggggggggactgatgcagtgtgaggaattgatagcgt
atctgcgggatgaatctgaatttagagacaaactcactccaattactatttttatggaatatcggttggattata
gaacagctgctgatacaacaggcttgcaacccattcttaaccagttcacgcctgctaacattagtcgacaggctc
acattctacttgactgtggtgaagacaatgtctgtaaacccaagctggaagtttctgtagatagtgatcaaaaga
agatctatattggggatgacaaccctctgacattgattgttaaggctcagaatcaaggagaaggtgcctacgaag
ctgagctcatcgtttccattccactgcaggctgatttcatcggggttgtccgaaacaatgaagccttagcaagac
tttcctgtgcatttaagacagaaaaccaaactcgccaggtggtatgtgaccttggaaacccaatgaaggctggaa
ctcaactcttagctggtcttcgtttcagtgtgcaccagcagtcagagatggatacttctgtgaaatttgacttac
aaatccaaagctcaaatctatttgacaaagtaagcccagttgtatctcacaaagttgatcttgctgttttagctg
cagttgagataagaggagtctcgagtcctgatcatatctttcttccgattccaaactgggagcacaaggagaacc
ctgagactgaagaagatgttgggccagttgttcagcacatctatgagctgagaaacaatggtccaagttcattca
gcaaggcaatgctccatcttcagtggccttacaaatataataataacactctgttgtatatccttcattatgata
ttgatggaccaatgaactgcacttcagatatggagatcaacccctttgagaattaagatctcatctttgcaaacaa
ctgaaaagaatgacacggttgccgggcaaggtgagcgggaccatctcatcactaagcgggatcttgccctcagtg
aaggagatattcacactttgggttgtggagttgctcagtgcttgaagattgtctgccaagttgggagattagaca
gaggaaagagtgcaatcttgtacgtaaagtcattactgtggactgagacttttatgaataaagaaaatcagaatc
attcctattctctgaagtcgtctgcttcatttaatgtcatagagtttccttataagaatcttccaattgaggata
tcaccaactccacattggttaccactaatgtcacctggggcattcagccagcgcccatgcctgtgcctgtgtgggg
tgatcattttagcagttctagcaggattgttgctactggctgttttggtatttgtaatgtacaggatgggctttt
ttaaacgggtccggccacctcaagaagaacaagaaagggagcagcttcaacctcatgaaaatggtgaaggaaact
cagaaactGAATTC **EcoRI**

Sequence of β3-chain (2395 bp):

EcoRV

GATATCcgccgcgggaggcggacgagatgcgagcgcggccgcggccccggccgctctgggcgactgtgctggcgc
tgggggcgctggcgggcgttggcgtaggagggcccaacatctgtaccacgcgaggtgtgagctcctgccagcagt
gcctggctgtgagccccatgtgtgcctggtgctctgatgaggccctgcctctgggctcacctcgctgtgacctga
aggagaatctgctgaaggataactgtgccccagaatccatcgagttcccagtgagtgaggcccgagtactagagg
acaggcccctcagcgacaagggctctggagacagctcccaggtcactcaagtcagtccccagaggattgcactcc
ggctccggccagatgattcgaagaatttctccatccaagtgcggcaggtggaggattaccctgtggacatctact
acttgatggacctgtcttactccatgaaggatgatctgtggagcatccagaacctgggtaccaagctggccaccc
agatgcgaaagctcaccagtaacctgcggattggcttcggggcatttgtggacaagcctgtgtcaccatacatgt
atatctccccaccagaggccctcgaaaaccccctgctatgatatgaagaccacctgcttgcccatgtttggctaca
aacacgtgctgacgctaactgaccaggtgacccgcttcaatgaggaagtgaagaagcagagtgtgtcacggaacc
gagatgccccagagggtggctttgatgccatcatgcaggctacagtctgtgatgaaaagattggctggaggaatg
atgcatcccacttgctggtgtttaccactgatgccaagactcatatagcattggacggaaggctggcaggcattg
tccagcctaatgacgggcagtgtcatgttggtagtgacaatcattactctgcctccactaccatggattatccct
ctttggggctgatgactgagaagctatcccagaaaaacatcaatttgatctttgcagtgactgaaaatgtagtca
atctctatcagaactatagtgagctcatcccagggaccacagttggggttctgtccatggattccagcaatgtcc
tccagctcattgttgatgcttatgggaaaatccgttctaaagtagagctggaagtgcgtgacctccctgaagagt
tgtctctatccttcaatgccacctgcctcaacaatgaggtcatccctggcctcaagtcttgtatgggactcaaga
ttggagacacggtgagcttcagcattgaggccaaggtgcgaggctgtccccaggagaaggagaagtcctttacca
taaagcccgtgggcttcaaggacagcctgatcgtccaggtcacctttgattgtgactgtgcctgccaggcccaag
ctgaacctaatagccatcgctgcaacaatggcaatgggacctttgagtgtggggtatgccgttgtgggcctggct
ggctgggatcccagtgtgagtgctcagaggaggactatcgcccttcccagcaggacgaatgcagccccgggagg
gtcagcccgtctgcagccagcggggcgagtgcctctgtggtcaatgtgtctgccacagcagtgactttggcaaga
tcacgggcaagtactgcgagtgtgacgacttctcctgtgtccgctacaaggggagatgtgctcaggccatggcc
agtgcagctgtggggactgcctgtgtgactccgactggaccggctactactgcaactgtaccacgcgtactgaca
cctgcatgtccagcaatgggctgctgtgcagcggccgcggcaagtgtgaatgtggcagctgtgtctgtatccagc
cgggctcctatggggacacctgtgagaagtgccccacctgcccagatgcctgcacctttaagaaagaatgtgtgg
agtgtaagaagtttgaccggggagccctacatgacgaaaatacctgcaaccgttactgccgtgacgagattgagt
cagtgaaagagcttaaggacactggcaaggatgcagtgaattgtacctataagaatgaggatgactgtgtcgtca
gattccagtactatgaagattctagtggaaagtccatcctgtatgtggtagaagagccagagtgtcccaagggcc
ctgacatcctggtggtcctgctctcagtgatgggggccattctgctcattggccttgccgccctgctcatctgga
aactcctcatcaccatccacgaccgaaaagaattcgctaaatttgaggaagaacgcgccagagcaaaatgggaca
cagccaacaacccactgtataaagaggccacgtctaccttcaccaatatcacgtaccggggcacTCTAGA **XbaI**

4.5 Enzymes and other proteins

Pfu-Turbo polymerase	Invitrogen Gibco, San Diego, USA
Pfu Ultra II polymerase	Stratagene, La Jolla, USA
Restriction enzymes	NEB, Ipswich, UK
T4 DNA Ligase	NEB, Ipswich, UK
Taq polymerase	Invitrogen Gibco, San Diego, USA
Integrin αvβ3 (purified from human plasma)	Millipore, Schwalbach
Fibronectin	Becton Dickinson BD, Bedford, USA
Poly-L-lysine	Sigma, St.Louis, USA
Vitronectin (purified from human plasma)	Becton Dickinson BD, Bedford, USA

Protein-G-agarose	Roche Diagnostics GmbH, Mannheim
Tetramethyl rhodamine iso-thiocyanate (TRITC)-conjugated phalloidin	Millipore, Schwalbach

4.6 Antibodies

Primary antibodies:

name	***antigen***	***company***	***conc. µg/µl***	***application***	***dilution***
Mab1976Z/ LM609	αvβ3/ CD51/61	Millipore	1	ICC	1:100
CBL 544/ # 23C6	αvβ3/ CD51/61	Millipore	0.1	ICC FACS IP	1:10 1:10 1:20
Anti-myc	c-myc	Invitrogen	1	ICC	1:100
PM 6/13	β3/ CD61	Southern Biotech	0.1	ICC	1:100
CBL 479	β3/ CD61	Millipore	0.1	ICC FACS WB	1:100 1:100 1:1000
MAB 2008	β3/ CD61	Millipore	1	WB	1:1000
MAB 2023Z	β3/ CD61	Millipore	1	WB	1:1000
Ab 1930	αv/ CD51	Millipore		WB	1:5000
CBL 490	αv/ CD51	Millipore	0.1	ICC FACS WB	1:300 1:300 1:2500
Anti-FAK	FAK	BD	0.25	ICC WB	1:100 1:1000
Anti-phospho-FAK	FAK pY397	BD	0.25	ICC WB	1:50 1:1000
MAB 374/ clone 6C5	Glyceraldehyde 3-phosphate dehydrogenase (GAPDH)	Millipore	1	WB	1:5000

name	***antigen***	***company***	***conc. µg/µl***	***application***	***dilution***
Anti-MAPK	p44/42 (erk1/2)	Cell Signaling	__	FACS WB	1:200 1:1000
Anti-phospho MAPK	phospho-p44/42 (erk1/2)	Cell Signaling	__	FACS WB	1:200 1:1000
Anti-Akt	PKB/Akt	Cell Signaling	__	FACS WB	1:200 1:1000
Anti-phospho-Akt	phospho-PKB/Akt Ser473	Cell Signaling	__	FACS WB	1:200 1:1000
Anti-talin	talin1	Cell Signaling	__	WB	1:1000
Anti-talin	talin1	Atlas Antibodies	0.06	ICC	1:50
Anti-phospho-paxillin	phospho-paxillin (Y118)	Cell Signaling	__	ICC	1:50
Mouse IgG2b	*aspergillus niger* glucose oxidase	Dako	__	IP	1:40

Secondary antibodies:

Alexa-488-conj. goat-anti-mouse Immunoglobulin G (IgG)	Invitrogen Gibco, San Diego, USA
Alexa-488-conj. goat-anti-rabbit IgG	Invitrogen Gibco, San Diego, USA
Alexa-568-conj. goat-anti-mouse IgG	Invitrogen Gibco, San Diego, USA
Peroxidase-conj. goat-anti-mouse IgG	Jackson ImmunoResearch, West Grove, USA
Peroxidase-conj. rabbit-anti-mouse IgG	Jackson ImmunoResearch, West Grove, USA

4.7 Technical devices

Atomic force microscope:	
Axiovert 200	Zeiss, Jena
BioCell sample holder	JPK Instruments AG, Berlin
Nanowizzard II	JPK Instruments AG, Berlin
AxioImager (microscope)	Zeiss, Jena
AxioScope Hal 100 (microscope)	Zeiss, Jena
Axiovert 25 (microscope)	Zeiss, Jena
Centrifuge Avanti 30	Beckmann Coulter, Krefeld
Centrifuge 5417R	Eppendorf, Hamburg
Centrifuge 5415C	Eppendorf, Hamburg
Centrifuge Labofug 400R	Heraeus, Hanau
Confocal laser-scanning microscope:	
Laser device	Leica, Wetzlar
Axiovert 35 (microscope)	Zeiss, Jena
ELISA Reader	SLT Spectra, Crailsheim
Flow cytofluorometer FACS Calibur	BD Biosciences, Franklin Lakes, NJ, USA
Gel electrophoresis apparatus GNA-100	Pharmacia Biotech AB Uppsala, Sweden
GeneAmp 2400 (PCR-Thermocycler)	Perkin Elmer, Weiterstadt
Heracell incubator-CO_2	Heraeus, Hanau
Herasafe biological safety cabinet	Heraeus, Hanau
Labcycler (PCR -Thermocycler)	Sensoquest, Göttingen
pH-Meter	Schott, Mainz
Photometer	Eppendorf, Hamburg
Power supply Bluepower 500	Serva, Heidelberg
Purelab classic (VE water)	Elga GmbH, Celle
Thermomixer 5436	Eppendorf, Hamburg
UV-Transiluminator	Biometra, Göttingen
Vortex Genie 2	Bender & Hobein AG Zürich, Schweiz
Wet blot device	Biorad, München
X-ray film processor Cawomat 2000IR	Cawo, Schrobenhausen

4.8 Expendable materials

Cell culture flasks, dishes, and plates, cell scraper, falcon tubes, petri dishes, sterile round bottom tubes, and 5/10/25 serological pipettes were obtained from BD Biosciences, Franklin Lakes, NJ, USA.

All pipette tips, 1.5/ 2 ml reaction tubes, and 0.2 ml polymerase chain reaction (PCR) tubes were purchased from Sarstedt, Nümbrecht.

Arrow TL2 (cantilever for AFM)	NanoWorld, Neuchâtel, Switzerland
Combitips® plus 1 /2.5 /5 ml	Eppendorf AG, Wesseling-Berzdorf
E-plate 16 (impedance measurements)	Roche Diagnostics GmbH, Mannheim
FACS tubes conical 4.5 ml	Greiner Bio-One, Frickenhausen
Immobilon™ PVDF transfer membrane	Millipore, Schwalbach
Minisart® sterile filter 0.1 /0.2 µm	Sartorius, Aubagne, France
Lab-Tek™ chamber slides	Nunc Thermo Fisher Scientific, Rockford, IL, USA
Pasteur pipette glass 120 mm	Hirschmann Laborgeräte, Eberstadt
Sterile syringe and injection needles	Braun, Melsungen

4.9 Chemicals

Acetone	Carl Roth, Karlsruhe
Ammonium persulfate (APS)	Carl Roth, Karlsruhe
Ampicillin	Sigma-Aldrich, St.Louis, USA
Arginine	Sigma-Aldrich, St.Louis, USA
Asparagine	Sigma-Aldrich, St.Louis, USA
Bacto™ Agar	Becton Dickinson BD, Heidelberg
Bacto™ Tryptone	Becton Dickinson BD, Heidelberg
Bacto™ Yeast Extract	Becton Dickinson BD, Heidelberg
Bovine Serum Albumin (BSA) purity ≥ 98%	Sigma-Aldrich, St.Louis, USA
BSA purity 95%	Sigma-Aldrich, St.Louis, USA
Brij V98	Sigma-Aldrich, St.Louis, USA
Bromophenol blue	Sigma-Aldrich, St.Louis, USA

(3',3",5',5"-tetrabromophenolsulfonphthalein)	
$CaCl_2$	Sigma-Aldrich, St.Louis, USA
DAPI (4',6-diamidino-2-phenylindole)	Invitrogen Gibco, Carlsbad, USA
D-MEM	Invitrogen Gibco, Carlsbad, USA
DMSO	Carl Roth, Karlsruhe
DMSO (cell culture)	Sigma-Aldrich, St.Louis, USA
DNA-ladder 1 kb peqGOLD	PeqLab, Erlangen
EDTA	Biochrom AG, Berlin
EDTA (cell culture)	Biochrom AG, Berlin
Ethanol 99.9% (v/v)	Merck, Darmstadt
Ethidium bromide	CarlRoth, Karlsruhe
FCS	Invitrogen Gibco, Carlsbad, USA
Geneticin® G 418 Sulphate Gentamycin	Invitrogen Gibco, Carlsbad, USA
Glycerol	CarlRoth, Karlsruhe
HEPES (4-(2-hydroxyethyl)-1-piperazineethanesulfonic acid)	CarlRoth, Karlsruhe
HEPES 1M (cell culture)	Invitrogen Gibco, Carlsbad, USA
Isopropanol	Merck, Darmstadt
KCl	CarlRoth, Karlsruhe
KH_2PO_4	CarlRoth, Karlsruhe
Lipofectin® Reagent	Invitrogen Gibco, Carlsbad, USA
Methanol	CarlRoth, Karlsruhe
2-Mercaptoethanol	Sigma-Aldrich, St.Louis, USA
$MgCl_2$	Sigma-Aldrich, St.Louis, USA
$MnCl_2$	Sigma-Aldrich, St.Louis, USA
MTT (3-(4,5-Dimethylthiazol-2-yl)-2,5-diphenyltetrazolium bromide)	Sigma-Aldrich, St.Louis, USA
NaCl	CarlRoth, Karlsruhe
NaF	CarlRoth, Karlsruhe
Na_2HPO_4	CarlRoth, Karlsruhe
PBS	Invitrogen Gibco, Carlsbad, USA
Paraformaldehyde (PFA)	Serva, Heidelberg
Protease inhibitor cocktail (Complete, EDTA free)	Roche Diagnostics GmbH, Mannheim
Rotiphorese 40	CarlRoth, Karlsruhe

Sodium dodecyl sulphate (SDS) Pellets	CarlRoth, Karlsruhe
TEMED	Merck, Darmstadt
(N,N,N',N', Tetramethylethylendiamin)	
Thiazolyl blue tertazolium bromide (MTT)	Sigma-Aldrich, St.Louis, USA
Triton® X-100	Sigma-Aldrich, St.Louis, USA
Tris-Ultra Pure	CarlRoth, Karlsruhe
Trypsin	Invitrogen Gibco, Carlsbad, USA
Trypan Blue Solution 0.4 % (w/v)	Sigma-Aldrich, St.Louis, USA
Tween®-20	Applichem, Gatersleben
Universal Agarose peqGOLD	PeqLab, Erlangen

4.10 Buffers

Application buffer for SDS-PAGE:

non-reducing conditions:

Tris/HCl pH 6.8	90 mM
SDS	7% (w/v)
Glycerol	30% (v/v)
Bromophenol blue	0.01% (w/v)

reducing conditions, add:

2-mercaptoethanol	20% (v/v)

Blocking solution for Western Blot:

5% Milk powder in 1x PBST

Cell lysis buffer for whole cell lysates:

HEPES, pH 7.5	50 mM
NaCl	150 mM
EDTA	1 mM
Glycerol	10% (v/v)
Triton-X-100	1% (v/v)
Complete™ proteases inhibitor cocktail	0.1% (w/v)

Cell lysis buffer for coimmunoprecipitation:

HEPES, pH 7.5	25 mM
NaCl	150 mM
NaF	1mM
$MgCl_2$	1mM
Brij V98	1% (v/v)
Complete^{TM} proteases inhibitor	0.1% (w/v)

DNA loading buffer for agarose gel electrophoresis:

Glycerol	50%
Bromophenol blue	0.05%

Solution in 1x TAE (Tris base, acidic acid, EDTA buffer-see below)

Electrophoresis buffer for SDS-PAGE:

Glycine	1.6 M
Tris	250 mM
SDS	1% (w/v)

PBS 10x (pH 7.4):

NaCl	1.37 M
KCl	26.8 mM
KH_2PO_4	14.7 mM
Na_2HPO_4	71.8 mM

for PBST: 1x PBS, 1% (v/v) Tween-20

PFA solution for cell fixation:

Solution A	0.1 M Na_2HPO_4
Solution B	0.1 M NaH_2PO_4
AB	adjust solution A with solution B to pH 7.4

dissolve 4% (w/v) PFA in solution AB by heating to ~80°C

Stripping solution for Western blot membranes:

Glycine	160 mM
SDS	0.1% (v/v)
Tween-20	1% (v/v)
adjust to pH 2.2	

TAE (Tris, acidic acid, EDTA) running buffer for agarose gel electrophoresis:

Tris-Acetate	40 mM
EDTA, pH 8.0	1 mM

TBS (Tris-buffered saline) 10x (pH 7.4):

NaCl	1 M
Tris	100 mM

Wet-blot buffer for blotting of Western blot membranes:

Tris	25 mM
Glycine	192 mM
Methanol	20% (v/v)

4.11 Kits

BCA™ Protein Determination Assay	Thermo Fisher Scientific, Rockford, IL, USA
DNA High Pure PCR Template Preparation Kit	Roche Diagnostics GmbH, Mannheim
Mycoplasma decontamination antibiotics for cell culture	Applichem, Gatersleben
NucleoBond® AX DNA Isolation	Macherey-Nagel, Düren
NucleoSpin® Plasmid DNA Isolation	Macherey-Nagel, Düren
NucleoSpin® Extract	Macherey-Nagel, Düren
Pierce ECL Western Blotting Substrate	Thermo Fisher Scientific, Rockford, IL, USA
QuikChange™ in vitro site-directed Mutagenesis	Invitrogen Gibco, Carlsbad, USA

5 Methods

Common molecular biological techniques like preparation of competent cells (*e.coli*), DNA cloning, DNA restriction, agarose-gel electrophoresis and preparation of plasmid DNA were performed according to methods published by Sambrook et al. 1989 and manufacturers' recommendations.

5.1 Cell culture

5.1.1 Cultivation of the human ovarian cancer cell line OV-MZ-6

Cell cultivation and cell splitting:

The origin and cultivation of human ovarian OV-MZ-6 cancer cells has previously been described (Möbus et al. 1992). Generally, cells were cultivated at 37°C, 5% (v/v) CO_2 in a water saturated atmosphere. Cells were passed into new cell culture flasks every 3-4 days. For this, adherent OV-MZ-6 cells were detached from the growth area of the cell culture flask by incubation in PBS, 0.02 % (v/v) EDTA at 37°C for 2 to 5 min. Cells were washed down from the flask with 5 ml PBS, transferred into 10 ml Falcon tubes and spun down at 246 x g for 3 min. After aspiration of the supernatant, cells were resuspended in growth medium and an appropriate portion was passed into a new cell culture flask.

Cryoconservation of cells:

For cryoconservation, cells were detached from the culture flasks by incubation in PBS, 0.02 % (v/v) EDTA at 37°C for 2 to 5 min, washed in 5 ml PBS and spun down. PBS was aspirated and cells resuspended in freezing medium containing FCS and DMSO (see material 4.3). Cells were quickly transferred into cryogenic tubes and incubated on ice before storage. Frozen OV-MZ-6 ovarian cancer cells stocks were long-term stored in fluid nitrogen at -196°C or temporarily at -80°C. For cultivation, they were slowly thawed and washed in 5 ml of ice cold cell culture medium. After centrifugation at 246 x g for 3 min, cells were resuspended in growth medium and passed into small cell culture flasks. Prior to experimental usage and after thawing, cells were at least once passed into a new cell culture flask.

5.1.2 Stable cell transfection and isolation of individual cell clones

For stable transfection, human ovarian cancer cells OV-MZ-6 were seeded on cell culture dishes (Ø 10 cm) one day prior to transfection, to reach a confluency of approximately 70%. Cells were washed once at the day of transfection in PBS and recovered with growth arrest cell culture medium free of FCS and additive amino acids (GAM). Stable transfection of OV-MZ-6 cells was performed upon usage of lipofectin. For this, 17 µl of lipofectin were preincubated with 100 µl GAM for 45 min at room temperature (RT). 15 µg of DNA were dissolved in 100 µl GAM and mingled with the lipofectin/GAM mixture. After 15 min of incubation at RT, the DNA/ lipofectin solution was dropped onto cell monolayers and incubated for 6 h at 37°C. Transfection medium was carefully aspirated and cells immediately recovered with cell culture growth medium. Successful transfection of cells with vector pCDNA 3.1/myc-His endowed the cells with an antibiotic resistance to Geneticin G418. Selection of stably transfected OV-MZ-6 cells was performed by inclusion of G418 into the cell culture medium at a concentration of 1g/l (Hapke et al. 2001). The selection process started on the 3rd day after transfection and was completed after about 10 days.

Isolation of single transfected cell clones was conducted by limited dilution. For this, a highly diluted cell suspension was seeded on cell culture dishes, allowing single cells to grow and form small colonies. Single colonies were picked and transferred into 96-well plates for further growth. Expression of integrin αvβ3 and mutants thereof was checked with immuncytochemical staining and FACS analysis (see Methods 5.5.1 and 5.6.2). The selection process was repeated for at least three cloning rounds.

5.1.3 Detection of mycoplasma contamination

Mycoplasma are small bacteria (0.2-2 µm) without cell walls. They mainly derive from humans (*mycoplasma orali*) and can infect cell cultures. This results in severe effects on cellular physiology and metabolism (Rottem et al. 1993). In order to avoid cell culture contamination, a regular screening for mycoplasma infection by PCR was performed. For this, total cellular DNA was obtained by using the DNA High Pure PCR Template Preparation Kit by Roche Diagnostics according to the manufactures'

recommendations. The PCR reaction, including a positive and a negative control, was performed in a 50 µl reaction volume in aqueous solution. PCR products were analysed by agarose gel electrophoresis. Amplified mycoplasma-DNA PCR product was detected at 500 bp.

Forward and reverse primer-sequence:

5'
5'- CGC CTG AGT AGT ACG TTC GC- 3'

3'
5'- GCG GTG TGT ACA AGA CCC GA- 3'

Protocol:

10x PCR reaction buffer	5 µl
dNTPs	0.15 mM
3' Primer	1.2 µM
5' Primer	1.2 µM
DNA template	1 µg
Taq polymerase	1 unit

PCR cycles:

94°C	5'		1x
94°C		30''	
60°C		1'	30x
72°C		30''	
72°C	5'		1x

5.2 Measurement of cellular adhesion

5.2.1 Impedance measurement

In order to determine cellular adhesive strength and cell spreading within the first 30 min after cell seeding, the microelectronic real time-cell electronic sensor system (*xCelligence system*™, Roche Diagnostics Corporation, Indianapolis, USA) was

used. The presence of cells on top of the E-plate electrodes affects the local ionic environment at the electrode/solution interface, correlating with an increase in electrode impedance that also depends on the quality of cell interaction with the electrodes. The electronic sensors provide a continuous and quantitative measurement of the cell index (C_I) that depends on the number of attached cells and the shape of the cells in each well. Cells were seeded onto the surface of either VN-coated or non-pretreated cell growth surfaces at a cell density of 15,000 cells per well in 150 µl DMEM containing 1% FCS. Total electrode impedance was recorded over time, resulting in a cell index number (C_I = ($impedance_{tx}$ - $impedance_{to}$)/15Ω) as measure of cell adhesion and spreading.

5.2.2 Atomic force microscopy

In the present work, binding events and forces between a VN-coated cantilever and cells, transfected with integrin αvβ3 and mutants thereof, were measured by atomic force microscopy (AFM). The basic principle of AFM is scanning a surface (e.g. cells) with a flexible cantilever, which is often loaded with an interaction partner. Thus, forces between the tip and the sample lead to a deflection of the cantilever according to Hooke's law. The cantilever is navigated by a piezoelectric scanner that facilitates accurate and precise movements by approaching onto a surface and retracting the cantilever. A laser beam is focused on the back of the cantilever and reflected towards a position-sensitive photo detector. Depending on the applied force, the cantilever deflection shifts and the position of the reflected laser beam changes. The photo detector converts the laser deflection in an electrical signal, as a measure of force between surface and cantilever (Fig. 11).

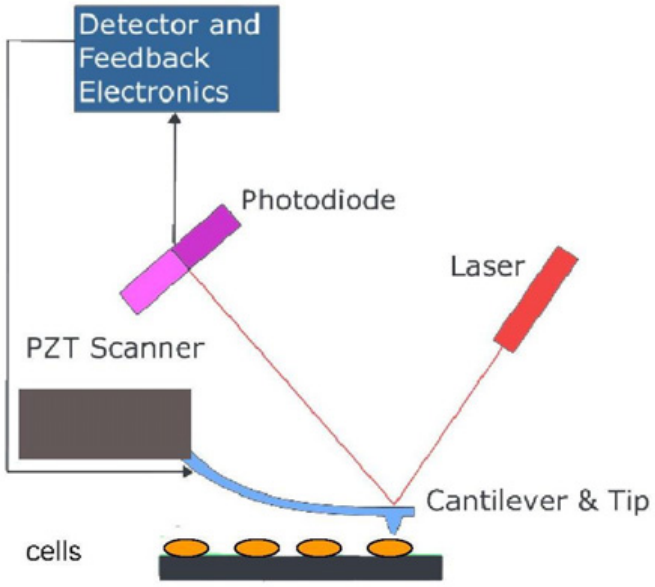

Fig. 11 Experimental set-up of an Atomic Force Microscope for measuring cell receptor/ligand forces

For measurement of forces between integrin αvβ3 and the ligand VN, a cantilever coated with VN, is approached to a single cell. Approach and retraction of the cantilever is controlled by a piezoelectric scanner. A laser beam is focused on the back of the cantilever and reflected towards a position-sensitive photo detector. Depending on the applied force, the cantilever deflection shifts and the position of the reflected laser beam changes. Laser deflection, as a result of changes in adhesive forces and disruption events, is detected by the photodiode.

All force measurements were conducted using a NanoWizard II atomic force microscope mounted on an inverted optical microscope (Axiovert 200). Silicon cantilever tips were coated with 2 µg/ml of the integrin αvβ3 ligand VN for 15 min at RT. The spring constants of the cantilevers were determined via thermal noise calibration at 16 ± 12 mN/m. Cells were allowed to attach to poly-L-lysine (PL)-coated cover slips (10 µg/ml v/v in PBS), put into 6-well cell culture plates for 24 h prior to AFM, at a cell density that allows single cell measurements. Cells were then washed in PBS in order to remove cell culture medium, followed by incubation in PBS, 1 mM $CaCl_2$, and 1 mM $MgCl_2$, at 37°C within a BioCell sample holder. During the AFM experiments, the approach and retract velocity was held constant at 4 µm/s. In order to obtain single binding events, the cantilever was moved towards cell surfaces with an applied force of 0.5 nN; the contact force was held for 100 ms. Subsequently, the cantilever was retracted at the same speed and the de-adhesion force of the integrin

αvβ3/VN-interaction recorded as a function of distance. The approach/retract-cycle was repeated for at least 200 times per cell within 2 h, with at least 10 cells measured per integrin αvβ3-transfection category. Control experiments were conducted by competition of VN-binding to integrin αvβ3 with the mAb LM609, raised to the binding site of integrin αvβ3. For these blocking experiments, mAb LM609 was added at a concentration of 2 µg/ml, 30 min at RT prior to measuring. The obtained force/distance-curves were analysed focussing on the work of de-adhesion (i.e. the area included by each curve), the peak force during de-adhesion (i.e. the global maximum force of each curve) and the number, height, and position of steps in the obtained force-distance curves (Fig. 12). The steps were found by selecting the peaks in the first derivative of the force. This was accomplished by using software written by Jan Opfer (Jan Opfer & Kay Gottschalk, unpublished data).

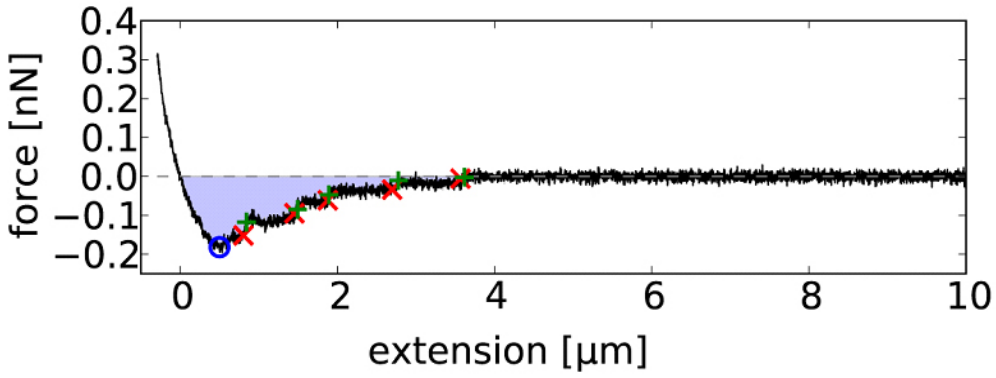

Fig. 12 Example of a typical AFM force/ distance curve

The obtained force/distance-curves from measuring live cell adhesion forces were analysed focussing on the work of de-adhesion (i.e. the area included by each curve, blue), the peak force during de-adhesion (i.e. the global maximum force of each curve, marked by blue circle) and the number, height, and position of steps (red crosses). For data evaluation, the steps were found by selecting the peaks in the first derivative of the force.

5.2.3 Spinning disc

In addition, adhesion force measurements were performed by utilising a spinning disc device, developed and described by David Boettiger and coworkers (Garcia et al. 1997) (Fig. 13). In principle, the spinning disc displays a centrifugation assay, where hydrodynamic shear is applied to cells adhering to a particular ligand. Upon centrifugation, shear forces, required to detach the cells, are distributed over the cell

surface and the shear stress is a linear function of radial distance of an individual cell on the spinning disc device from the axis of rotation. The assay allows to determine the mean shear stress required for cell detachment of one cell population adhering to a ligand coated disc. Experimental data were evaluated as precisely described before (Boettiger 2007).

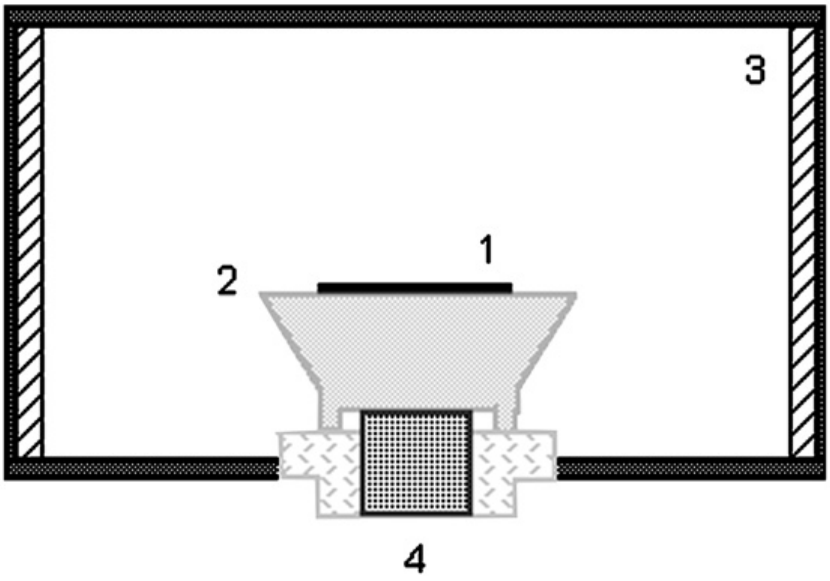

Fig. 13 Experimental set-up of a spinning disc device

Cells are seeded on VN pretreated cover slips and shear stress (4000 rpm) is applied after 20, 40, 60 and 90 min of adhesion time. After spinning, cells remaining on the cover slip are counted and evaluated as described (Boettiger 2007). Shear stress (τ50) is calculated and plotted as a function of time. 1) glass coverslip with attached cells; 2) spinning disc; 3) baffled fluid chamber; 4) shaft connected to motor (Figure modified from Garcia et al. 1998).

For the experiment, OV-MZ-6 cells expressing integrin TMD-αvβ3, TMD-GpA, and TMD-GpA-I, respectively, were harvested from cell monolayers at a confluency of approximately 60%. 300000 cells were seeded onto cover slips (Ø 2.5 cm), which were pretreated with VN (2µg/ml in PBS) for 30 min at RT, followed by a blocking step in PBS, 1% (w/v) BSA. After 20, 40, 60 and 90 min time of cellular adhesion, cell-loaded cover slips were subjected to the spinning disc device at 224 x g (4000 rpm, r = 12.5 mm) for 5 min. The spinning disc device consists of an engine driven rotating pole with cells on top of the cover slip that is dipped into a fluid (in our case PBS) filled barrel. During spinning, cells are exposed to a radius-dependent shear stress (τ) that is caused by radial fluid motion over the surface of the cover slips on

the spinning disc. The shear stress for each measured radial position is given by the equation:

$\tau = 0.8\ r \sqrt{(\rho \mu \omega^3)}$

where τ represents the shear stress; r, the radial distance from the centre of rotation; ρ, the fluid density; μ, the fluid viscosity, and ω the rotational velocity in radians per minute. After the spinning step, cells were fixed in 4% (w/v) PFA, for 15 min at RT, thereafter stained with 4',6-diamidino-2-phenylindole (DAPI), and slides mounted for analysis by a Zeiss AxioScope Hal 100 microscope. By using the software *Meta Morph*® (Molecular Devices, Sunnyvale, CA, USA), cells were automatically counted at defined radial positions and normalised to the cell numbers of an average of the 5 fields located closest to the center of the disc and fit to the sigmoid equation:

$f = 1/ (a- \exp[b(\tau-c)])$

where a, represents the asymptote (0.95-1.05); c, (τ_{50}) the inflection point (= point where 50% of cells are detached); and b, the slope at the inflection point. c values (τ_{50}) of each time point were normalised to expression levels for integrin αvβ3 and the two TMD mutants, respectively, based on FACS measurements and plotted as non-linear regression curves, indicating the standard error of estimate. Data are given in dyne/cm² (1 dyne/cm² = 0.1 N/m²), this unit is mainly used for specifying pressures associated with the measurement of hydrodynamic shear stress.

5.3 Cell proliferation assay

The proliferative activity of OV-MZ-6 cells was measured by a modification of the assay format by Mosmann (Mosmann 1983). In this assay, yellow MTT reagent, a tetrazole, is added to cell monolayers of a certain cell number. In living cells it is then reduced intracellularly to purple formazan crystals by mitochondrial reductases. DMSO is added as solvent for the purple formazan crystals. Consequently, the extent of colour change is proportional to the number of living cells.

OV-MZ-6 cell transfectants were seeded in triplicates on 96-well cell culture plates, either pretreated with VN (2 µg/ml in PBS) or left non-coated. To exclude possible effects of growth factors and bovine VN on cell growth, cells were seeded in cell culture medium containing 1% FCS. Every 24 h, 2 nM MTT reagent solution was added and incubated for 2 h at 37°C. The accumulated blue formazan crystals were dissolved in 100 µl DMSO. Optical density, as a measure of living cells, was recorded at the starting point and every other 24 h at 590 nm by a SLT Spectra ELISA Reader. For normalisation of the obtained values served the optical densities of wells containing only cell culture medium, MTT reagent, and DMSO. These were measured at each individual time point and subtracted from the obtained values.

5.4 Cell migration assay

The cellular migrative capacity was evaluated by wound scratch assays. When wounded or scratched, cell monolayers are starting to repopulate the scratch wound again. Cells polarise towards the wound, initiate protrusions and migrate into the gap. Progression of these events can be observed by imaging the size of the scratch at distinct time points between 2 and 48 h.

For wound scratch assays, cells were passed to 12-well cell culture dishes either pretreated with VN or left uncoated. After cell monolayers reached a confluency of approximately 90%, in order to generate a homogeneous wound into cell monolayers, a scratch was set by using a sterile pipette tip. Directly after wounding, detached cells caused by the procedure were removed by five to ten extensive washes in PBS. Microscopical images of cell monolayers were taken immediately after wounding and after 24 h of further incubation. Cells invading the gap were manually counted by using the marking-function of the computer programme *Photoshop*.

5.5 Immunocytochemical staining

5.5.1 Detection of integrin αvβ3

Human ovarian OV-MZ-6 cancer cells were cultivated ON in cell culture microchamber slides, which had been pretreated with FN (5 µg/ml PBS) for 30 min at RT. Cells were fixed in 4% (w/v) PFA for 15 min at RT, washed in PBS, and blocked in PBS, 2% (w/v) BSA, for 30 min at RT. Monoclonal Ab directed to integrin αvβ3 or the individual subunits αv, and β3, respectively, were incubated with the cells for 1.5 h at RT followed by secondary Alexa 488-labeled goat-anti-mouse IgG for 45 min at RT. Slides were mounted in PBS and fluorescence intensity determined by confocal laser-scanning microscopy (CLSM). In order to convert fluorescence staining intensity into colours of a glow scale, the look-up table “glowOv/Un LUT” provided with the CLSM scanning software was applied: low intensity (red), medium intensity (yellow), and high intensity (white) (Beck et al. 2005; Lössner et al. 2008). Staining procedures in the absence of any Ab as measure of cell autofluorescence or in the presence of the secondary Alexa-488-labeled IgG alone served as controls and did not result in noticable fluorescence signals (data not shown).

5.5.2 Detection of FAK/ phosphorylated FAK (Y397)

OV-MZ-6 cells were cultivated in VN-coated (2 µg/ml) cell culture microchamber slides for 24 h, subsequently fixed in 4% (w/v) PFA, and permeabilised in PBS, 0.025% (w/v) saponin for 5 min at RT. After washes in PBS, cells were blocked in PBS, 2% (w/v) BSA, for 30 min at RT and then incubated with mAb directed to FAK or p-FAK (Y397), for 1.5 h at RT, followed by the addition of secondary Alexa 488-labeled goat-anti-mouse IgG for 45 min at RT. Fluorescence intensity was evaluated by CLSM as described before.

5.5.3 Double immunocytochemical staining of integrin αvβ3 with phosphorylated paxillin (Y118) and talin

Human OV-MZ-6 cells were cultivated in cell culture microchamber slides overnight, subsequently fixed in 4% (w/v) PFA, and permeabilised in PBS, 0.025% (w/v) saponin for 5 min at RT. Alternatively, cells were fixed with methanol/ acetone 1:1 for 5 min at -20°C. After washes in PBS and a blocking step in PBS, 2% (w/v) BSA, cells were simultaneously incubated with the respective primary Ab for 1.5 h at RT. Binding of Ab directed to p-paxillin (Y118) or talin, respectively, was detected by secondary Alexa 488-goat-anti-rabbit IgG (green) and mAb # 23C6 directed to integrin αvβ3 was detected by Alexa 568-conjugated goat-anti-mouse IgG (red) for 45 min at RT. Colocalisation of the stained proteins in merged pictures is depicted in "yellow". Double stains were visualised by an AxioImager (Zeiss).

5.6 Flow cytofluorometry

5.6.1 Principle of fluorescence activated cell sorting

Fluorescence activated cell sorting (FACS) is used for examining different cell characteristics by passing them through an electronic detection apparatus. Here, a beam of laser light of a single wavelength is focused onto a stream of fluid carrying single cells of interest. Different detectors are aimed at the point where the stream passes through the light beam:

→ one in line with the light beam: forward scatter (FSC) = size of cell
→ and several perpendicular to it: side scatter (SSC) = granularity of cell (e.g. shape of the nucleus, the amount and type of cytoplasmic granules or the membrane roughness) and one or more fluorescent detectors

Each suspended particle/cell, varying in size from 0.2 to 150 micrometers, passes through the beam scatters the light in a specific way. Fluorescence-conjugated antibodies, which are located in the cell or attached to cell surface, according to the antigen targeted, may be excited into emitting light at a longer wavelength than the light source. This combination of scattered and fluorescent light is picked up by the

detectors. By analysing fluctuations in brightness at each detector it is then possible to derive information about cell shape or morphology and the fluorescence intensity emitted through antibodies, bound to a certain antigen of interest.

5.6.2 Detection of integrin αvβ3

Cells were grown in T25 cell culture flasks and harvested after 2-4 days of cultivation. In order to prevent unspecific binding, cells were blocked in PBS, 2% (w/v) BSA in the presence of 1 mM Ca^{2+} ($CaCl_2$) and 1 mM Mg^{2+} ($MgCl_2$). Immunostaining was performed on living cells, using the mAb directed to integrin αvβ3 (# 23C6) for 1h at RT, followed by detection with secondary Alexa 488-conjugated goat-anti-mouse IgG for 45 min at RT.
All experiments were performed with a FACS Calibur and data analysed by using the software *CellQuest*™ (Becton Dickinson).

5.6.3 Detection of (phosphorylated) MAPK p44/42$^{(erk-1/erk-2)}$

Cells were grown in 6-well cell culture plates and harvested after 24 h of cultivation. For detection of activated phospho-p44/42$^{(erk-1/erk-2)}$, in order to fully activate integrin αvβ3, cells were incubated with 5 mM Mn^{2+} ($MnCl_2$) for 2 h at 37°C. Cells were fixed in 4% (w/v) PFA, permeabilised in 0.025% (w/v) saponin, blocked in PBS, 2% (w/v) BSA, and stained with mAb directed to MAPK p44/42$^{(erk-1/erk-2)}$ or p-p44/42$^{(erk-1/erk-2)}$ for 1 h at RT, followed by detection with secondary Alexa 488-conjugated goat-anti-rabbit IgG for 45 min at RT.

5.6.4 Detection of (phosphorylated) PKB/Akt (Ser 473)

Cells were grown in 6-well cell culture plates and harvested after 24 h of cultivation. For detection of activated phospho-PKB/Akt, cells were incubated with 5 mM Mn^{2+} ($MnCl_2$) for distinct time points at 37°C and subsequently fixed in PBS, 4% (w/v) PFA, permeabilised in 0.025% (w/v) saponin, and blocked in PBS, 2% (w/v) BSA. For immunostaining, cells were incubated with mAb directed to PKB/Akt or p-PKB/Akt

(S473) for 1 h at RT, followed by detection with secondary Alexa 488-labeled goat-anti-rabbit IgG for 45 min at RT.

5.7 Western blot analysis

Detection of cellular antigens in cell lysates was performed by Western blot. For the preparation of cell lysates containing total protein, vector- and integrin αvβ3-transfected human OV-MZ-6 cells were passed to 6 well cell culture plates, which were either pretreated with VN (2 µg/ml in PBS, 1 h at RT) or left uncoated. After 1.5 h, 3 h, or 6 h, cells were lysed in 150 µl lysis buffer for whole cell lysates (see material 4.10). Cell lysates were cleared by centrifugation and total protein content determined using the BCA™ Protein Assay Kit according to the manufactures recommendations. At least 20 µg total protein of each lysate were applied to sodium dodecyl sulphate polyacrylamide gel electrophoresis (SDS-PAGE). Proteins were transferred onto PVDF membranes using a wet blotting device in wet blot buffer (see material 4.10). Membranes were blocked in PBS, 5% (w/v) milk powder, and 1% (v/v) tween-20 at 4°C overnight. After incubation with the respective mAb (FAK/p-FAK [Y397], p44/42$^{(erk-1/erk-2)}$/p-p44/42$^{(erk-1/erk-2)}$, PKB/Akt and p-PKB/Akt [Ser 473]) and addition of horse radish peroxidase-conjugated anti-rabbit (PKB/Akt, MAPK) or anti-mouse IgG (FAK), proteins were visualised by using the ECL^{TM} chemiluminescent substrate according to the manufacturers´ recommendations. In order to normalise differences in protein loading and blotting efficiency, membranes were subsequently stripped and reprobed with mAb directed to GAPDH. Then, band intensities of the antigens of interest were densitometrically evaluated by the software *Scion Image* and compared to the respective protein band intensity obtained for GAPDH.

5.8 Coimmunoprecipitation analysis

Colocalisation of integrin αvβ3 with cytoskeletal protein phospho-paxillin (Y118) was detected by coimmunoprecipitation (IP) analysis. For this, cells were grown on T75 cell culture flasks and harvested at a confluency of 70%. Cells were lysed in 1 ml lysis buffer (see material 4.10) over night (ON), at 4°C in order to maintain protein complexes. Lysates were cleared by centrifugation and pre-incubated with 30 µl of

protein-G-sepharose. Unspecific bound protein was spun down and protein concentration was determined. 1 mg of total protein was incubated with 5 µg of mAb # 23C6 directed to integrin αvβ3, ON at 4°C on a rotating wheel. 30 µl of protein-G-sepharose, which binds the Fc-region of IgG, was added. Bound integrin αvβ3 and all linked proteins were spun down and applied to 7.5% (w/v) SDS-PAGE. Phospho-paxillin (Y118), co-localised with integrin αvβ3, was detected by subsequent Western blot analysis. As control served IP performed in the presence of an irrelevant mouse control IgG 2b.

5.9 Cultivation and transformation of bacteria

Cultivation of *E.coli*:

Bacteria were cultivated in LB-medium in agitated flasks or on LB-agar plates at 37°C. Transformation of bacteria with pCDNA3.1/myc-His endowed the cells with antibiotic resistance to ampicillin. For the selection process of transformed bacterial cell clones, 0.1 mg/ml ampicillin was added to the LB-medium.

Transformation of *E.coli*:

100 µl of competent XL-1 blue/ SURE cells were incubated with either 10 µl of in vitro site-directed mutagenesis PCR product after digestion with DpnI or 1 µl of prepared plasmid DNA, for 20 min on ice. This was followed by a heat shock at 42°C for 45 s. The bacteria were chilled for 2 min on ice and afterwards incubated in 1 ml LB-medium, for 1 h at 37°C. The bacteria were spun down at 5000 x g, for 5 min at RT, and resuspended pellets plated on LB-agar containing ampicillin, ON at 37°C. After at least 12 h of incubation, single cell clones were picked and grown in 2 ml LB-medium containing ampicillin, ON at 37°C. The following day, DNA preparation was conducted according to the manufacturers' recommendations.

5.10 Mutation of integrin αv- and β3-sequence

5.10.1 In vitro site-directed mutagenesis

The sequences of the cDNA encoding the integrin αv- and β3-subunit, respectively, cloned into the vector pCDNA 3.1/myc-His were mutated by in vitro site-directed mutagenesis. This work was accomplished by Lilli Anne Volkhardt and Leonora Brunie and the plasmids expressing the mutated integrin αv- and β3-subunits were kindly provided by them for the present study. For the mutagenesis PCR, oligonucleotid primers containing the desired mutation were used in a PCR reaction by adding Pfu-Turbo polymerase without proofreading capability (Invitrogen, San Diego, USA). Extention and incorporation of the mutagenic primers resulted in nicked, circular, new DNA strands. The non-mutated, methylated parental DNA template was digested by the methylation-sensitive restriction enzyme DpnI. Competent *e.coli* (XL-1 blue or SURE) were transformed with the nicked dsDNA. After transformation the competent cells repaired the nicks in the mutated plasmid-DNA, thus adopting the desired mutation in the DNA.

5.10.2 Exchange of integrin αvβ3 transmembrane domain

Exchange of the complete integrin αv- and β3-TMD, respectively, by the complete TMD of GpA was conducted by sequential in vitro site-directed mutagenesis utilising the QuikChange™ kit. The point mutation of αv- and β3-TMD-GpA leading to the control TMD-GpA-I was also conducted by utilising the in vitro site-directed mutagenesis QuikChange™ kit. PCR reactions were composed and PCR cycles designed according to the manufacturers' recommendations. Success of mutagenesis was verified by DNA sequencing (Fig. 14).

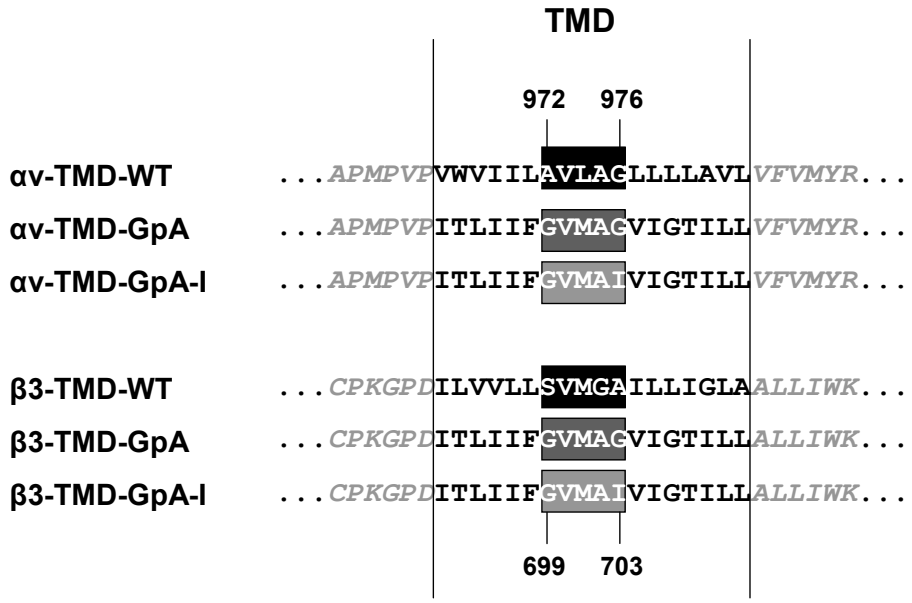

Fig. 14 Scheme of the exchange of the complete integrin αv- and β3-TMD by the GpA TMD
By in vitro site-directed mutagenesis, the complete TMD of the integrin αv- and β3-subunit was exchanged into the TMD of GpA. Moreover, a control mutation with an additional isoleucin, TMD-GpA-I was introduced .

5.10.3 Exchange of integrin αvβ3 salt bridge forming amino acids

Exchange of the integrin αv (R995) and β3 (D723) salt bridge generating amino acids, vice versa, was conducted by in vitro site-directed mutagenesis utilising the QuikChange™ kit. PCR reactions were composed and PCR cycles designed according to the manufacturers' recommendations. Success of mutagenesis was verified by DNA sequencing (Fig. 15).

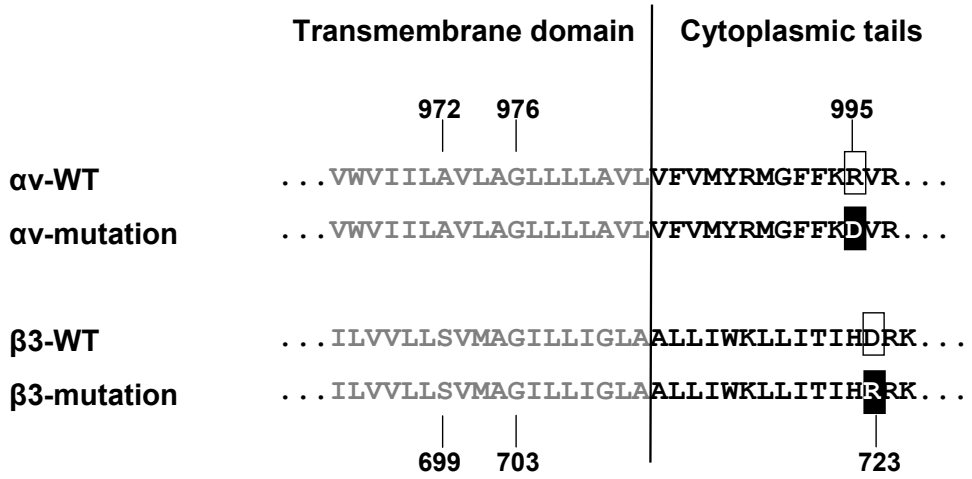

Fig. 15 Scheme of the exchange of the integrin αvβ3 salt bridge forming amino acids

By in vitro site-directed mutagenesis, the salt bridge generating amino acids of the integrin αv (R995D)- and β3 (D723R)-subunit were exchanged vice versa.

6 Results

6.1 Regulation of integrin activation by the integrin αvβ3 transmembrane domain

6.1.1 Establishment of a cellular model system transfected with integrin αvβ3 and its TMD mutants

6.1.1.1 Transfection of human ovarian cancer cells

In the present work, the human ovarian cancer cell line OV-MZ-6 was chosen as a model system. This cell line is of epithelial origin, deriving from the ascites of a patient afflicted with a cystadenocarcinoma of the ovary (Möbus et al. 1992). OV-MZ-6 ovarian cancer cells have previously been well characterised. The cell line itself expresses very low endogenous integrin αvβ3 levels. Overexpression of wild type integrin αvβ3 in OV-MZ-6 cells demonstrated, with respect to the ligand VN, its enhancing effect on cell proliferation, adhesion, migration, and signalling (Hapke et al. 2003).

Integrin αv- and β3-cDNA, cloned into the mammalian expression vector pCDNA3.1/myc-His (Hapke et al. 2001) was used for in vitro site-directed mutagenesis (see dissertations of Lilli Volkhardt and Leonora Brunie). The whole TMD of the αv- as well as the β3- integrin subunit was exchanged by the TMD of GpA, which is known to mediate strong association of α-helical TMD helices (Senes et al. 2004). An additional control mutation was introduced in both αv- and β3-integrin subunits. Here, the second G residue of the GxxxG was mutated to isoleucine (TMD-GpA-I). This mutation abrogates GpA TMD association (Lemmon et al. 1992b). OV-MZ-6 cells were stably transfected with integrin TMD-αvβ3, TMD-GpA, and TMD-GpA-I. As a control served OV-MZ-6 cells that were transfected with the empty expression vector pCDNA3.1/myc-His (vector) (Fig.16).

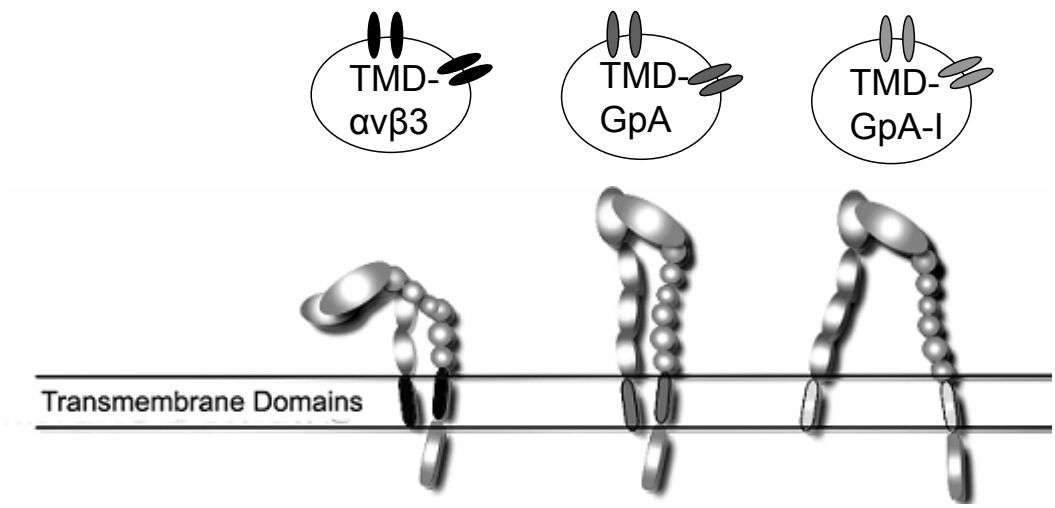

Fig. 16 Transfection of OV-MZ-6 cancer cells with integrin αvβ3 and its TMD mutants

By in vitro site-directed mutagenesis, the full length TMD of the integrin αv- and β3-subunits, respectively, were exchanged by the TMD of GpA containing a strongly dimerising GxxxG motif. An additional control mutation resulted in a motif that does not longer allow TMD association (integrin TMD-GpA-I). OV-MZ-6 cells were transfected with integrin TMD-αvβ3, TMD-GpA, and TMD-GpA-I, respectively.

6.1.1.2 Selection of stably transfected cell clones

Successful transfection of cells with pCDNA 3.1/myc-His endowed the cells with antibiotic resistance to G418. Stably transfected cell clones were isolated by limited dilutions. Integrin αvβ3 expression levels were determined after each cloning round by immunocytochemical staining and subsequent CLSM analysis. Integrin αvβ3 and its TMD mutated variants were detected as heterodimers, predominantly localised on the cell surface, by using the mAb # 23C6. Additionally, single integrin αv- and β3-subunits were detected by using the respective Ab with an Axiovert 35, Zeiss, Jena (Fig. 17). Cell surface staining of the single TMD-mutated integrin subunits proved their correct embedding in the cell membrane, despite the altered TMD. Since the receptor density largely influences cellular characteristics towards the ligand VN, cell clones expressing integrin αvβ3 and its TMD mutants to the same extent were chosen for all further studies.

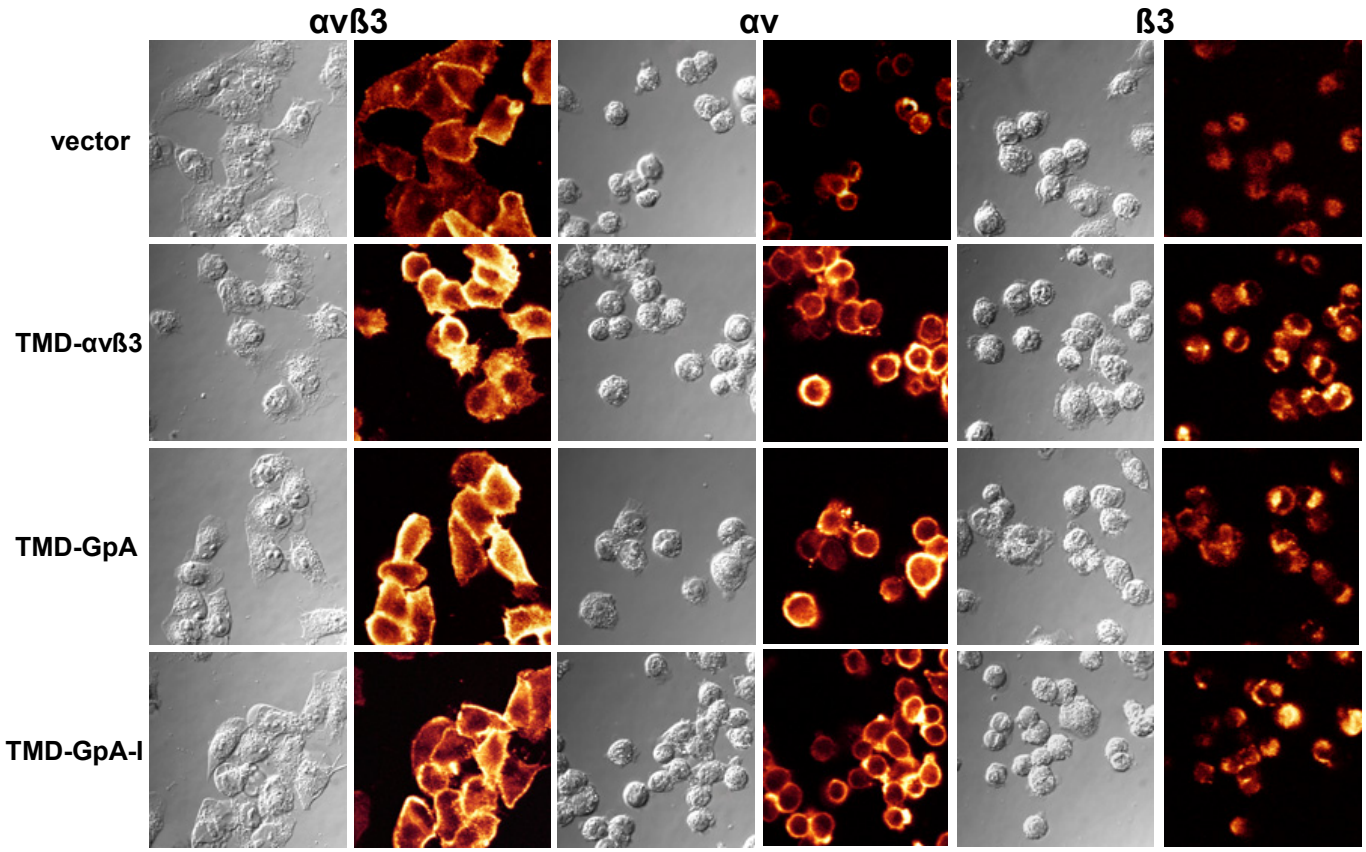

Fig. 17 Immunocytochemical detection of integrin αvβ3 expression levels of the selected cell transfectants

Human ovarian cancer cells, stably transfected with integrin TMD-αvβ3, TMD-GpA, and TMD-GpA-I were immunocytochemically stained with mAb directed to integrin αvβ3, αv or β3 as described. Representative fluorescence images together with the corresponding differential interference contrast images are depicted. The pictures demonstrate integrin αvβ3 expression on the cell surface of the cell clones, selected for further studies, in comparison to vector-transfected cells. In order to convert fluorescence staining intensity into colours of a glow scale, the look-up table glowOv/Un LUT provided with the CLSM scanning software *Scanware* (Leica, Heidelberg) was applied: low intensity (red), medium intensity (yellow), and high intensity (white).

Furthermore, expression levels of integrin αvβ3 and its TMD mutants were regularly analysed by FACS measurement. In this type of test, every cell transfectant expressed elevated levels of integrin αvβ3 and its TMD mutants, approximately 2- to 3-fold compared to vector-transfected cells (Fig. 18).

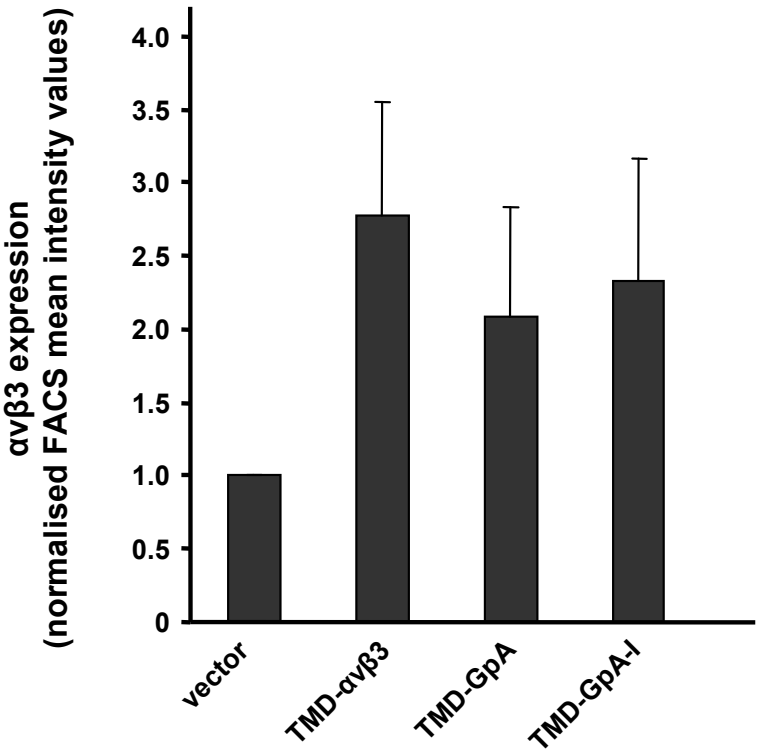

Fig. 18 Determination of integrin αvβ3 expression by FACS analysis

Expression levels of integrin αvβ3 and its TMD mutants, respectively, in stably transfected in OV-MZ-6 cells were regularly checked by FACS analysis. Normalised FACS mean fluorescence intensity values of 10 individual experiments are depicted (n=10, ±S.D.).

6.1.2 Changes in integrin αvβ3-mediated cellular signalling as a function of TMD sequence

6.1.2.1 Activation of FAK as a function of integrin αvβ3 TMD sequence

One of the most important kinases involved in integrin-mediated signalling pathways is the focal adhesion kinase (FAK), localised within focal adhesion sites. This 125-kDa non-receptor tyrosine kinase is involved in integrin-regulated cellular signalling pathways that regulate cell proliferation, survival, and migration. Differences between cells expressing the integrin αvβ3 TMD mutants regarding total expression of FAK as well as of activated and thus phosphorylated (p-)FAK (Y397) were determined. For this, cells were plated on 6-well cell culture plates and lysed after 6 h as described. Protein content was measured and 20 µg of total protein were applied onto SDS-

PAGE under reducing conditions, followed by subsequent Western blotting. Western blot membranes were probed with mAb directed to FAK and p-FAK, respectively. To detect variations in protein loading and in order to normalise blotting efficiency, membranes were stripped and reprobed with mAb raised against house keeping gene GAPDH (Fig.19A). Signal intensities of p-FAK, obtained by Western blot analysis were also normalised against intensity of the respective GAPDH band with the software *Scion Image* (Fig. 19B). No considerable differences in total FAK expression levels between the different cell transfectants were noticed. However, investigating activated and thus phosphorylated FAK, significant elevation was noticed in OV-MZ-6 cell transfectants displaying integrin TMD-GpA-I with an open TMD, which were seeded on VN coated cell culture plates. This was followed by those cells expressing integrin TMD-αvβ3. OV-MZ-6 cells displaying integrin TMD-GpA with strong TMD association expressed similar p-FAK levels like vector-transfected cells, which served as controls. Even in the absence of VN, cells displaying integrin TMD-GpA-I provoked high levels of p-FAK, which denotes for a constitutive activation of this integrin αvβ3 variant (Fig.19B).

In addition, p-FAK expression in cells adherent to VN was checked by immunocytochemical staining and subsequent evaluation by CLSM. All OV-MZ-6 cell transfectants displayed a similar and prominent FAK expression, which was located all over the cytoplasm with predominant perinuclear expression pattern. Furthermore, OV-MZ-6 cells expressing integrin TMD-GpA-I and to a smaller extent, cells displaying integrin TMD-αvβ3, showed intense clustered staining signals for p-FAK within focal adhesion sites formed onto VN. In contrast, in vector- or TMD-GpA-transfected cells, a merely weak and diffuse p-FAK staining pattern and little formation of focal adhesion contacts was noticeable (Fig. 20). Staining procedures in the presence of Alexa-488-labeled secondary Ab alone served as controls and were negative (data not shown).

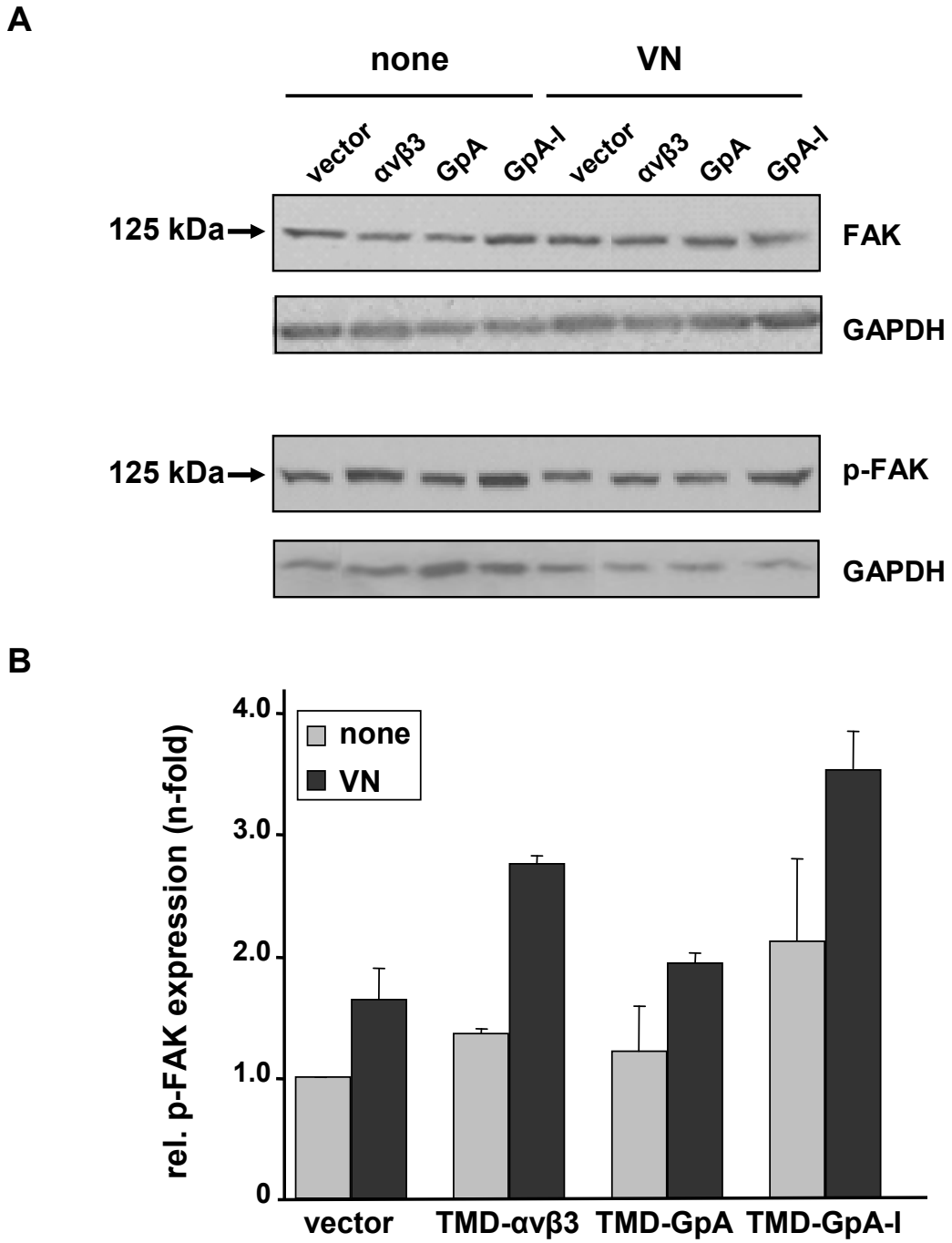

Fig.19 Determination of cellular FAK/p-FAK expression levels as a function of the integrin TMD sequence by Western blot analysis

A) Detection of FAK/p-FAK expression by Western blot analysis. Cells transfected with integrin TMD-αvβ3, TMD-GpA, TMD-GpA-I, or empty vector were cultivated in the absence (none) or presence of VN and processed for Western blot analysis as described. In order to normalise variations of protein concentrations and blotting efficiency, membranes were stripped and reprobed with mAb directed to GAPDH. A representative image of a typical Western blot analysis is depicted. **B**) Densitometrical analysis of p-FAK expression. Signal intensity of protein bands on membranes was evaluated by using the software Scion Image and normalised to the signals obtained for GAPDH. Mean values for relative p-FAK expression are given as 'n-fold' by setting the normalised signal for the respective vector-transfected cells on uncoated cell growth areas to "1" (n = 2, ± S.D.).

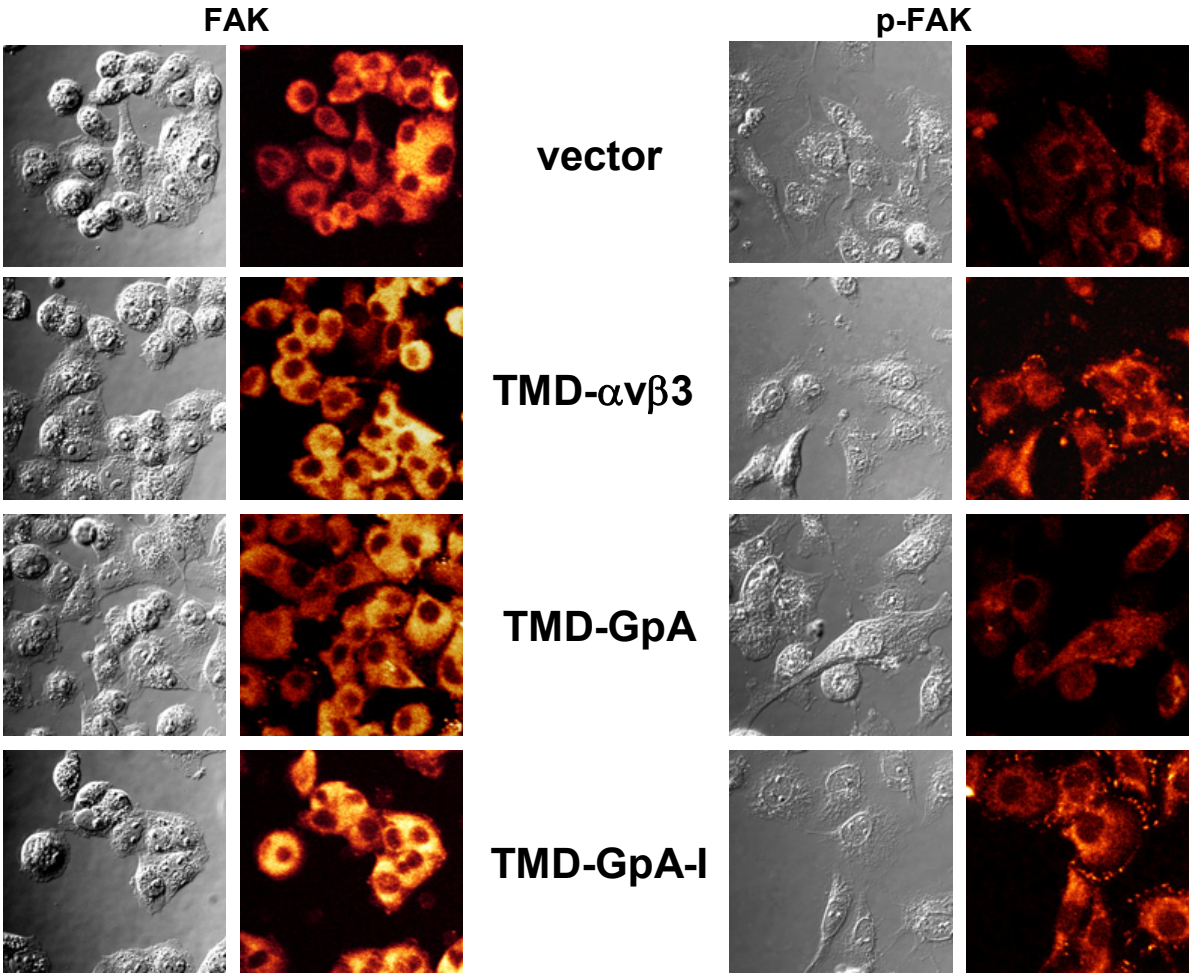

Fig. 20 Immunocytochemical detection of cellular FAK/p-FAK expression as a function of integrin αvβ3 activation

Extent of FAK/ p-FAK expression was evaluated by immunocytochemical detection. For this, all cell transfectants were grown on micro chamber slides and stained with mAb directed to (p-)FAK as described. Representative fluorescence images together with the corresponding transmission images are illustrated. Similar FAK expression was observed in all OV-MZ-6 cell transfectants. However, only cells expressing integrin TMD-GpA-I and to a smaller extent those expressing integrin TMD-αvβ3 showed intense clustered staining signals for p-FAK within focal adhesion sites.

6.1.2.2 Activation of MAPK p44/p42$^{(erk-1/erk-2)}$ as a function of integrin αvβ3 TMD sequence

Various studies report an important role of integrin signalling via the mitogen-activated protein kinase (MAPK) pathway, especially p44/p42$^{(erk-1/erk-2)}$ (Hotchin et al. 1995; Shin et al. 1999). Activation of this pathway regulates several transcription factors, leading to changes in cell proliferation, differentiation, migration, and survival. In order to determine the expression and activation status of p44/p42$^{(erk-1/erk-2)}$ as a function of the integrin αvβ3 TMD sequence, cells were seeded on 6-well cell culture plates, either pretreated with VN or left uncoated. After 6 h, cells were lysed and p44/p42$^{(erk-1/erk-2)}$ as well as phosphorylated-p44/p42$^{(erk-1/erk-2)}$ determined by Western blot analysis (Fig. 21A). To detect variations in protein loading and in order to normalise blotting efficiency, membranes were stripped and reprobed with mAb raised against GAPDH. Content of total p44/p42$^{(erk-1/erk-2)}$ did not display large variations among cells expressing the different integrin αvβ3 TMD mutants. In contrast, even in the absence of VN, cells transfected with integrin TMD-GpA-I displayed highest levels of p-p44/p42$^{(erk-1/erk-2)}$. This was followed by p-p44/p42$^{(erk-1/erk-2)}$ levels of cells expressing integrin TMD-αvβ3. Vector as well as integrin TMD-GpA transfectants displayed lowest p44/p42$^{(erk-1/erk-2)}$ activation and thus phosphorylation. Signal intensities of p-p44/p42$^{(erk-1/erk-2)}$, obtained by Western blot analysis were also normalised against intensity of the respective GAPDH band with the software *Scion Image* (Fig. 21B).

Moreover, integrin αvβ3-mediated activation of p44/p42$^{(erk-1/erk-2)}$ was evaluated by FACS measurements. For this, transfected OV-MZ-6 cells were either activated by ligand mimetic 5 mM Mn^{2+} (Bazzoni et al. 1995; Takagi et al. 2002a; Pesho et al. 2006) for 2 h at RT or left untreated. For the following flow cytofluorometrical analysis, cells were harvested and stained as described. Expression levels of phosphorylated p44/p42$^{(erk-1/erk-2)}$ of Mn^{2+}-activated cells were normalised to p-p44/p42$^{(erk-1/erk-2)}$ levels of the respective OV-MZ-6 cell transfectant incubated without Mn^{2+} (Fig. 22).

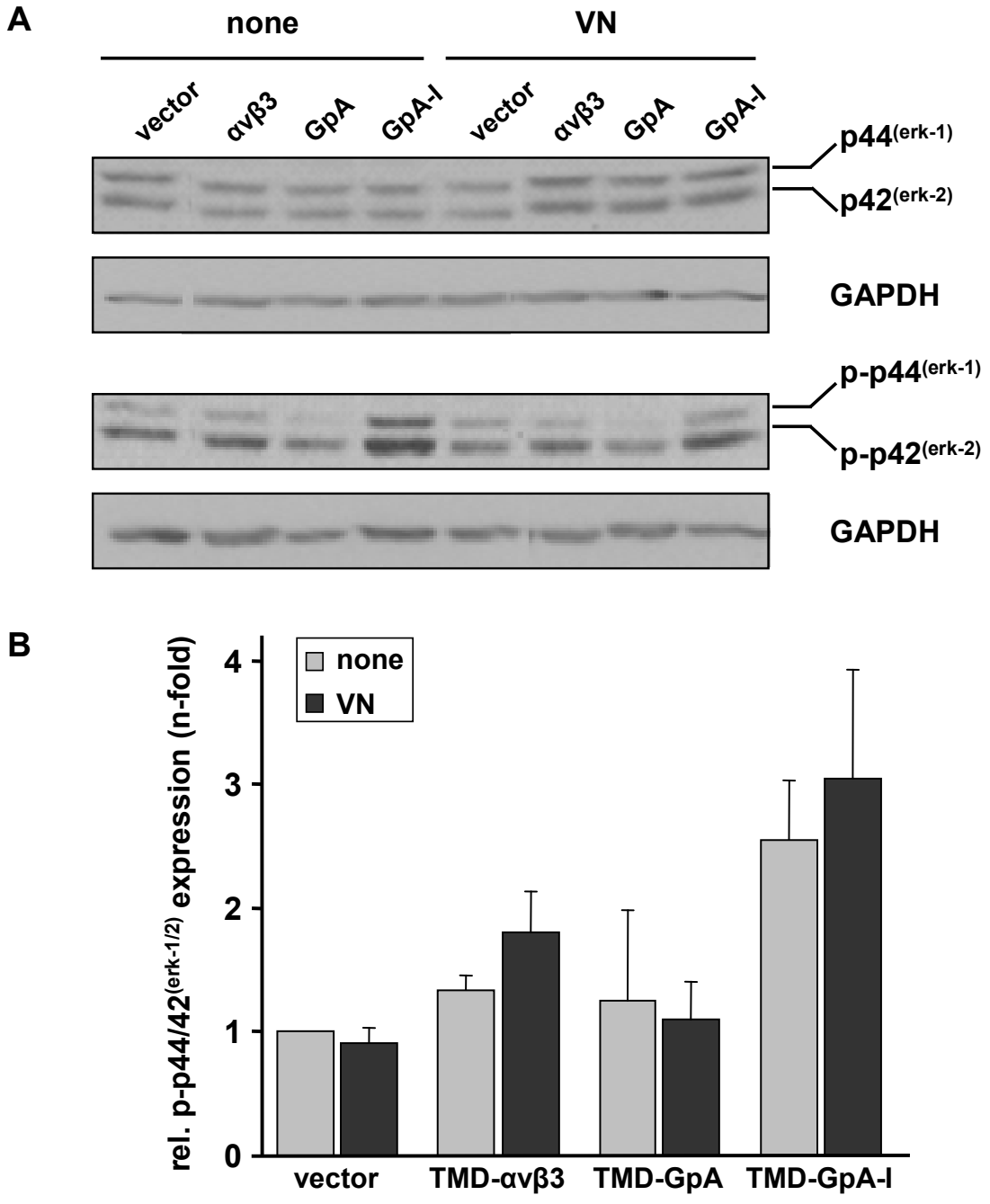

Fig. 21 Determination of cellular p44/p42$^{(erk-1/erk-2)}$/ phospho-p44/p42$^{(erk-1/erk-2)}$ expression levels as a function of the integrin TMD sequence by Western blot analysis

A) Detection of (p-)p44/42$^{(erk-1/2)}$ by Western blot analysis. Cells transfected with integrin TMD-αvβ3, TMD-GpA, TMD-GpA-I, or empty expression vector, were cultivated in the absence (none) or presence of VN and processed for Western blotting as described. A representative image of a typical Western blot is depicted. **B**) Densitometrical analysis of p-p44/42$^{(erk-1/2)}$ expression was conducted as described. Mean values for relative p-p44/42$^{(erk-1/2)}$ expression are given as 'n-fold' by setting the normalised signal for the respective vector-transfected cells grown in the absence of VN to "1" (n = 2, ± S.D.).

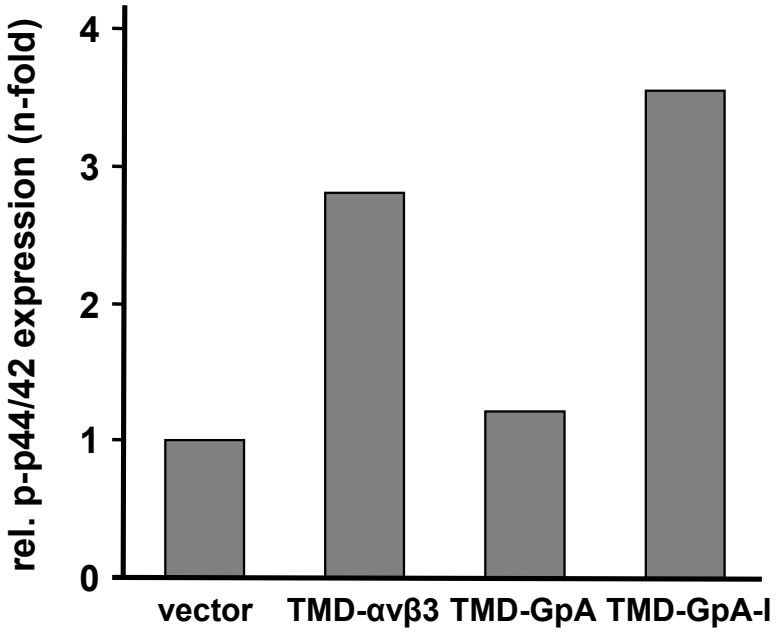

Fig. 22 Determination of activated p44/42$^{(erk-1/2)}$ expression levels by FACS analysis

Cell were grown on 6-well plates, activated by the addition of 5 mM Mn^{2+} for 2 h, and processed for FACS analysis of p-p44/42$^{(erk-1/2)}$-expression as described. FACS intensity mean channel values obtained for p-p44/42$^{(erk-1/2)}$ expression were normalised to the data obtained for respective cells incubated without Mn^{2+}. Relative p-MAPK expression is given as 'n-fold' by setting the normalised signal for vector-transfected cells to "1". One representative experiment is depicted.

6.1.2.3 Activation of PKB/Akt as a function of integrin αvβ3 TMD sequence

Another important integrin-triggered signalling pathway implies phosphorylation of PI3K that in turn phosphorylates the seronine-threonine kinase PKB/Akt (Khwaja et al. 1997). This pathway plays an important role in regulation of cell survival and metabolism by controlling downstream effectors like NF-κB or members of the Bcl-2 family (Desgrosellier et al. 2010).

For the analysis of activation and thus phosphorylation of PKB/Akt as a function of integrin αvβ3-mediated signalling, cells displaying the different integrin αvβ3 TMD mutants were seeded on 6-wells cell culture plates either pretreated with VN (2 µg/ml in PBS) or left uncoated. Cells were lysed after 1.5 h and PKB/Akt as well as p-PKB/Akt (Ser 473) expression was determined by Western blot analysis (Fig. 23A). To detect variations in protein loading and in order to normalise blotting efficiency,

membranes were stripped and reprobed using mAb directed to GAPDH. Total PKB/Akt expression levels did not show significant alterations in the different integrin αvβ3 TMD transfectants. However, even in absence of VN, cells expressing integrin TMD-GpA-I displayed highest p-PKB/Akt levels. These were followed by cells transfected with integrin TMD-αvβ3, grown on VN coated cell culture plates. Lowest p-PKB/Akt levels, comparable to those observed for vector-transfected cells, were noticed in cells expressing integrin TMD-GpA. Signal intensities of p-PKB/Akt, obtained by Western blot analysis were also normalised against intensity of the respective GAPDH band with the software *Scion Image* (Fig. 23B).

In addition, integrin αvβ3-mediated activation of PKB/Akt was evaluated by FACS analysis. For this, transfected OV-MZ-6 cells were either activated by ligand mimetic 5 mM Mn^{2+} for distinct time points at RT or left untreated. For the following flow cytofluorometrical analysis, cells were processed and stained as described. Expression levels of phosphorylated PKB/Akt of Mn^{2+}-activated cells were normalised to p-PKB/Akt levels of the respective OV-MZ-6 cell transfectant incubated without Mn^{2+} (Fig. 24).

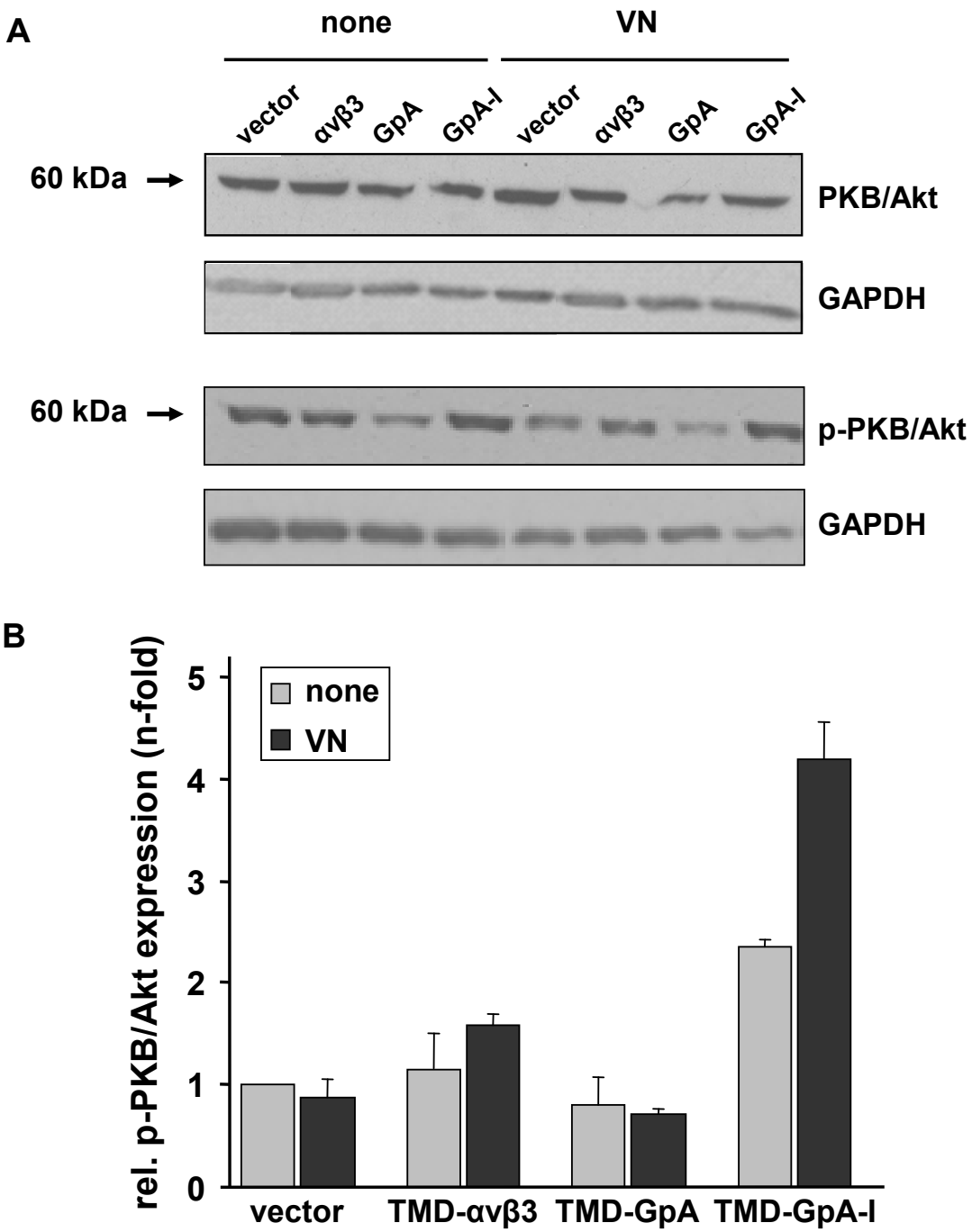

Fig.23 Determination of cellular PKB/Akt and p-PKB/Akt expression levels as a function of the integrin TMD sequence by Western blot analysis

A) Detection of (p-)PKB/Akt expression by Western blot analysis. Lysates of cells grown in the absence (none) or presence of VN were processed for Western blot analysis as described and stained with mAb directed to either PKB/Akt or p-PKB/Akt. A representative image of a typical Western blot is depicted. **B)** Densitometrical analysis of p-PKB/Akt expression. Densitometrical evaluation of protein band intensity was performed as described. Mean values for relative p-PKB/Akt expression are given as 'n-fold' by setting the normalised signal for the respective vector-transfected cells grown in the absence of VN to "1" (n = 2, ± S.D.)

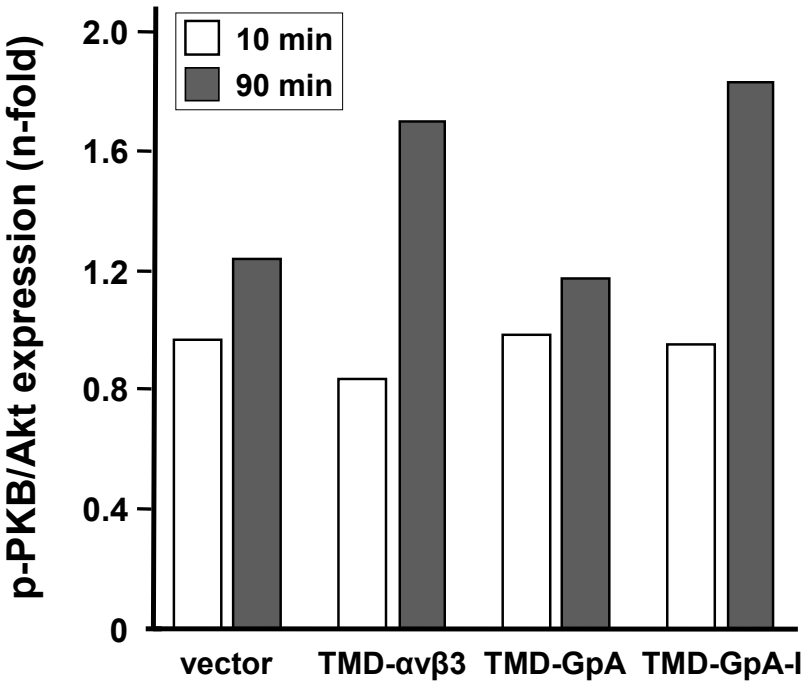

Fig. 24 Determination of activated PKB/Akt expression levels by FACS analysis

Cells were grown in the absence and presence of 5 mM Mn^{2+} (for 10 min, 90 min), and processed for FACS analysis of p-PKB/Akt expression as described. FACS intensity mean channel values obtained for p-PKB/Akt expression were normalised to the data obtained for respective cells incubated without Mn^{2+}. Relative p-PKB/Akt expression is given as 'n-fold' by setting the normalised signal for vector-transfected cells to "1". One representative experiment is depicted.

6.1.2.4 Linkage of integrin αvβ3 and its TMD mutants with cytoskeletal proteins talin and phospho-paxillin (Y118)

Talin binding to the integrin β-cytoplasmic tail is a crucial step during integrin activation (Tadokoro et al. 2003). The initiated changes of the integrin conformation are required for further downstream signalling (Anthis et al. 2009). In order to investigate colocalisation of integrin αvβ3 and its TMD mutants (TMD-GpA, TMD-GpA-I) with talin as a function of integrin activation, immunocytochemical double staining was performed as described. For this, OV-MZ-6 cells expressing integrin αvβ3 and its TMD mutants were passed to VN-coated cell culture microchamber slides and cultivated 24 h prior to the staining procedure. Cells expressing integrin TMD-GpA as well as vector-transfected control cells showed no obvious colocalisation of talin with integrin αvβ3. On the contrary, cells expressing integrin

TMD-αvβ3 and TMD-GpA-I displayed a clear colocalisation pattern, demonstrated in the merged pictures in “yellow” (Fig. 25).

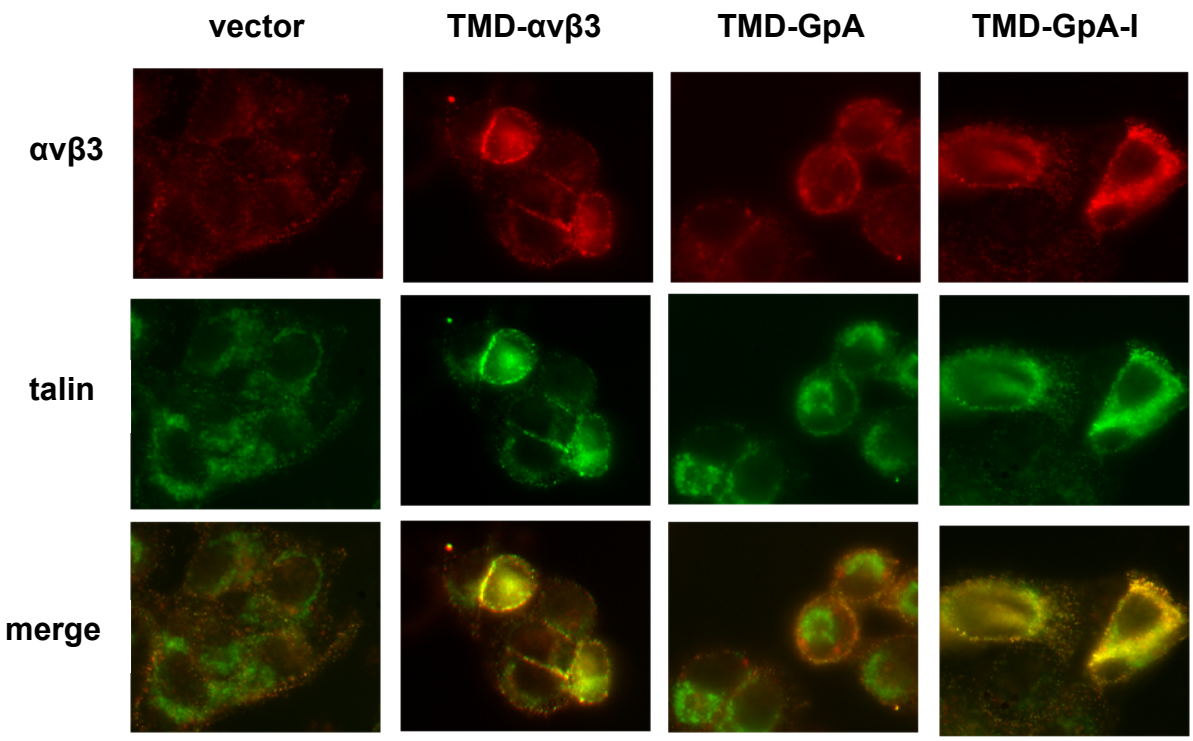

Fig. 25 Evaluation of colocalisation between integrin αvβ3 and talin as a function of the integrin TMD sequence

Colocalisation of the integrin αvβ3 TMD mutants with talin was visualised by immunocytochemical double staining and subsequent CLSM analysis. For this, cells expressing integrin αvβ3 and its TMD mutants were passed to VN-coated cell culture microchamber slides and cultivated for 24 h prior to staining procedure. In order to characterise colocalisation of integrin αvβ3 with talin, immunocytochemical double staining was performed as described. In case of integrin αvβ3, signals were detected by secondary Alexa-568-labeled goat-anti-mouse IgG, for talin, Alexa-488-labeled goat-anti-rabbit IgG served as secondary Ab. Depicted are typical and representative fluorescence images. Colocalisation of integrin αvβ3 and talin was documented by merging the two fluorescence images in “green” (488 nm, talin) and “red” (568 nm, αvβ3), indicating similar distribution patterns of both proteins within merged images in “yellow”.

Moreover, colocalisation of integrin αvβ3 and its TMD mutants (TMD-GpA, TMD-GpA-I) with the cytoskeletel protein, p-paxillin, was investigated. Paxillin is a focal adhesion associated adaptor protein, which plays a role in several signalling pathways. The protein undergoes a tyrosine phosphorylation (Y118) in response to

integrin-triggered signalling and is a marker of integrin clustering and enhanced outside-in signalling (Fuortes et al. 1994; Graham et al. 1994; Zhou et al. 2001).

Colocalisation of integrin αvβ3 and its TMD mutants with p-paxillin was visualised by immunocytochemical double staining and subsequent CLSM analysis. For this, stably transfected OV-MZ-6 cells were seeded on VN-coated cell culture microchamber slides and double stained as described. Here, colocalisation between p-paxillin and integrin αvβ3 was most apparent in cells displaying integrin TMD-GpA-I, when compared to vector-transfected cells, followed in intensity by that seen in cells expressing integrin TMD-αvβ3. No obvious colocalisation was visible in TMD-GpA-expressing as well as vector-transfected cells (Fig. 26).

In addition, in order to analyse physical association of p-paxillin (Y118) with integrin αvβ3 and its TMD mutants (TMD-GpA, TMD-GpA-I), coimmunoprecipitation analysis was carried out. For this, whole cell lysates were immunoprecipitated with mAb directed to integrin αvβ3 (# 23C6) or an irrelevant mouse IgG2b as control. Immune complexes were analysed by electrophoretical separation and subsequent Western blot analysis for the presence of p-paxillin (Y118) and the integrin β3-subunit, respectively. These analyses revealed that in cells expressing the constitutively active integrin TMD-GpA-I mutant, integrin αvβ3 immune complexes also contained p-paxillin, even in the absence of VN (Fig. 27). In case IP were carried out in the presence of an irrelevant IgG, no specific, p-paxillin-related protein bands were detectable. In order to prove band identity of p-paxillin, whole cell lysates were applied to SDS-PAGE and subsequent Western blotting without prior IP (Fig. 27).

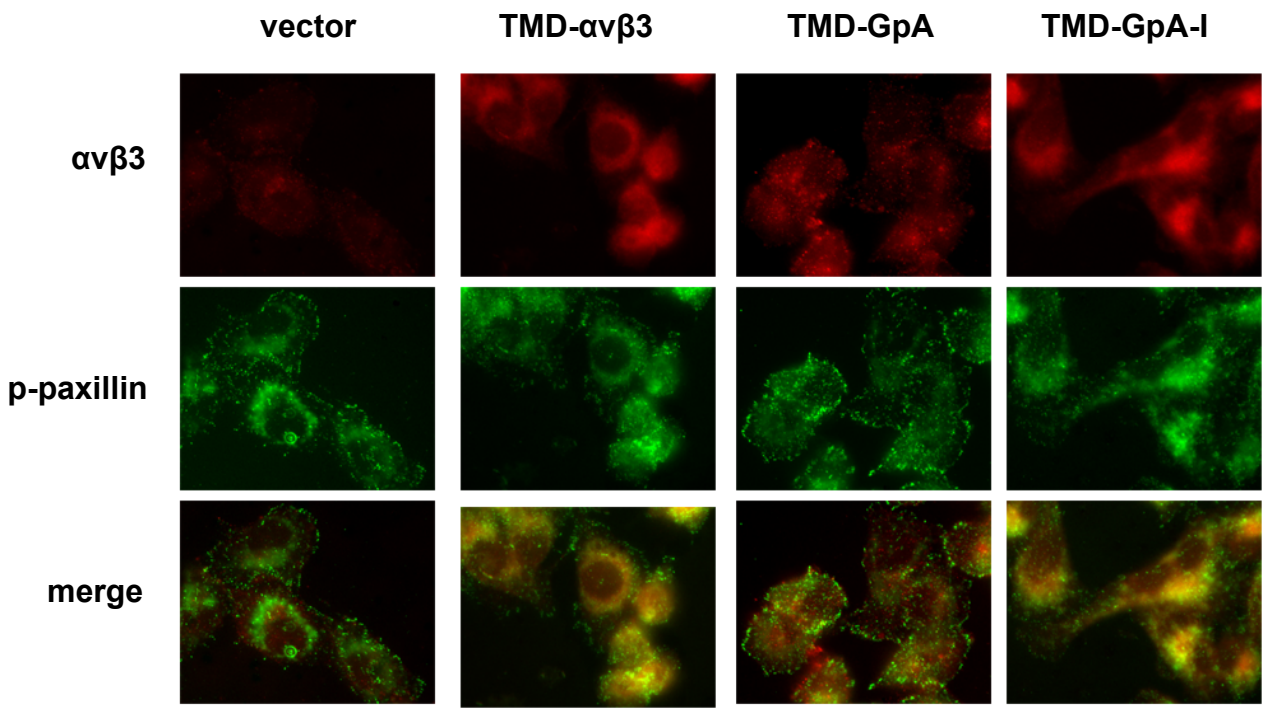

Fig. 26 Double immunocytochemical staining of integrin αvβ3, the respective TMD-mutants, and p-paxillin (Y118)

Colocalisation of the integrin αvβ3 TMD mutants with p-paxillin (Y118) was visualised by immunocytochemical staining and subsequent CLSM analysis. For this, cells expressing integrin αvβ3 and its TMD mutants were passed to VN-coated cell culture microchamber slides and cultivated for 24 h prior to staining procedure. Immunocytochemical double staining was performed as described. In case of integrin αvβ3, signals were detected by secondary Alexa-568-labeled goat-anti-mouse IgG, for p-paxillin, Alexa-488-labeled goat-anti-rabbit IgG served as secondary Ab. Depicted are typical and representative fluorescence images. Colocalisation of integrin αvβ3 and p-paxillin was documented by merging the two fluorescence images in "green" (488 nm, p-paxillin) and "red" (568 nm, αvβ3), indicating similar distribution patterns of both proteins within merged images in "yellow".

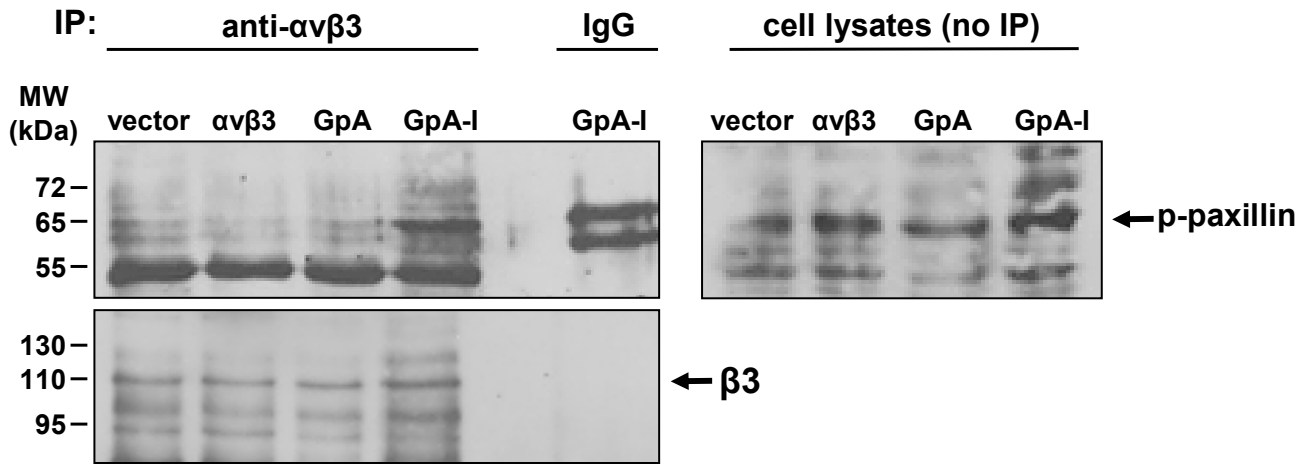

Fig. 27 Coimmunoprecipitation analysis of the integrin αvβ3 TMD mutants and p-paxillin (Y118)

Coimmunoprecipitations were conducted by incubating lysates of cells displaying integrin TMD-αvβ3 (αvβ3), TMD-GpA (GpA), or TMD-GpA-I (GpA-I) with mAb directed to integrin αvβ3 (# 23C6) ON at 4°C. After separation of immune complexes by protein G-coupled agarose beads, aliquots were applied to SDS-PAGE. Phospho-paxillin (Y118) and the integrin β3-subunit, respectively, contained within immune complexes, were analysed by subsequent Western blotting as described. As controls served IP performed in the presence of a control mouse IgG2b. Whole cell lysates, without prior IP procedure served as control for protein band identity.

6.1.3 Impact of the TMD conformation on integrin αvβ3-dependent cellular proliferation

It has been described earlier that OV-MZ-6 cells, upon elevation of integrin αvβ3 and cellular attachment to the preferred ECM ligand VN, respond with enhanced proliferative activity (Hapke et al. 2003). In order to investigate changes of integrin αvβ3-mediated proliferative activity of cells expressing integrin αvβ3 and its TMD mutants, a colorimetric MTT cell proliferation assay was performed. For this, cells were seeded in triplicates on 96-well cell culture plates, either pretreated with VN or left uncoated. MTT reagent was added every 24 h and incubated for 2 h at 37°C. The reaction was stopped by the addition of DMSO. The absorbance of generated blue formazan crystals, as a measure of living cells, was determined at 590 nm with an ELISA spectral photometer.

Within 90 h, highest proliferative activity was noted for OV-MZ-6 cells expressing integrin TMD-GpA-I in the presence of VN, followed by cells expressing integrin

TMD-αvβ3 as well as cells expressing integrin TMD-GpA adherent to VN. Vector-transfected OV-MZ-6 cells, adherent to both VN and uncoated cell culture dishes, served as control. They displayed a drastically reduced proliferative activity compared to integrin αvβ3 expressing cells. On non-pretreated cell growth surfaces, an only low proliferation rate was noticeable in all cases (Fig. 28).

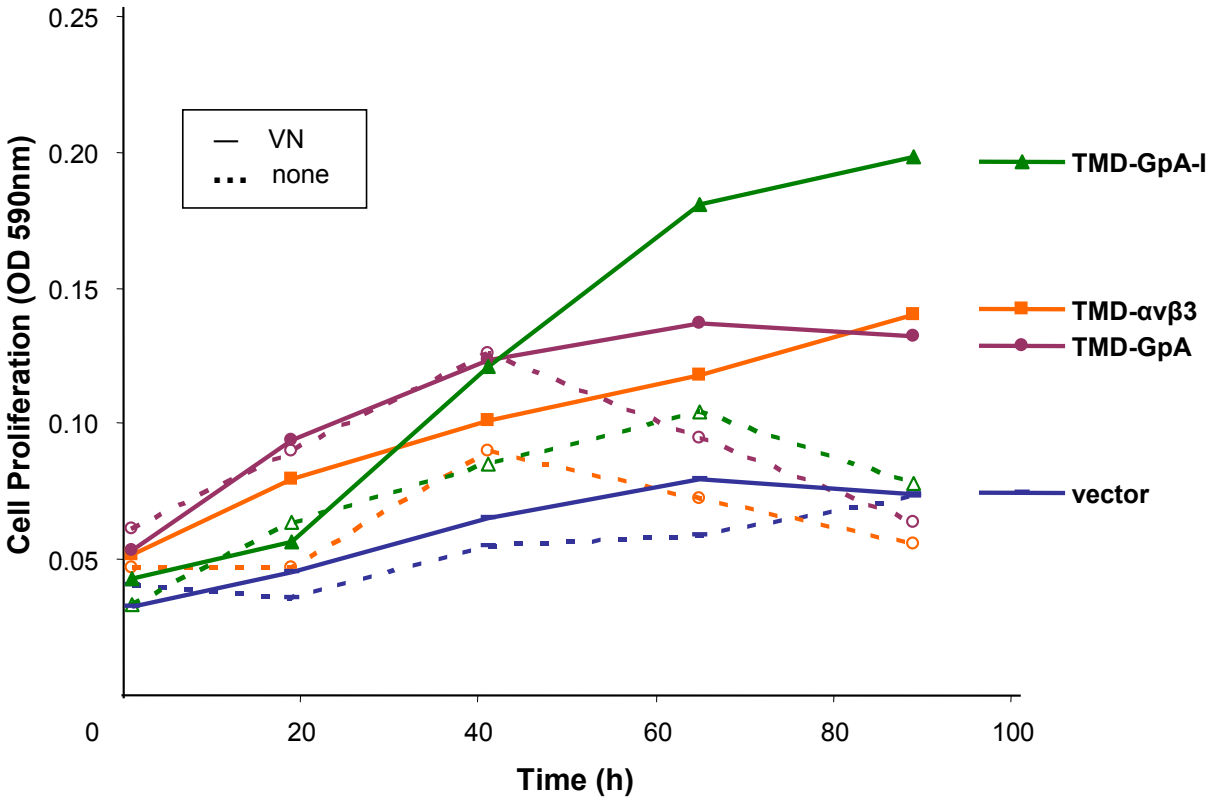

Fig. 28 Proliferative activity of OV-MZ-6 ovarian cancer cells as a function of the integrin αvβ3 TMD sequence

In order to determine cell proliverative activity a colorimetric MTT cell proliferation assay was performed. For this, cells transfected with the integrin αvβ3 TMD mutants were seeded on VN coated or non-pretreated 96-well cell culture plates. Every 24 h, 2 nM MTT reagent solution was added and and incubated for 2 h at 37°C. Accumulated formazan crystals were disolved by the addition of 100 µl DMSO. The absorbance of generated formazan crystals, as a measure of living cells, was determined with an ELISA spectral photometer at 590 nm. One representative experiment out of three is depicted.

6.1.4 Influence of the integrin αvβ3 TMD conformation on cellular motility

In order to investigate changes in integrin αvβ3-provoked outside-in signalling, dependent on its TMD conformation and the impact on cell migratory activity, a wound scratch assay was performed. For this, integrin TMD-αvβ3-, TMD-GpA-, TMD-

GpA-I-, and vector-transfected OV-MZ-6 cells, respectively, were cultivated on VN-coated or non-pretreated cell culture plates. When cell monolayers reached a confluency of approximately 90%, a wound scratch was set into the monolayer with a sterile pipette tip. Within 24 h, a significantly increased migratory capacity of integrin TMD-GpA-I-transfected OV-MZ-6 cells was observed. This allowed an enlarged number of cells to invade the wound scratch area when compared to those cells expressing integrin TMD-αvβ3. The enhanced migratory behaviour of cells transfected with integrin TMD-GpA-I was obvserved on either non-coated or VN pretreated wells. In contrast, in vector- as well as TMD-GpA-transfected cells, only negligible migratory activity was noticed independent of the presence of VN (Fig. 29).

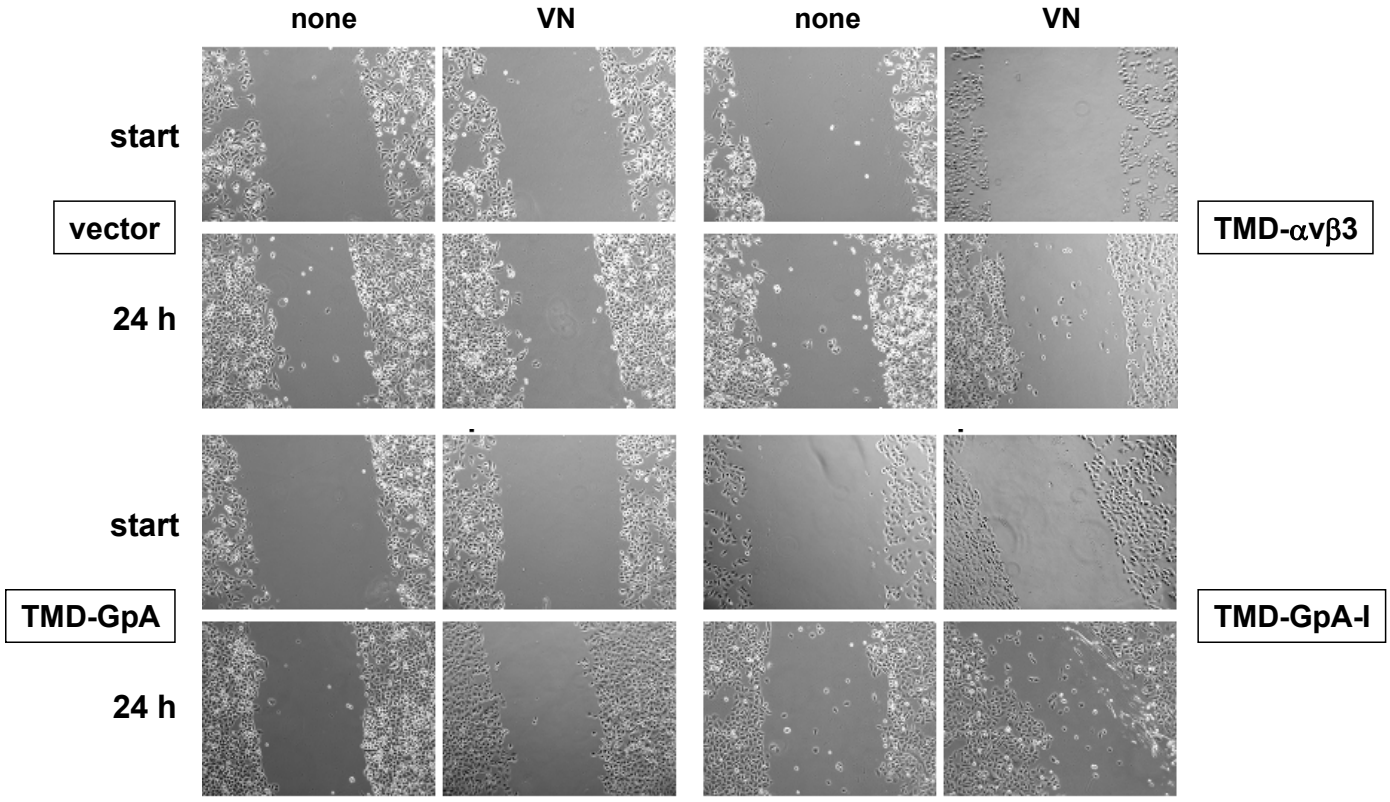

Fig. 29 Effect of the integrin αvβ3 TMD conformation on cellular motility

For wound scratch cell migration assays, cells expressing the integrin TMD mutants were passed to non- or VN-coated 12-well cell culture dishes. After cell monolayers reached a confluency of approximately 90%, a homogeneous wound scratch was set by using a sterile pipette tip. Cells that were detached during the wounding procedure were immediately removed by PBS washes. Microscopical images of monolayers were taken immediately after wounding (start) and after 24 h of further cell incubation at 37°C. Pictures of one representative experiment are depicted.

To evaluate the number of invasive cells, cells that obviously migrated into the gap of the wound scratch of three representative experiments were manually counted. For this, pictures were transferred to the software *Photoshop* and cells invading the wound scratch were marked and manually counted. Mean values of counted cells ± S.D. were plotted as 'n-fold' by setting the number of invaded vector-transfected cells adherent to VN to “1” (Fig. 30).

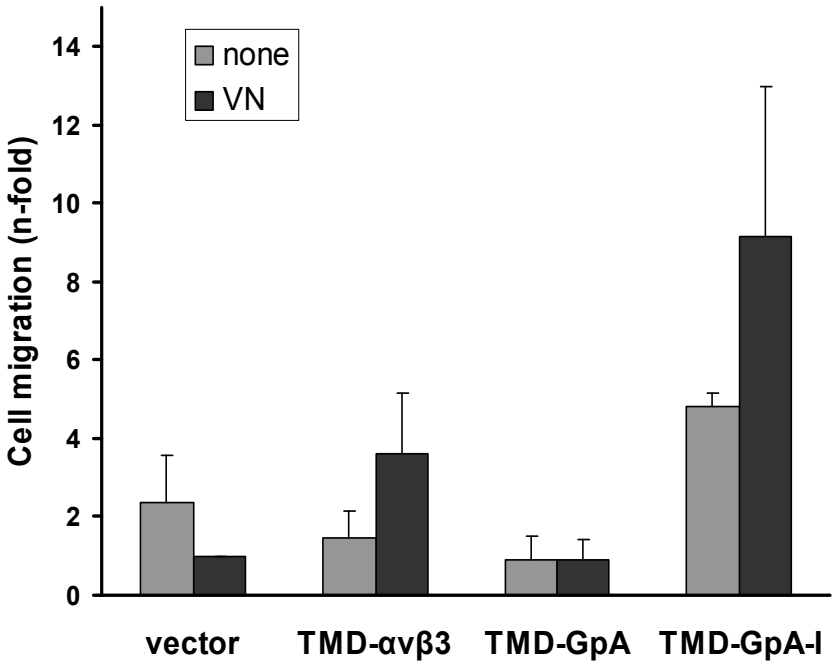

Fig. 30 Quantitative evaluation of cellular motility, dependent on integrin αvβ3 TMD conformation

The migratory activity of each integrin αvβ3 cell transfectant was quantified by counting the numbers of cells that had invaded the wounds. Mean values for relative cell migratory capacity are given as ‘n-fold’ by setting the normalised signal for the respective vector-transfected cells grown on VN to “1” (n = 3, ± S.D.).

6.1.5 Changes in integrin αvβ3-mediated cellular adhesion as a function of TMD conformation

6.1.5.1 Measurement of initial cellular adhesion

Integrin αvβ3/ ECM-dependent adhesion profiles for human ovarian OV-MZ-6 cancer cells have been previously established (Hapke et al. 2003). By performing competition studies utilising the synthetic integrin αvβ3-directed cyclic peptide

cRGDfV, it was shown that in OV-MZ-6 cells, integrin αvβ3 preferably binds to VN, since soluble cRGDfV inhibited OV-MZ-6 cell adhesion to this ECM ligand.

The initial cellular adhesive strength and spreading capacity of the different integrin αvβ3 TMD cell transfectants was determined by use of the *xCelligence system*^{TM} (Roche). It measures electrical impedance across interdigitated microelectrodes, integrated on the bottom of tissue culture E-plates. This enables the system to detect changes in cellular adhesion and spreading in real time. For this, cells were seeded on E-plates, pretreated with VN, at a density of 15000 cells and total electrode impedance recorded over a time period of 30 min. Interestingly, OV-MZ-6 cells displaying elevated levels of integrin TMD-GpA or TMD-GpA-I showed strongest and almost comparable adhesive capacity, followed by cells expressing integrin TMD-αvβ3. Vector-transfected control cells, displaying low endogenous integrin αvβ3 levels, showed lowest adhesion/spreading capacity (Fig. 31).

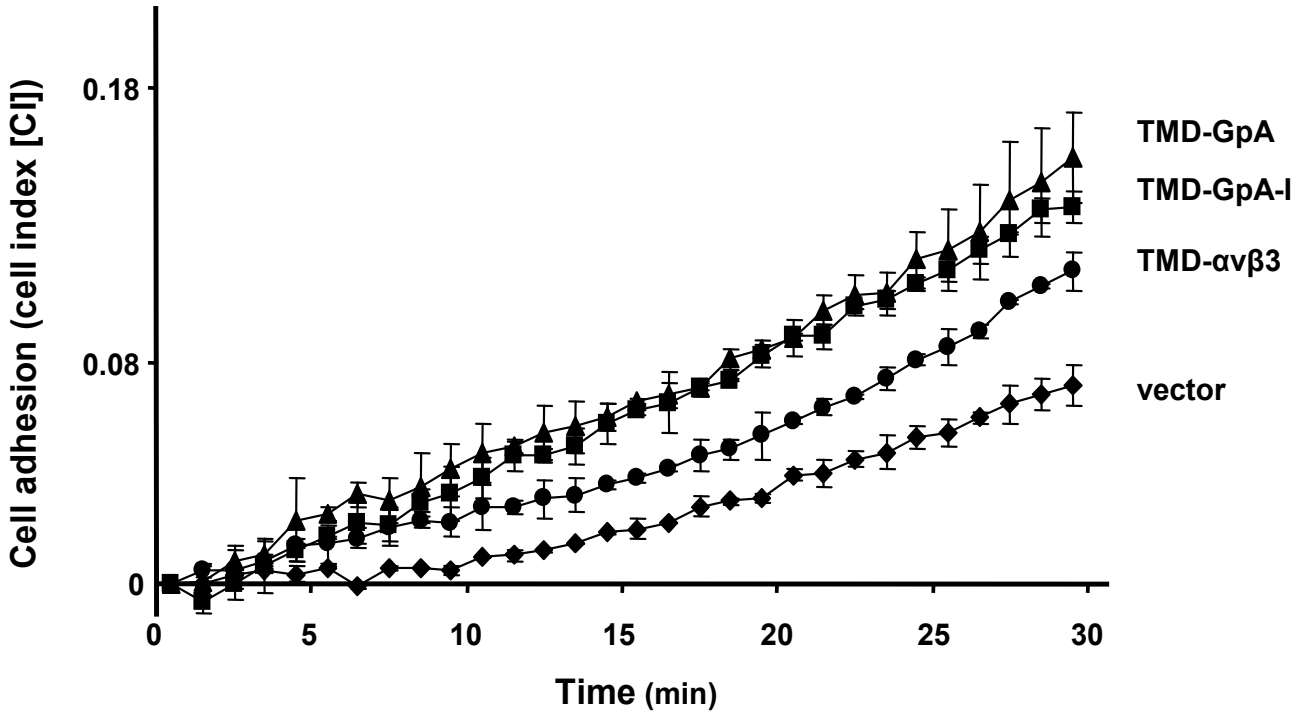

Fig. 31 Integrin αvβ3-provoked changes in initial cellular adhesion, dependent on the TMD sequence

The initial adhesive strength and spreading capacity of cells expressing integrin TMD-αvβ3, TMD-GpA, or TMD-GpA-I was determined by use of the microelectronic real time cell electronic sensor system *xCelligence system*^{TM}. For this, cells were seeded on VN coated E-plates and cell adhesion recorded over 30 min. Data are given as cell index (CI), representing relative changes in electrical impedance as measure of cell attachment and spreading (n=2, ±S.D.). One representative experiment out of three is depicted.

6.1.5.2 Evaluation of binding forces by atomic force microscopy

Integrin αvβ3 TMD conformation-dependent adhesive strength of OV-MZ-6 cells was further analysed by AFM. For this, cells were seeded on PL-coated glass cover slips in normal cell culture medium for 24 h. For the AFM experiments, cell culture medium was exchanged by PBS containing 1 mM Mg^{2+}/1 mM Ca^{2+}. During the AFM experiment (approx. 2 h), no obvious damaging effects on living cells were noticeable. Knowledge of the cantilevers' spring constant was used to calculate the forces needed for cantilever retraction. The cantilever was coated with VN to determine specific adhesive binding forces between the different integrin αvβ3 TMD variants and the ligand VN. Upon application/retraction cycles of the cantilever force to a single cell, membrane tethers were pulled out of the cell membrane. Strength and flexibility of the binding events between integrin αvβ3 and the ligand VN were determined. The retraction curves showed steps, typically observed during cell adhesion measurements (Helenius et al. 2008; Schmitz et al. 2008) (Fig. 32A). Based on these force-distance curves, different parameters were evaluated. First, the average number of adhesive events and the number of steps per adhesive force curve were counted (Fig. 32B). For cells expressing integrin TMD-GpA, nearly 8 force steps per adhesive event were observed, compared to approximately 3 force steps for those cells displaying integrin TMD-αvβ3 and TMD-GpA-I. Upon blockade of integrin αvβ3/VN-interactions by usage of functional blocking mAb (# LM609) both, the number of force jumps and the number of adhesive events were reduced. However, we still observed frequent unspecific adhesion events, which, as shown below, are much weaker than the integrin-mediated adhesions. Further evaluated were the peak force (Fig. 32C), the work needed to retract the cantilever (which equals the area under the force-distance curves) (Fig. 32D), as well as height and position of the force steps (Fig. 32E and 32F). The median of the peak force increased from 91.2 pN for unspecific adhesion measured after blocking by the αvβ3-directed mAb (data not shown) over 102.3 pN for integrin TMD-αvβ3, 126.8 pN for integrin TMD-GpA-I and up to 188.8 pN for integrin TMD-GpA (Fig. 32C). The work required for detaching the cantilever from the cells increased from 52.9 aJ (blocking by mAb – data not shown) over 125.8 aJ (TMD αvβ3), 188.5 aJ (TMD-GpA-I), and up to 287.1 aJ (TMD-GpA) (Fig. 32D). The low forces and low work after treatment with the integrin αvβ3-directed mAb demonstrated the importance of this integrin for strong cell adhesion and also the integrin αvβ3-specificity of the AFM measurements.

The increase in peak force and work required to detach the cantilever from integrin TMD-GpA-expressing cells demonstrated a surprisingly strong cell adhesive capacity despite TMD clasping caused by the GpA TMD sequence. This was also reflected by an increase in the step height from 21.5 pN for integrin TMD-αvβ3 to 27.0 pN for integrin TMD-GpA and TMD-GpA-I, respectively (Fig. 32E). Interestingly, the strengthened adhesion correlated with a decrease in the median step position for integrin TMD-GpA-I in comparison to TMD-αvβ3 from 0.9 μm to 0.5 μm, while integrin TMD-GpA-expression exerted no effect on the step position with a median position of 1.0 μm (Fig. 32F).

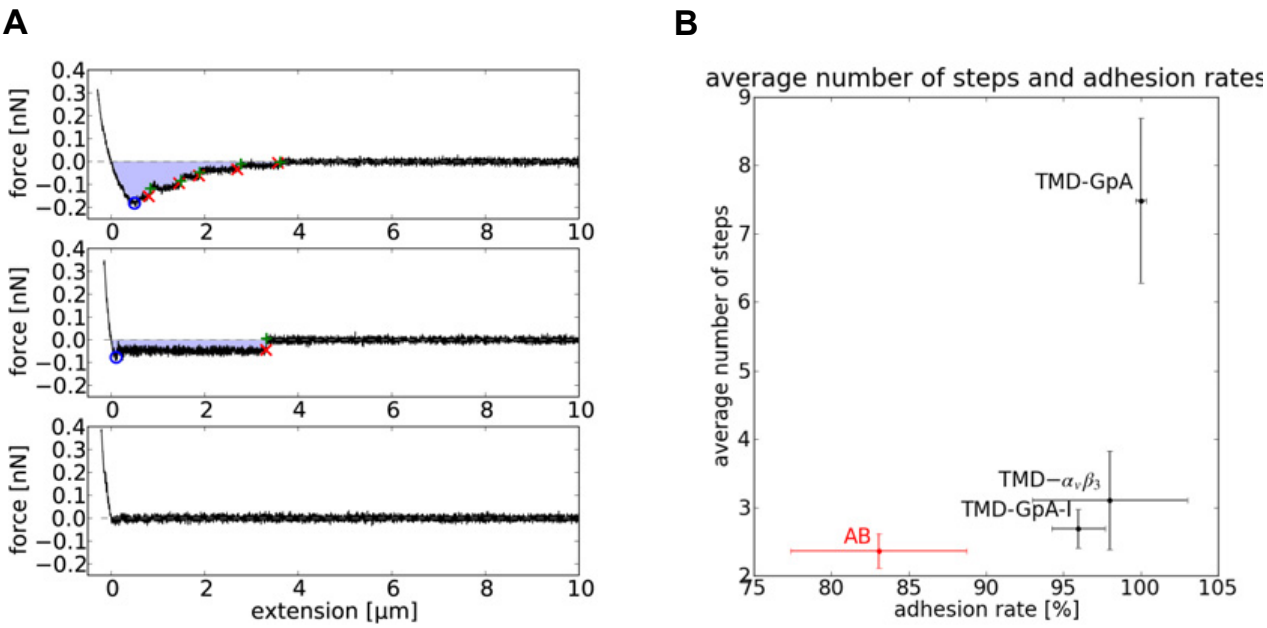

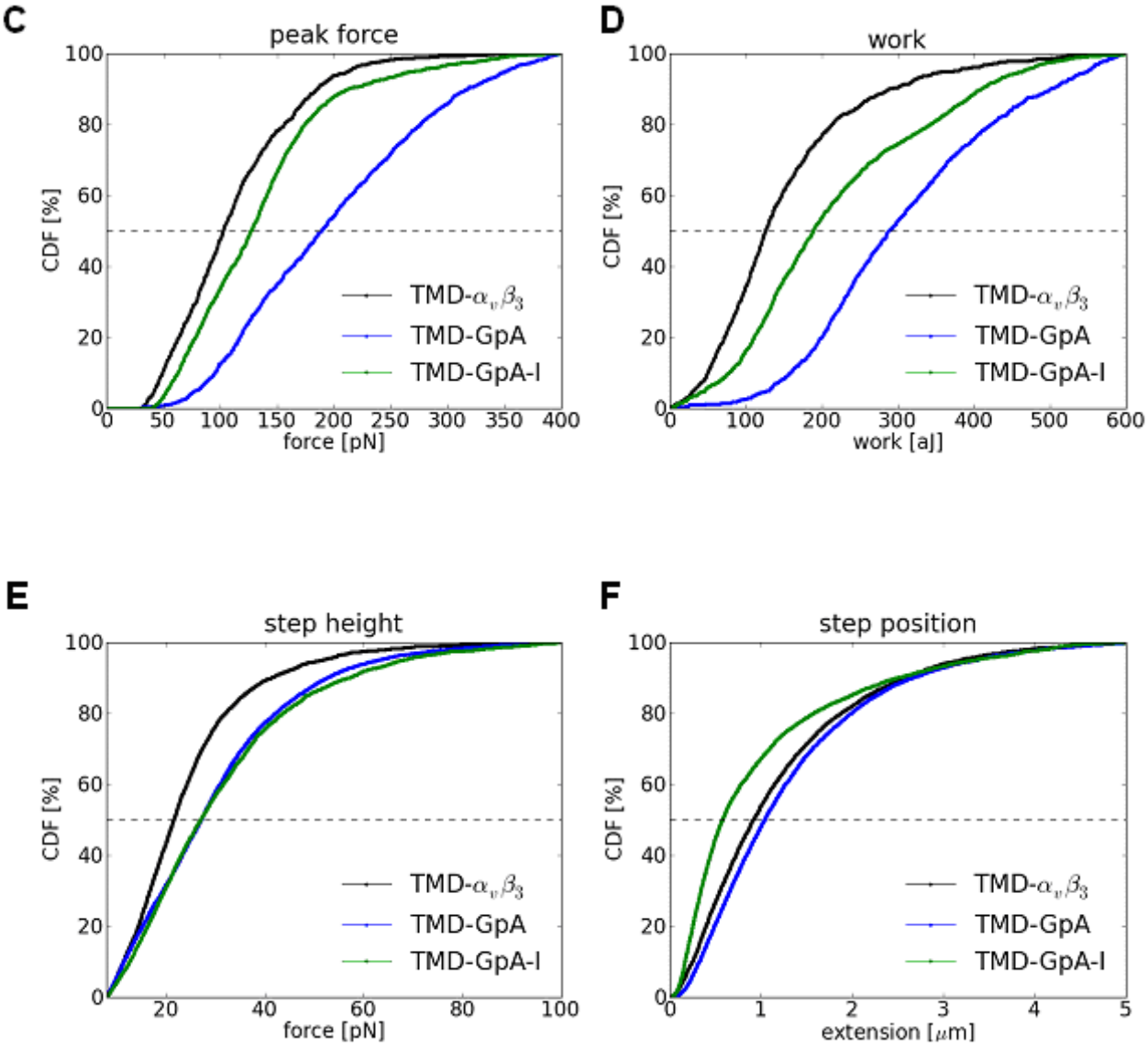

Fig. 32 Evaluation of adhesive strength between cells expressing the different integrin αvβ3 TMD mutants and the ligand VN by AFM

Cells were seeded on PL coated cover slips one day prior to measurement. Cantilevers were coated with VN (2 µg/ml). The cantilever was applied onto a single cell with a force of 0.5 nN at a constant approach- and retract-velocity of 4 µm/s. **A)** Examples of AFM force/distance curves. The first two curves show adhesions with a different number of force steps. The last force curve shows no adhesion. Evaluated were the peak force (blue circle), the work of cantilever retraction (blue area under curve), as well as height and position of force steps (force steps indicated by red 'X' (begin of force step) and green '+' (end of force step)). **B)** Average adhesion rate and average number of steps per adhesive force-distance curves for the different constructs. **C)** Cumulative distribution function (CDF) of the peak force (blue circle in A). **D)** CDF of the work of cantilever retraction (blue area in A). **E)** CDF of the step height. **F)** CDF of step position.

6.1.5.3 Determination of cellular adhesive capacity with a spinning disc device

While AFM measures the capability of cells to adhere to their environment on short time scales, the final adhesive strength of cells needs measurements on longer time scales, which allow for cytoskeletal reorganization and the formation of focal contacts or focal adhesions. In order to reach these longer time scales, the strength of adhesion was further evaluated by a spinning disc device. Experimental data were evaluated as described before (Garcia et al. 1997; Boettiger 2007; Engler et al. 2009). The spinning disc exposes a cell population to a linear hydrodynamic shear stress gradient and measures the mean shear stress required for cell detachment (Garcia et al. 1997; Boettiger 2007). Experimental analyses have demonstrated that the mean detachment shear stress is proportional to the number of adhesive integrin-ligand bonds (Garcia et al. 1997; Boettiger et al. 2001; Shi et al. 2003).
For the experimental procedure, the different integrin αvβ3 cell transfectants were passed to VN-coated cover slips (adhesion time 20 up to 90 min) and exposed to a constant velocity (ω) on the spinning disc device. The resulting fluid flow across the sample creates a shear profile that scales with the distance of the location of a respective adherent cell to the center (r) of the cover slips. After the spinning step, highest cell concentrations were detectable close to the center of the discs, where the shear stress approaches zero (τ_0) and gradually declined towards the edges of the cover slips. Cell numbers were quantified at specific positions on the cover slips and normalised to cell numbers in the centre at τ_0. The extent of adhesive strength, which is defined as the point where 50% of the cells remain attached to the cover slip during spinning (τ_{50}) as a function of number of integrin αvβ3/VN-bonds, was determined. Because this assay measures the reaction between integrin αvβ3 and VN, the rate and steady state level of adhesion is proportional to the number of integrin αvβ3 receptors on the cell surface. Therefore, the data from the spinning disc analysis were corrected by determining cell surface expression levels of integrin αvβ3 and its TMD variants by FACS analysis and normalised to values obtained for integrin TMD-αvβ3 expression (see Fig. 18). Normalised adhesion strength (τ_{50}) was plotted as non-linear regression curves, indicating the standard error of estimate, as a function of cell adhesion time (Fig. 33). All different integrin αvβ3 cell transfectants displayed increases of their adhesive strengths (τ_{50}) onto VN-coated cover slips as a function of time of adhesion prior to spinning. However, cells expressing integrin

TMD-GpA or TMD-GpA-I exerted a higher adhesive strength per expressed αvβ3-receptor density reaching plateau levels of approximately 336 ± 2.3 dynes/cm² and 338 ± 13 dynes/cm², respectively, when compared to cells expressing integrin TMD-αvβ3 (288 ± 12.3 dynes/cm²) (Fig. 33).

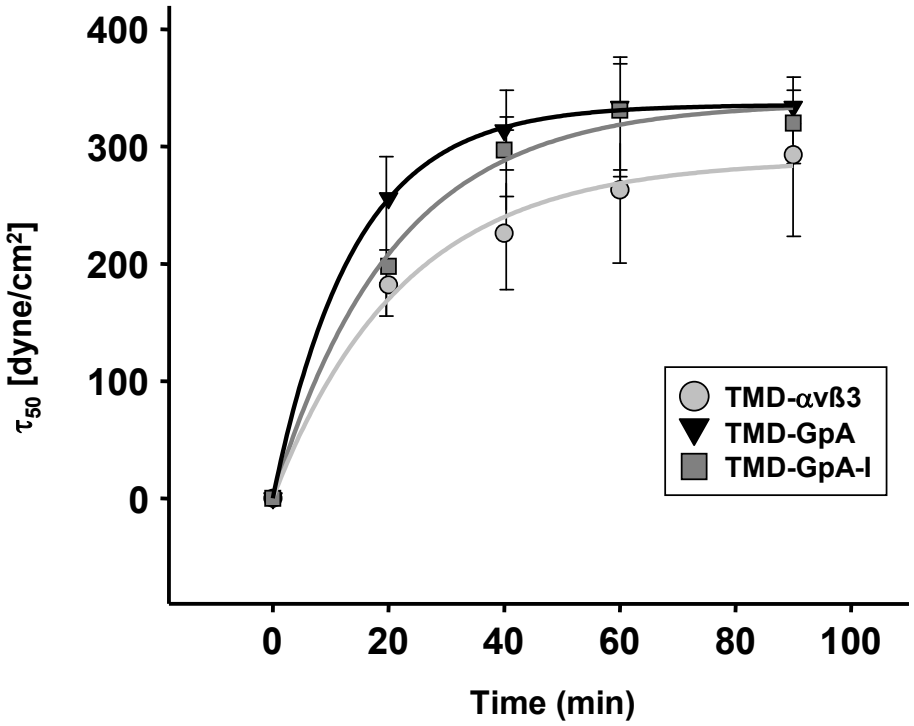

Fig. 33 Evaluation of integrin αvβ3-provoked cellular adhesive forces by a spinning disc device

Adhesion force measurements were performed by utilising a spinning disc device, developed and described by David Boettiger and coworkers (Garcia et al. 1997). Cells expressing integrin TMD-αvβ3, TMD-GpA, or TMD-GpA-I were harvested from appr. 60% confluent cell monolayers and seeded onto VN-pretreated cover slips, followed by a blocking step in PBS, 1% (w/v) BSA. At 20, 40, 60, and 90 min after cell plating, cover slips were spun at 4000 rpm for 5 min. After spinning, cells were fixed in PBS, 4% (w/v) PFA, stained with DAPI, and counted using an AxioScope Hal 100 microscope with the software *Meta Morph*™. Evaluation of three different experiments was conducted as described before (Boettiger 2007). Adhesive strengths (τ_{50}) of the distinct time points were plotted as non-linear regression curves, indicating the standard error of estimate. The relative differences in the extent of integrin αvβ3 surface expression, as measured by FACS analysis, were used to normalise the obtained adhesion data.

6.2 Role of the integrin αvβ3 cytoplasmic salt bridge during integrin activation

6.2.1 Establishment of a cellular model system transfected with integrin αvβ3 and its salt bridge mutants

The human ovarian cancer cell line OV-MZ-6 was chosen to study the effects of integrin αvβ3 cytoplasmic salt bridge formation on cellular signalling and adhesion. For this, integrin αv- and β3-cDNA cloned into mammalian expression vector pCDNA 3.1/myc-His, was modified by in vitro site-directed mutagenesis (see doctoral thesis by Lilli Volkhardt and Leonora Brunie). Mutants of WT integrin αvβ3 were generated by exchanging the salt bridge forming amino acids on each subunit, αvR995D and β3D723R, respectively. Upon cellular transfections with different combinations of these constructs, we established cell culture models either displaying integrin αvβ3 capable of forming a putative salt bridge (αvβ3-WT or the charge reversal mutant $\alpha v^{R995D}\beta 3^{D723R}$) or with a deficiency in this interchain interaction ($\alpha v^{R995D}\beta 3$ or $\alpha v\beta 3^{D723R}$) (Fig. 34).

αv-WT + β3-WT ➔ **αvβ3-WT (= TMD-αvβ3)**
αv-mutation + β3-mutation ➔ **$\alpha v^{R995D}\beta 3^{D723R}$**
αv-WT + β3-mutation ➔ **$\alpha v\beta 3^{D723R}$**
αv-mutation + β3-WT ➔ **$\alpha v^{R995D}\beta 3$**

Fig. 34 The integrin αvβ3 salt bridge mutants, expressed by OV-MZ-6 cancer cells
The salt bridge forming amino acids of αv- and β3-integrin chains were exchanged by site-directed mutagenesis. An arginine of αv (R995) and an aspartic acid of β3 (D723) were each replaced, generating a charge reversal mutation. OV-MZ-6 cells were transfected with WT αv-/ β3-integrin subunits and salt bridge mutated αv-/ β3-subunits in different combinations. The following cell transfectants were generated: αvβ3-WT; $\alpha v^{R995D}\beta 3^{D723R}$; $\alpha v\beta 3^{D723R}$; $\alpha v^{R995D}\beta 3$.

Successful transfection of cells with pCDNA 3.1/myc-His endowed the cells with antibiotic resistance to G418. Stably transfected cell clones were isolated by limited dilutions. Integrin expression levels were determined after each cloning round by immunocytochemical staining and subsequent CLSM analysis. Integrin αvβ3 and its salt bridge mutated variants were detected as heterodimers, predominantly localised

on the cell surface, with mAb # 23C6. Vector-transfected cells served as control (Fig. 35).

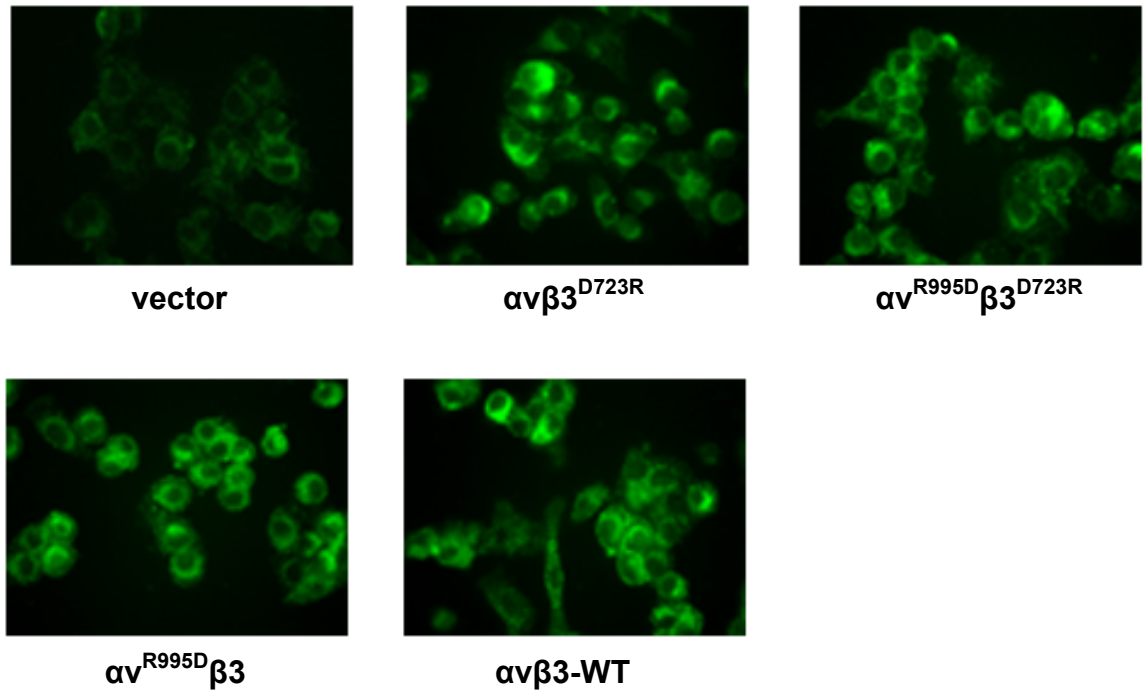

Fig. 35 Isolation of individual transfected cell clones, expressing integrin αvβ3 and the salt bridge mutants

Human ovarian cancer cells, stably transfected with integrin αvβ3-WT, $\alpha v^{R995D}\beta 3^{D723R}$, $\alpha v^{R995D}\beta 3$, or $\alpha v\beta 3^{D723R}$ were immunocytochemically stained with mAb (#23C6) directed to integrin αvβ3 as described. Representative fluorescence images are depicted. The pictures demonstrate integrin αvβ3 expression on the cell surface of the cell clones, selected for further studies, in comparison to vector-transfected cells.

Furthermore, expression levels of the different integrin transfectants were regularly analysed by FACS measurement. In order to compare experimental data obtained for the different cell transfectants, individual cell clones of each transfection category with very similar αvβ3 receptor density on the cell surface were isolated. Every cell transfectant expressed elevated levels of integrin αvβ3 and mutants thereof, approximately 2- to 3.5-fold compared to vector-transfected cells (Fig. 36).

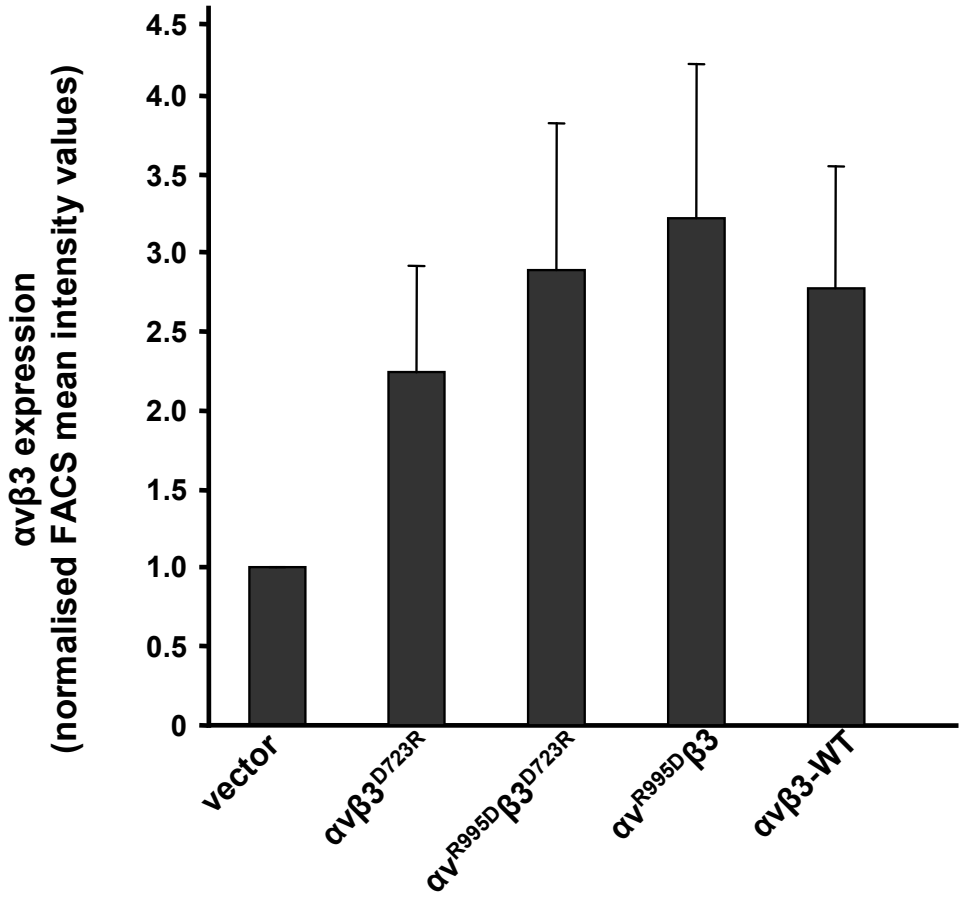

Fig. 36 Determination of integrin αvβ3 expression levels by FACS analysis

Expression levels of integrin αvβ3 of selected OV-MZ-6 cell clones, transfected with integrin αvβ3 and the salt bridge mutants, respectively, were regularly analysed by FACS measurements. Normalised FACS mean fluorescence intensity values of 10 individual experiments are depicted.

6.2.2 Changes of integrin αvβ3-mediated cellular signalling as a function of salt bridge formation

6.2.2.1 Activation of FAK as a function of integrin αvβ3 salt bridge formation

The importance of FAK as a signal transducing gateway of integrin-induced intracellular signalling cascades has already been described. Differences in activation/phosphorylation status of FAK (Y397), depending on integrin activation, were detected by Western blot analysis. For this, cells were plated on 6-well cell culture plates and lysed after 6h as described. Protein content was determined and 20 µg of total protein were applied onto SDS-PAGE under reducing conditions, followed by subsequent Western blotting. Western blot membranes were probed with mAb directed to FAK and p-FAK, respectively. To detect variations in protein loading

and in order to normalise blotting efficiency, membranes were stripped and reprobed with mAb directed to GAPDH (Fig.37A). Signal intensities of p-FAK, obtained by Western blot analysis, were also normalised against intensity of the respective GAPDH band with the software *Scion Image* (Fig. 37B). No considerable differences in total FAK expression levels between the different cell transfectants were noticed. However, investigating activated and thus phosphorylated FAK we noticed an elevation up to 5 fold of p-FAK levels in cells expressing integrin αvβ3 with a disrupted salt bridge ($\alpha v^{R995D}\beta 3$), even in the absence of ligand VN (Fig. 37B). This was followed by FAK phosphorylation in cells expressing integrin $\alpha v\beta 3^{D723R}$, αvβ3-WT and integrin $\alpha v^{R995D}\beta 3^{D723R}$. Vector-transfected cells served as controls and did not display sigificant elevation of p-FAK levels, when attached to VN.

Additionally, in order to detect p-FAK expression within focal adhesion sites, formed on VN, cells expressing integrin αvβ3 and its salt bridge mutants were seeded on VN coated microchamber slides and immunocytochemically stained as described. Cells expressing integrin αvβ3 with a disrupted salt bridge ($\alpha v^{R995D}\beta 3$ and $\alpha v\beta 3^{D723R}$), showed the brightest staining signal intensity for p-FAK within clustered focal adhesions. Cells displaying αvβ3-WT and $\alpha v^{R995D}\beta 3^{D723R}$ established lower but also elevated levels of p-FAK in their focal adhesion sites. In comparison, vector-transfected cells did not express a specific staining pattern (Fig. 38).

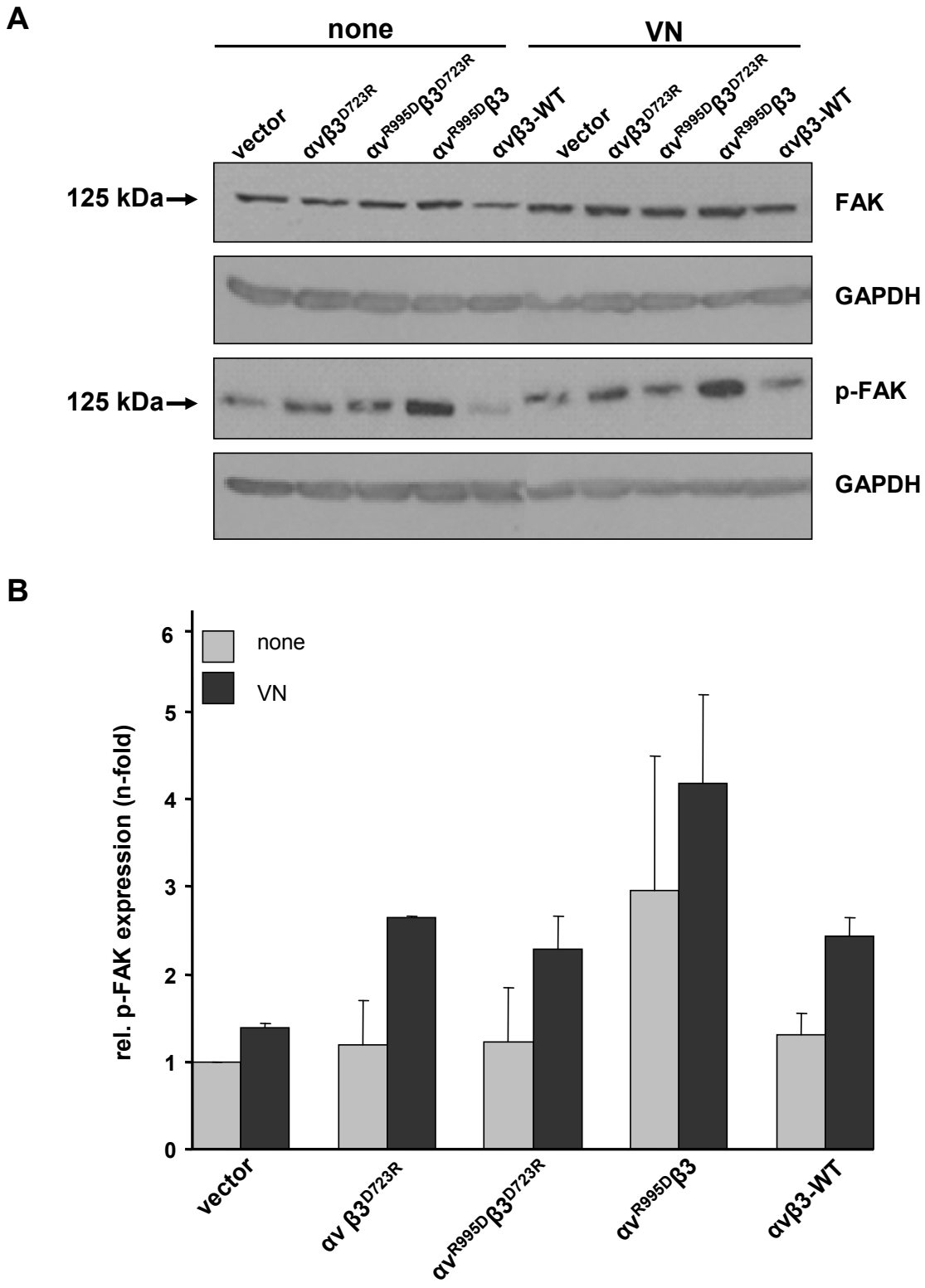

Fig. 37 Determination of cellular FAK/p-FAK expression levels by Western blot analysis

A) Detection of (p-)FAK by Western blot analysis. Cells transfected with integrin αvβ3 and its salt bridge mutants, or empty expression vector, were cultivated in the absence (none) or presence of VN and processed for Western blotting as described. A representative image of a typical Western blot is depicted. **B)** Densitometrical analysis of p-FAK expression was conducted as described by using the software *Scion Image*. Mean values for relative p-FAK expression are given as 'n-fold' by setting the normalised signal for the respective vector-transfected cells grown in the absence of VN to "1" (n = 2, ± S.D.).

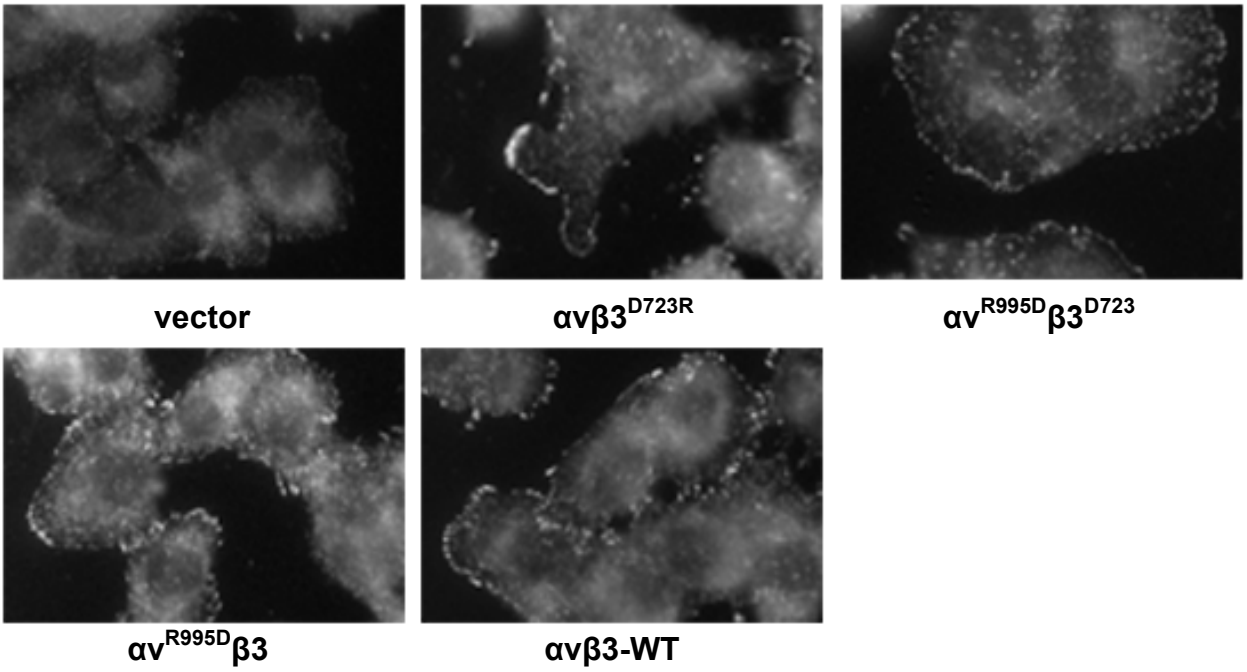

Fig. 38 Immunocytochemical detection of p-FAK expression in focal adhesions of cells expressing integrin αvβ3 and the salt bridge mutants

For the detection of p-FAK in cellular focal adhesions, cells expressing integrin αvβ3 and the salt bridge mutants were grown on VN pretreated micro chamberslides and immunocytochemical staining performed as described. Vector-transfected cells served as controls. Representative fluorescence images were taken with an AxioImager.

6.2.2.2 Activation of MAPK p44/p42$^{(erk-1/erk-2)}$ as a function of integrin αvβ3 salt bridge formation

The integrin αvβ3-mediated activation/phosphorylation status of MAPK p44/p42$^{(erk-1/erk-2)}$, depending on integrin cytoplasmic salt bridge formation, was examined by Western Blot analysis. In order to determine the expression and activation status of p44/p42$^{(erk-1/erk-2)}$ as a function of integrin αvβ3 salt bridge formation, cells were seeded on 6-well cell culture plates, either pretreated with VN or left uncoated. After 6 h, cells were lysed and p44/p42$^{(erk-1/erk-2)}$ as well as phosphorylated-p44/p42$^{(erk-1/erk-2)}$ determined by Western blot analysis (Fig. 39A). To detect variations in protein loading and in order to normalise blotting efficiency, membranes were stripped and reprobed with mAb raised against GAPDH. Signal intensities of p-p44/p42$^{(erk-1/erk-2)}$, obtained by Western blot analysis, were also normalised against intensity of the respective GAPDH band with the software *Scion*

Image (Fig. 39B). No considerable differences in total p44/p42$^{(erk-1/erk-2)}$ expression levels between the different cell transfectants were noticed. However, cells expressing integrin αvβ3 with a disrupted salt bridge (αv^{R995D}β3; αvβ3^{D723R}), displayed highest p-p44/p42$^{(erk-1/erk-2)}$ levels on VN (Fig. 39B). Cells transfected with integrin αv^{R995D}β3 displayed highest p-p44/p42$^{(erk-1/erk-2)}$ levels, even in the absence of VN. This was followed by p-p44/p42$^{(erk-1/erk-2)}$ activation in cells expressing integrin αvβ3-WT and integrin αv^{R995D}β3^{D723R}. Vector-transfected cells served as controls and did not display significant elevation of p-p44/p42$^{(erk-1/erk-2)}$ levels when attached to VN.

Additionally, activation and thus phosphorylation of p44/p42$^{(erk-1/erk-2)}$ as a function of integrin αvβ3 cytoplasmic salt bridge formation was evaluated by FACS analysis. For this, cells expressing integrin αvβ3 or the different salt bridge mutants were either activated by ligand mimetic 5 mM Mn^{2+} (Bazzoni et al. 1995; Takagi et al. 2002a) for 2 h at RT or left untreated. For the following flow cytofluorometrical analysis, cells were harvested and stained as described. Expression levels of phosphorylated p44/p42$^{(erk-1/erk-2)}$ of Mn^{2+}-activated cells were normalised to p-p44/p42$^{(erk-1/erk-2)}$ levels of the respective OV-MZ-6 cell transfectant incubated without Mn^{2+} (Fig. 40).

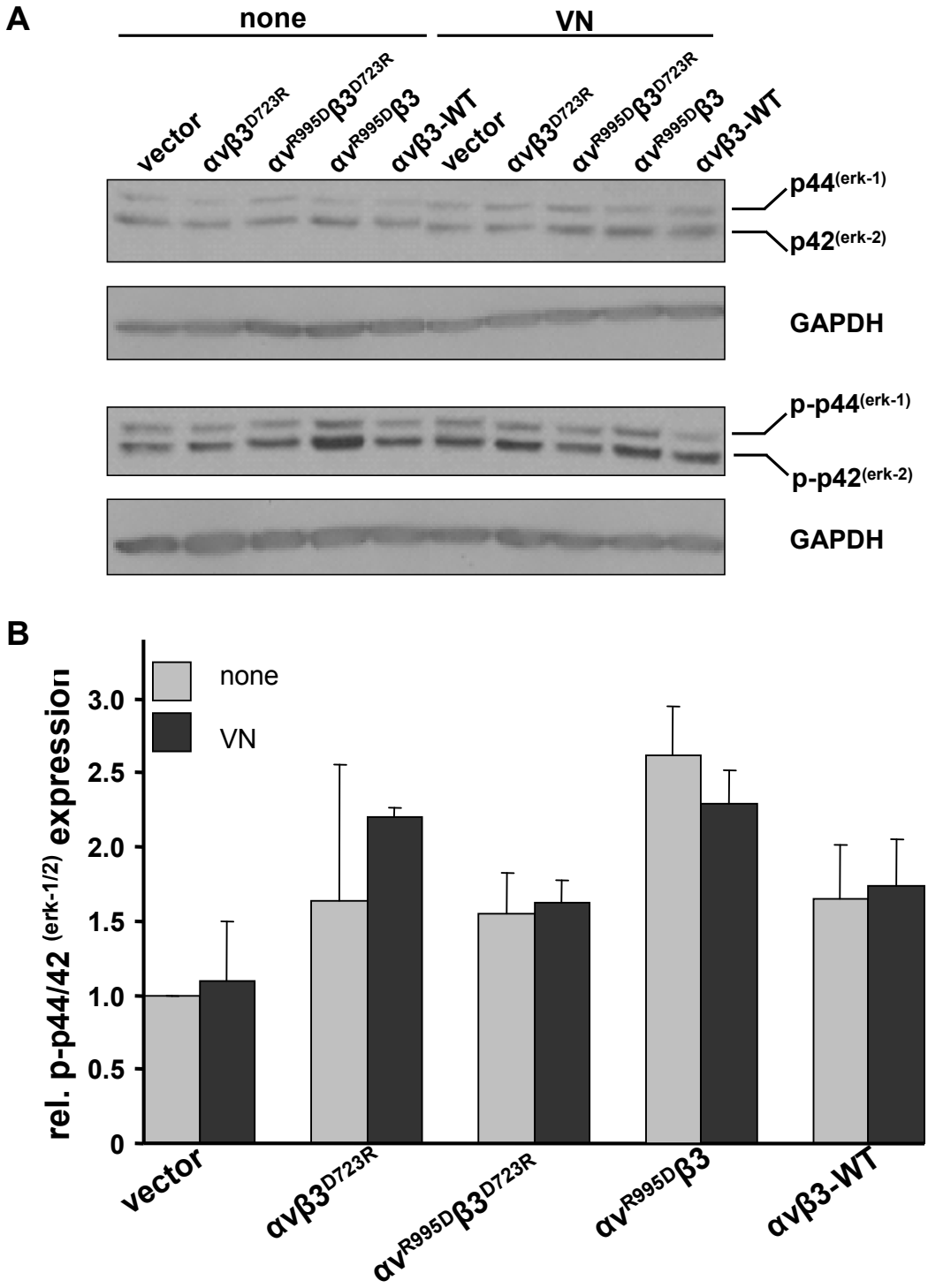

Fig. 39 Determination of cellular (p-)p44 /p42$^{(erk-1/erk-2)}$ expression levels as a function of integrin αvβ3 salt bridge formation by Western blot analysis

A) Detection of (p)-p44 /p42$^{(erk-1/erk-2)}$ by Western blot analysis. Cells transfected with integrin αvβ3 and its salt bridge mutants, or empty expression vector, were cultivated in the absence (none) or presence of VN and processed for Western blotting as described. A representative image of a typical Western blot is depicted. **B)** Densitometrical analysis of p-p44/42$^{(erk-1/2)}$ expression was conducted as described by using the software *Scion Image*. Mean values for relative p-p44/42$^{(erk-1/2)}$ expression are given as 'n-fold' by setting the normalised signal for the respective vector-transfected cells grown in the absence of VN to "1" (n = 2, ± S.D.).

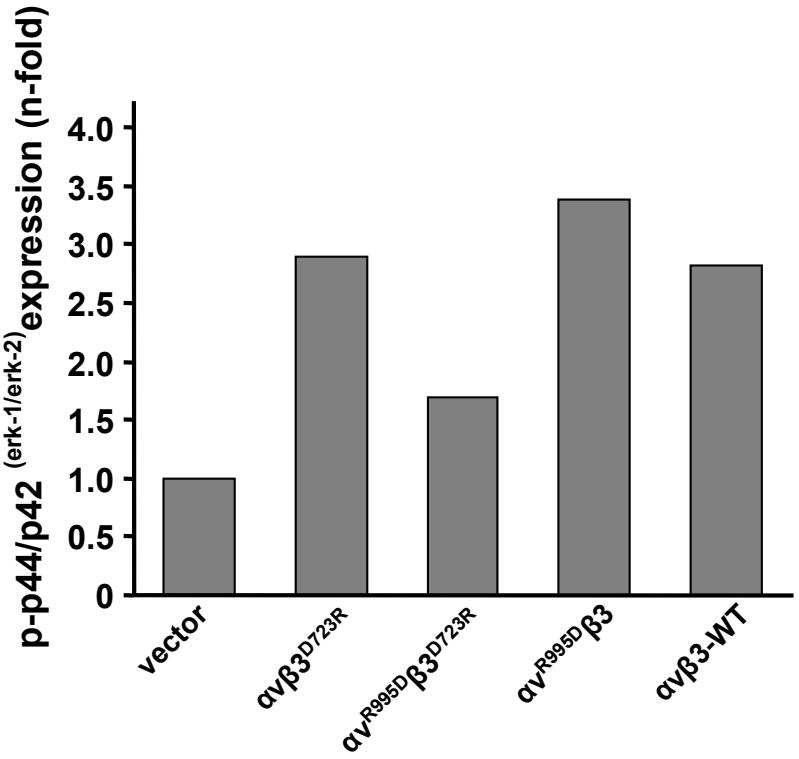

Fig. 40 Determination of activated p44/42$^{(erk-1/2)}$ expression levels as a function of integrin αvβ3 salt bridge formation by FACS analysis

Cells were grown on 6-well plates, activated by the addition of 5 mM Mn^{2+} for 2 h, and processed for FACS analysis of p-p44/42$^{(erk-1/2)}$ expression as described. FACS intensity mean channel values obtained for p-p44/42$^{(erk-1/2)}$ expression were normalised to the data obtained for respective cells incubated without Mn^{2+}. Relative p-MAPK expression is given as 'n-fold' by setting the normalised signal for vector-transfected cells to "1". One representative experiment is depicted.

6.2.2.3 Activation of PKB/Akt as a function of integrin αvβ3 TMD salt bridge formation

In order to determine integrin αvβ3-mediated activation/phosphorylation of PKB/Akt, depending on integrin cytoplasmic salt bridge formation, cells were seeded on 6-well plates, which were either pretreated with VN or left uncoated. After 3 h, cells were lysed and 20 µg of protein were applied to SDS-PAGE and analysed by subsequent Western blotting. Western blot membranes were probed with Ab directed to PKB/Akt and p-PKB/Akt, respectively (Fig. 41A). To detect variations in protein loading and in order to normalise blotting efficiency, membranes were stripped and reprobed with antibody directed to GAPDH. Intensities of protein bands were densitometrically analysed by the software *Scion Image* and normalised against the respective

GAPDH signal intensity (Fig. 41B). Total PKB/Akt was quite consistently expressed in all cell transfectants. However, we noticed a significant elevation of p-PKB/Akt levels in cells expressing integrin αvβ3 with a disrupted salt bridge (αv^{R995D} β3), even in the absence of ligand VN (Fig. 41B). This was followed by PKB/Akt phosphorylation in cells expressing integrin $\alpha v\beta 3^{D723R}$, αvβ3-WT and integrin $\alpha v^{R995D}\beta 3^{D723R}$. Vector-transfected cells served as controls and did not display significant elevation of p-PKB/Akt levels when attached to VN.

Additionally, activation of PKB/Akt as a function of integrin αvβ3 salt bridge formation was evaluated by FACS measurement. For this, transfected OV-MZ-6 cells were either activated by ligand mimetic 5 mM Mn^{2+} for 30 min at RT or left untreated. For the following flow cytofluorometrical analysis, cells were harvested and stained as described. Expression levels of phosphorylated PKB/Akt of Mn^{2+}-activated cells were normalised to p-PKB/Akt levels of the respective OV-MZ-6 cell transfectant incubated without Mn^{2+} (Fig. 42).

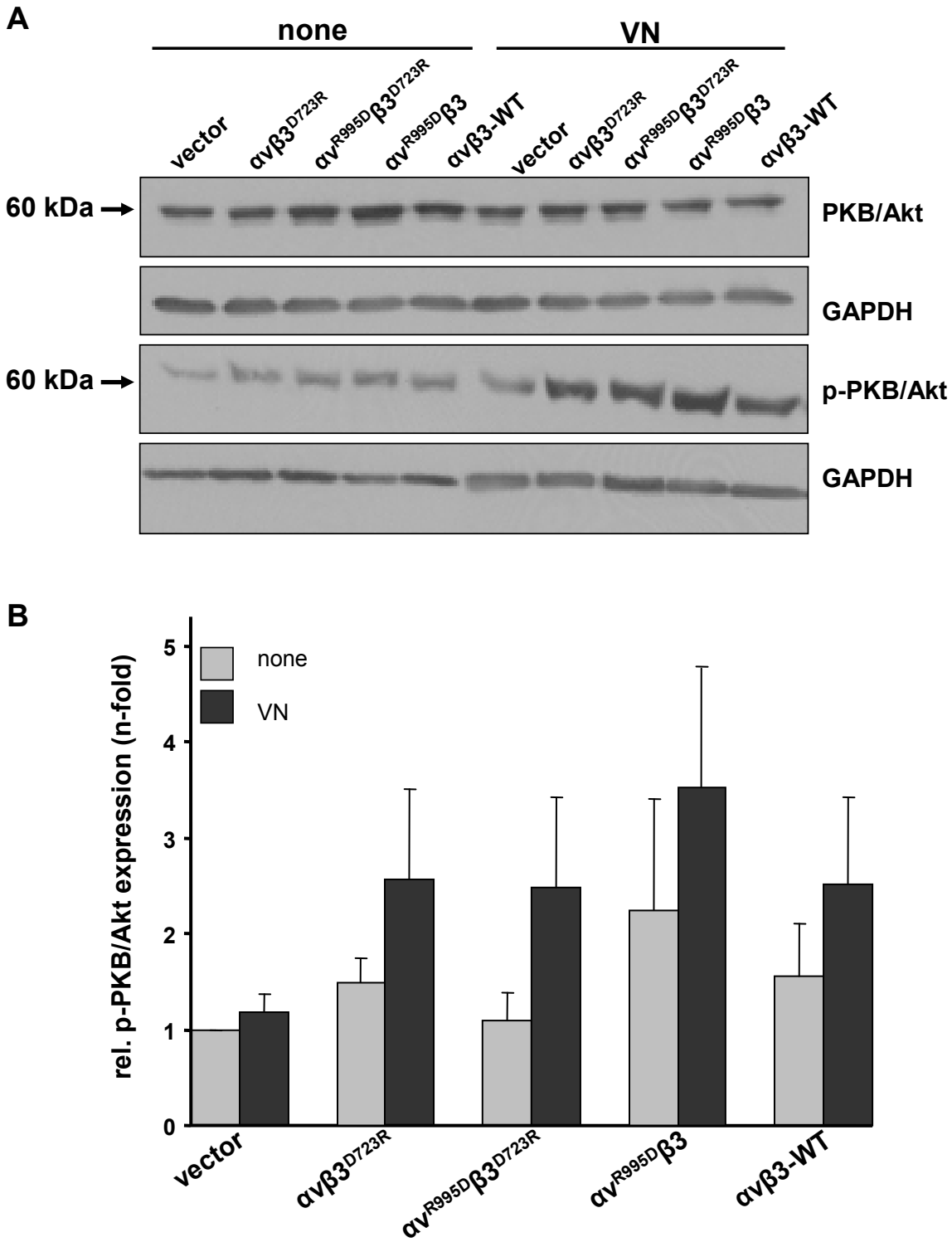

Fig. 41 Determination of cellular (p-)PKB/Akt expression levels as a function of integrin αvβ3 salt bridge formation by Western blot analysis

A) Detection of (p-)PKB/Akt by Western blot analysis. Cells transfected with integrin αvβ3 and its salt bridge mutants, or empty expression vector, were cultivated in the absence (none) or presence of VN and processed for Western blotting as described. A representative image of a typical Western blot is depicted. **B)** Densitometrical analysis of p-PKB/Akt expression was conducted as described by using the software Scion Image. Mean values for relative p-PKB/Akt expression are given as 'n-fold' by setting the normalised signal for the respective vector-transfected cells grown in the absence of VN to "1" (n = 2, ± S.D.).

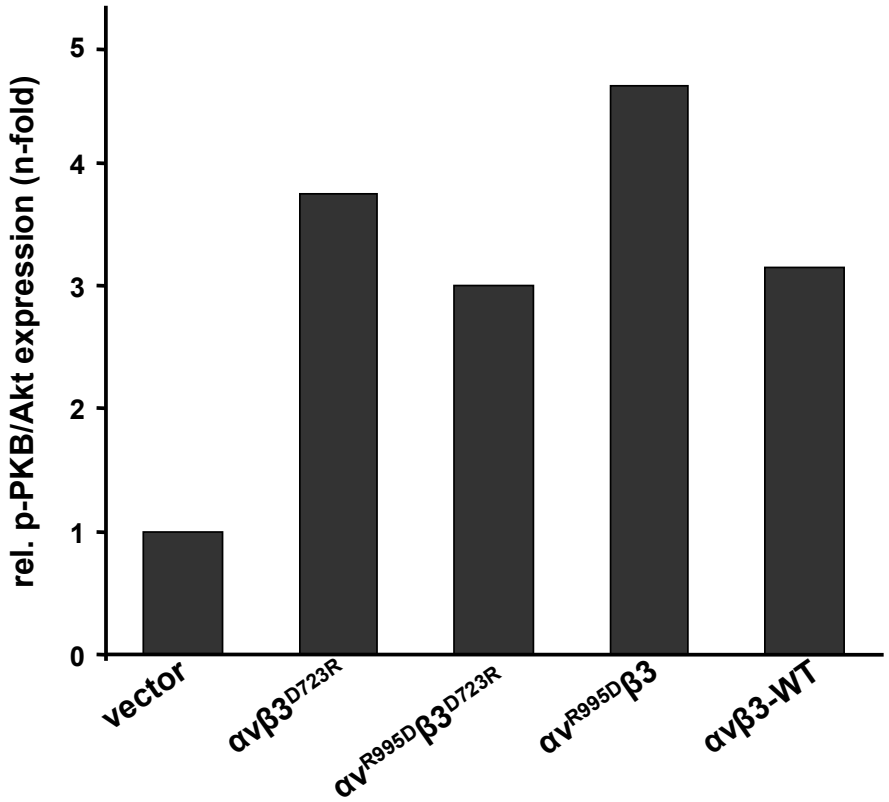

Fig. 42 Determination of activated p-PKB/Akt expression levels as a function of integrin αvβ3 salt bridge formation by FACS analysis

Cells were grown on 6-well plates, activated by the addition of 5 mM Mn^{2+} for 30 min, and processed for FACS analysis of p-PKB/Akt expression as described. FACS intensity mean channel values obtained for p-PKB/Akt expression were normalised to the data obtained for respective cell transfectants incubated without Mn^{2+}. Relative p-PKB/Akt expression is given as 'n-fold' by setting the normalised signal for vector-transfected cells to "1".

6.2.2.4 Linkage of integrin αvβ3 and its salt bridge mutants with cytoskeletal proteins talin and phospho-paxillin (Y118)

Talin binding to the integrin cytoplasmic tails is an essential event during integrin activation (Tadokoro et al. 2003). Disruption of the integrin cytoplasmic tails, facilitated by lack of the cytoplasmic salt bridge, theoretically enables constitutive binding of talin to the integrin β3-subunit. In order to test colocalisation of integrin αvβ3 with talin, cells expressing integrin αvβ3 and its salt bridge mutants were immunocytochemically double stained, followed by subsequent CLSM analysis. For this, cells were seeded on non-activating PL coated cell culture microchamber slides, 24 h prior to the staining procedure, and stained as described. Here, cells expressing integrin αvβ3 with a disrupted salt bridge $αv^{R995D}β3$, displayed a clear colocalisation

pattern, as demonstrated in the merged pictures in “yellow”. This was followed by cells expressing the other integrin variant with a disrupted salt bridge ($\alpha v\beta 3^{D723R}$). No colocalisation was observed in cells expressing integrin αvβ3-WT, $\alpha v^{R995D}\beta 3^{D723R}$, and vector-transfected control cells (Fig. 43).

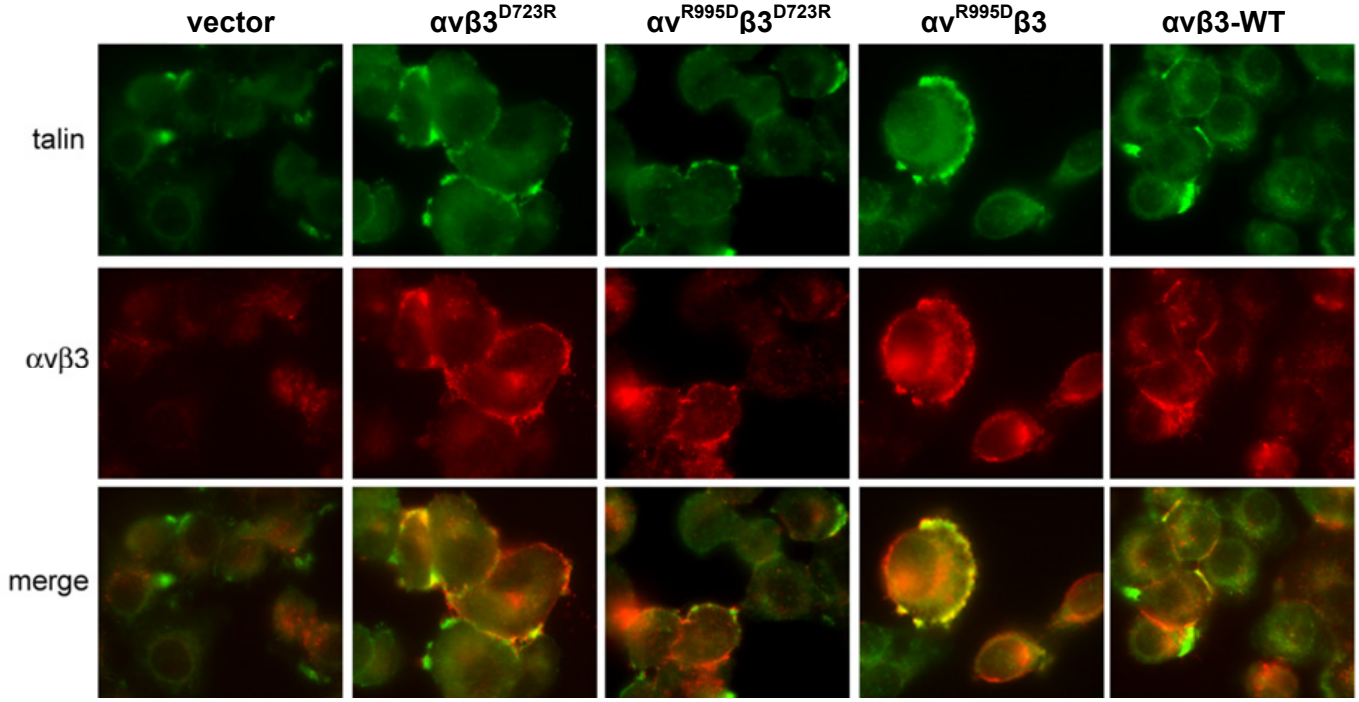

Fig. 43 Double immunocytochemical staining of integrin αvβ3, the respective salt bridge mutants, and talin

Colocalisation of the integrin αvβ3 TMD mutants with talin was visualised by immunocytochemical double staining and subsequent CLSM analysis. For this, cells expressing integrin αvβ3 and its salt bridge mutants were passed to PL-coated cell culture microchamber slides and cultivated for 24 h prior to staining procedure. In order to characterise colocalisation of integrin αvβ3 with talin, immunocytochemical double staining was performed as described. In case of integrin αvβ3, signals were detected by secondary Alexa-568-labeled goat-anti-mouse IgG, for talin, Alexa-488-labeled goat-anti-rabbit IgG served as secondary Ab. Depicted are typical and representative fluorescence images. Colocalisation of integrin αvβ3 and talin was documented by merging the two fluorescence images in “green” (488 nm, talin) and “red” (568 nm, αvβ3), indicating similar distribution patterns of both proteins within merged images in “yellow”.

Phosphorylation of the cytoskeletal protein paxillin (Y118) is a marker of integrin clustering (Fuortes et al. 1994; Graham et al. 1994; Zhou et al. 2001). In order to test constitutive integrin activation, colocalisation of integrin αvβ3 and its salt bridge mutants with p-paxillin was visualised by immunocytochemical staining and subsequent CLSM analysis. For this, cells were seeded on non-activating PL coated

cell culture microchamber slides and immunocytochemically double stained as described. Here, cells expressing integrin αvβ3 with a disrupted salt bridge ($\alpha v^{R995D}\beta 3$) showed the most distinct colocalisation with p-paxillin. This was followed by cells expressing the other integrin with a disrupted salt bridge ($\alpha v\beta 3^{D723R}$). No colocalisation was observed in cells expressing integrin αvβ3-WT, $\alpha v^{R995D}\beta 3^{D723R}$, and vector-transfected control cells (Fig. 44).

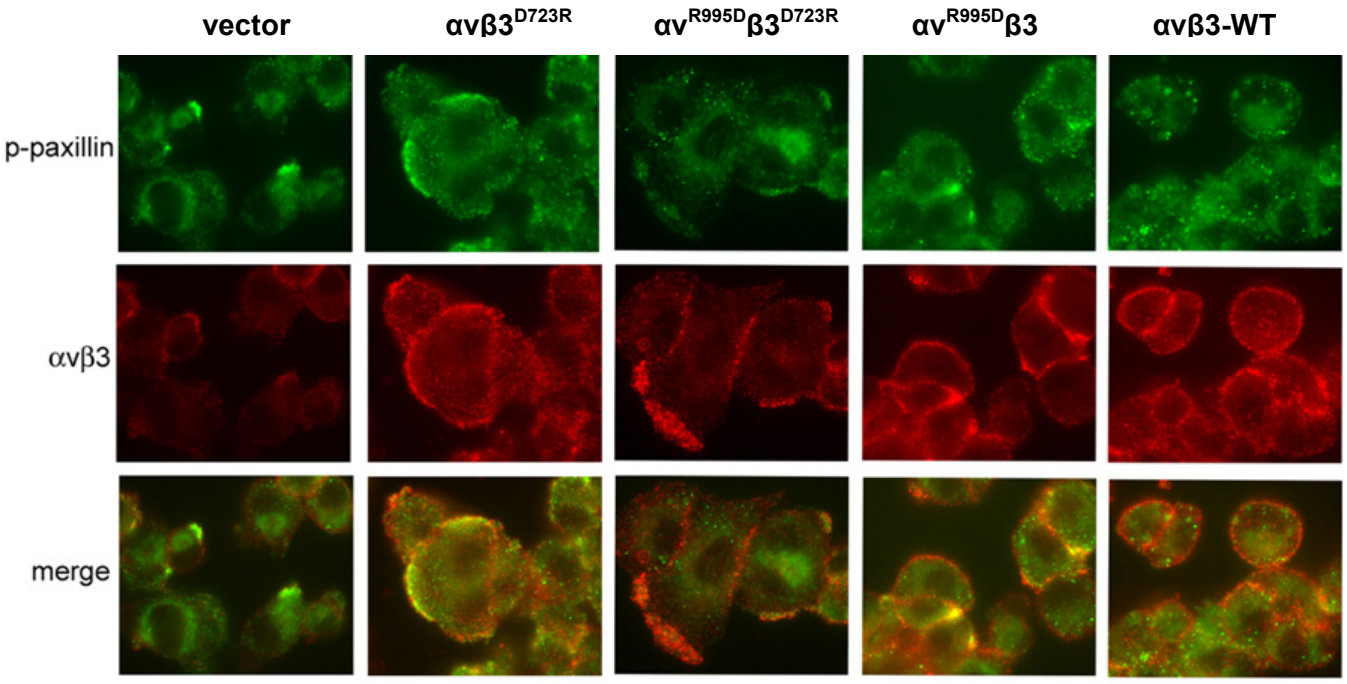

Fig. 44 Double immunocytochemical staining of integrin αvβ3, the respective salt bridge mutants, and p-paxillin (Y118)

Colocalisation of integrin αvβ3 and its salt bridge mutants with p-paxillin (Y118) was visualised by immunocytochemical double staining and subsequent CLSM analysis. For this, cells expressing integrin αvβ3 and its salt bridge mutants were passed to PL-coated cell culture microchamber slides and cultivated for 24 h prior to staining procedure. In order to characterise colocalisation of integrin αvβ3 with p-paxillin, immunocytochemical double staining was performed as described. In case of integrin αvβ3, signals were detected by secondary Alexa-568-labeled goat-anti-mouse IgG, for p-paxillin, Alexa-488-labeled goat-anti-rabbit IgG served as secondary Ab. Depicted are typical and representative fluorescence images. Colocalisation of integrin αvβ3 and p-paxillin was documented by merging the two fluorescence images in “green” (488 nm, p-paxillin) and “red” (568 nm, αvβ3), indicating similar distribution patterns of both proteins within merged images in “yellow”.

6.2.3 Impact of cytoplasmic salt bridge formation on integrin αvβ3-dependent cellular proliferation

In order to investigate changes of integrin αvβ3-mediated proliferative activity of cells expressing integrin αvβ3 and its salt bridge mutants, a colorimetric MTT cell proliferation assay was performed. For this, OV-MZ-6 cell transfectants were seeded in triplicates on VN coated 96-well cell culture plates. One hour after seeding and every 24 following hours, MTT reagent solution was added and and incubated for 2h at 37°C. The reaction was stopped by addition of DMSO. The absorbance of generated formazan crystals, as a measure of living cells, was determined at 590 nm with an ELISA spectral photometer. Within 90 h, highest proliferative activity was noticed for cells expressing integrin αvβ3 with a disrupted salt bridge ($\alpha v^{R995D}\beta 3$; $\alpha v\beta 3^{D723R}$), followed by cells expressing αvβ3-WT and $\alpha v^{R995D}\beta 3^{D723R}$. Vector-transfected control cells displayed a drastically reduced proliferative activity (Fig. 45).

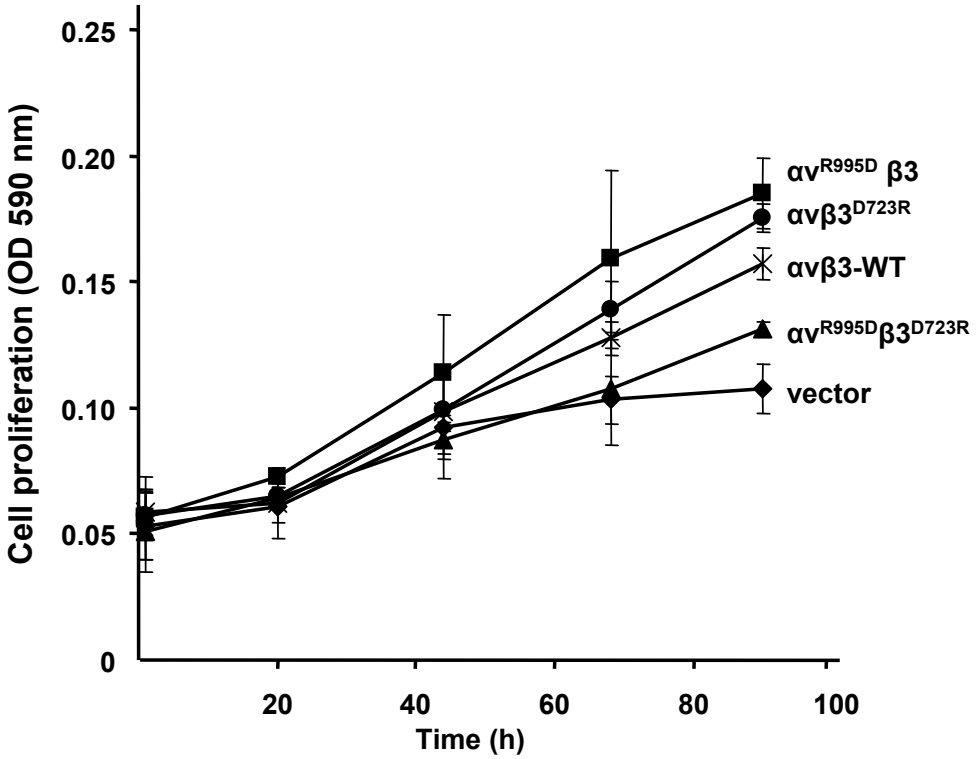

Fig. 45 Impact of integrin αvβ3 cytoplasmic salt bridge formation on cell proliferation

In order to determine cell proliverative activity a colorimetric MTT cell proliferation assay was performed. For this, cells transfected with integrin αvβ3 and its salt bridge mutants were seeded on VN coated 96-well cell culture plates. Every 24 h, 2 nM MTT reagent solution was added and incubated for 2 h at 37°C. Accumulated formazan crystals were disolved by the addition of 100 µl DMSO. The absorbance of generated formazan crystals, as a measure of living cells, was determined with an ELISA spectral photometer at 590 nm. Three independent proliferation assays were evaluated and mean OD_{590nm} values ±S.D. were plotted as a function of time (n = 3, ± S.D.).

6.2.4 Influence of integrin αvβ3 cytoplasmic salt bridge formation on cellular motility

Cellular migration is dependent on activation of intracellular signalling cascades. In order to investigate integrin αvβ3-provoked changes in outside-in signalling, dependent on cytoplasmic salt bridge formation, a wound scratch assay was performed. For this, cells expressing integrin αvβ3 and its salt bridge mutants were cultivated on VN-coated or non-pretreated cell culture plates. When cell monolayers reached a confluency of approximately 90%, a wound scratch was set into the monolayer with a sterile pipette tip. Plates were extensively washed in PBS, and pictures of the wound scratches were taken immediately after wounding, and after 24 h of further incubation (Fig. 46). Within 24 h, a significantly increased migratory capacity (up to 12 fold) of cells expressing integrin αvβ3 with a disrupted salt bridge ($\alpha v^{R995D}\beta 3$), even in the absence of VN, was noticed (Fig. 47). This was followed by cells expressing the other integrin αvβ3 with disrupted salt bridge, $\alpha v\beta 3^{D723R}$. However, these cells did not invade the gap on non-coated plates. Integrin αvβ3-WT and $\alpha v^{R995D}\beta 3^{D723R}$ transfected cells showed, on VN, an up to 4 fold enhanced migratory capacity compared to vector-transfected cells.

For the evaluation of the number of invasive cells, cells within the gap of the wound scratches of three representative experiments were counted. For this, pictures were transferred to the software *Photoshop* and cells invading the wound scratch were marked and manually counted. Mean values of counted cells ± S.D. were plotted as 'n-fold' by setting the number of invaded vector-transfected cells adherent to VN to “1” (Fig. 47).

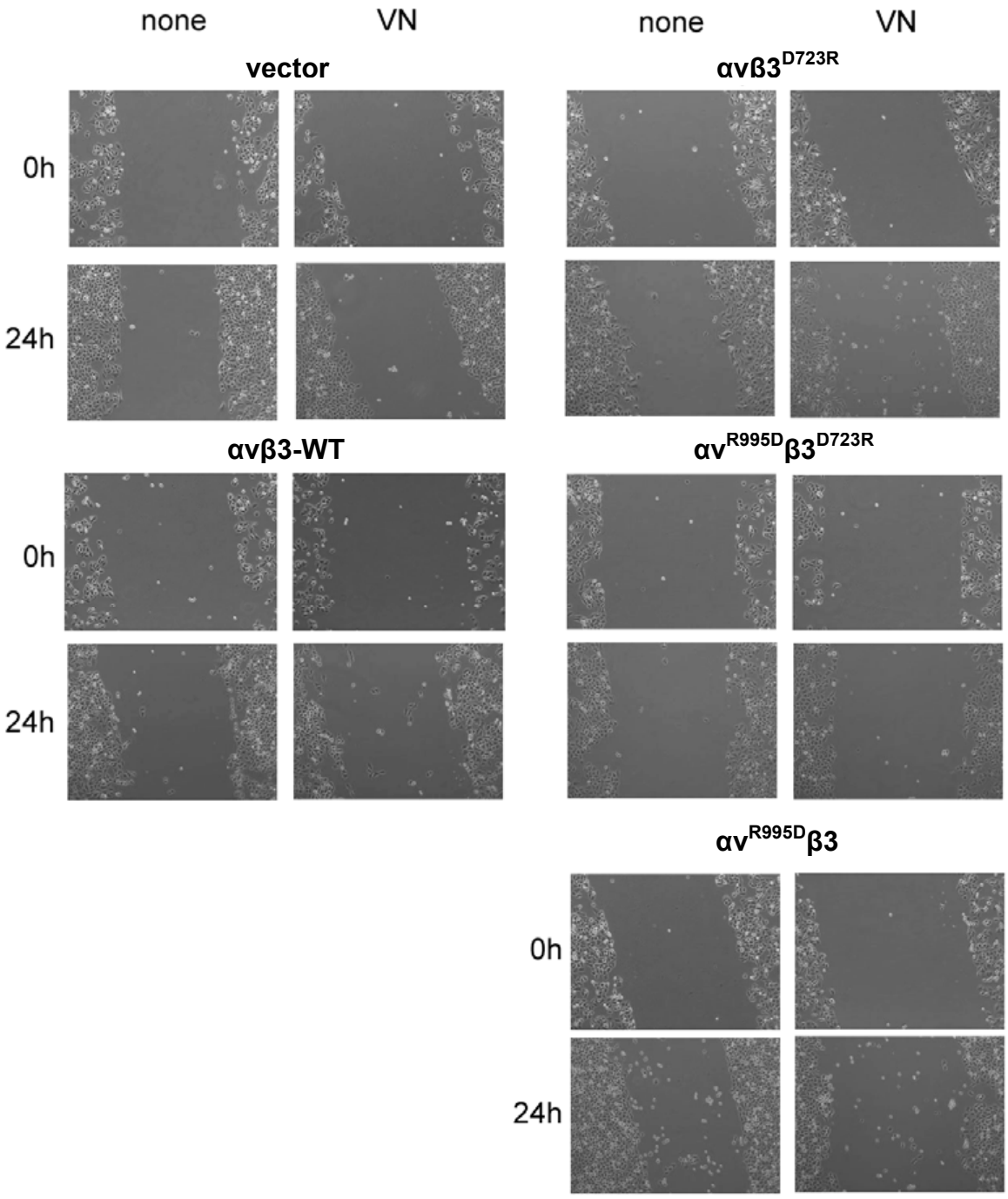

Fig. 46 Effect of integrin αvβ3 salt bridge formation on cell motility

For wound scratch cell migration assays, cells expressing integrin αvβ3 and its salt bridge mutants were passed to non- or VN-coated 12-well cell culture dishes. After cell monolayers reached a confluency of approximately 90%, a homogeneous wound scratch was set by using a sterile pipette tip. Cells that were detached during the wounding procedure were immediately removed by PBS washes. Microscopical images of monolayers were taken immediately after wounding (start) and after 24 h of further cell incubation at 37°C. Pictures of one representative experiment are depicted.

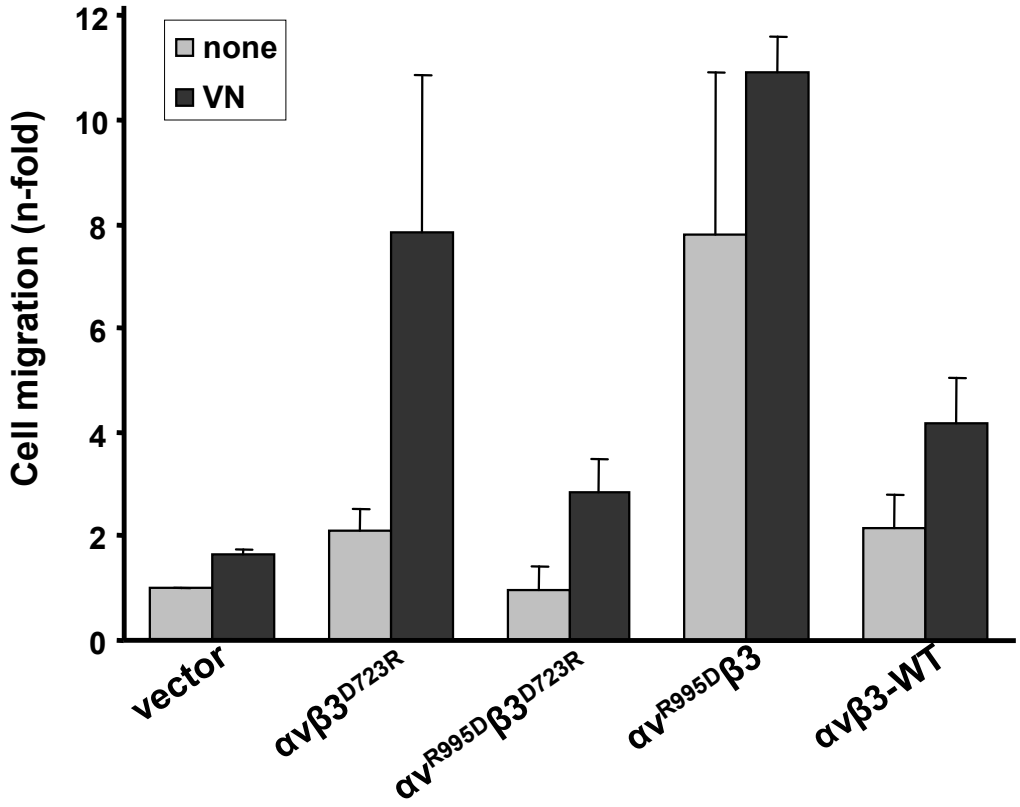

Fig. 47 Quantitative evaluation of cellular motility, dependent on integrin αvβ3 salt bridge formation

The migratory activity of each integrin αvβ3 cell transfectant was quantified by counting the numbers of cells that had invaded the wounds. Mean values for relative cell migratory capacity are given as 'n-fold' by setting the normalised signal for the respective vector-transfected cells grown on VN to "1" (n = 3, ± S.D.).

6.2.5 Changes in integrin αvβ3-dependent cellular adhesion as a function of cytoplasmic salt bridge formation

At sites of focal adhesion, cellular spreading and adhesion is mediated by integrins that bind their respective ligand. To analyse the impact of integrin αvβ3 salt bridge formation on integrin-dependent cellular adhesive capacity, impedance measurements were carried out by use of the xCelligence™ system (Roche). It measures electrical impedance across interdigitated microelectrodes, integrated on the bottom of tissue culture E-plates. This enables the system to detect changes in cellular adhesion and spreading in real time. For this, cells were seeded on E-plates pretreated with VN at a density of 15000 cells and total electrode impedance recorded over a time period of 30 min. Here, cells expressing integrin αvβ3 with a disrupted salt bridge ($\alpha v^{R995D}\beta 3$) showed the highest adhesive capacity. This was

followed by cells expressing the other integrin with abrogated salt bridge formation, αvβ3^{D723R}. Cells displaying integrin αvβ3-WT and αv^{R995D}β3^{D723R} expressed an enhanced adhesive capacity, to the same extent, compared to vector-transfected cells (Fig. 48).

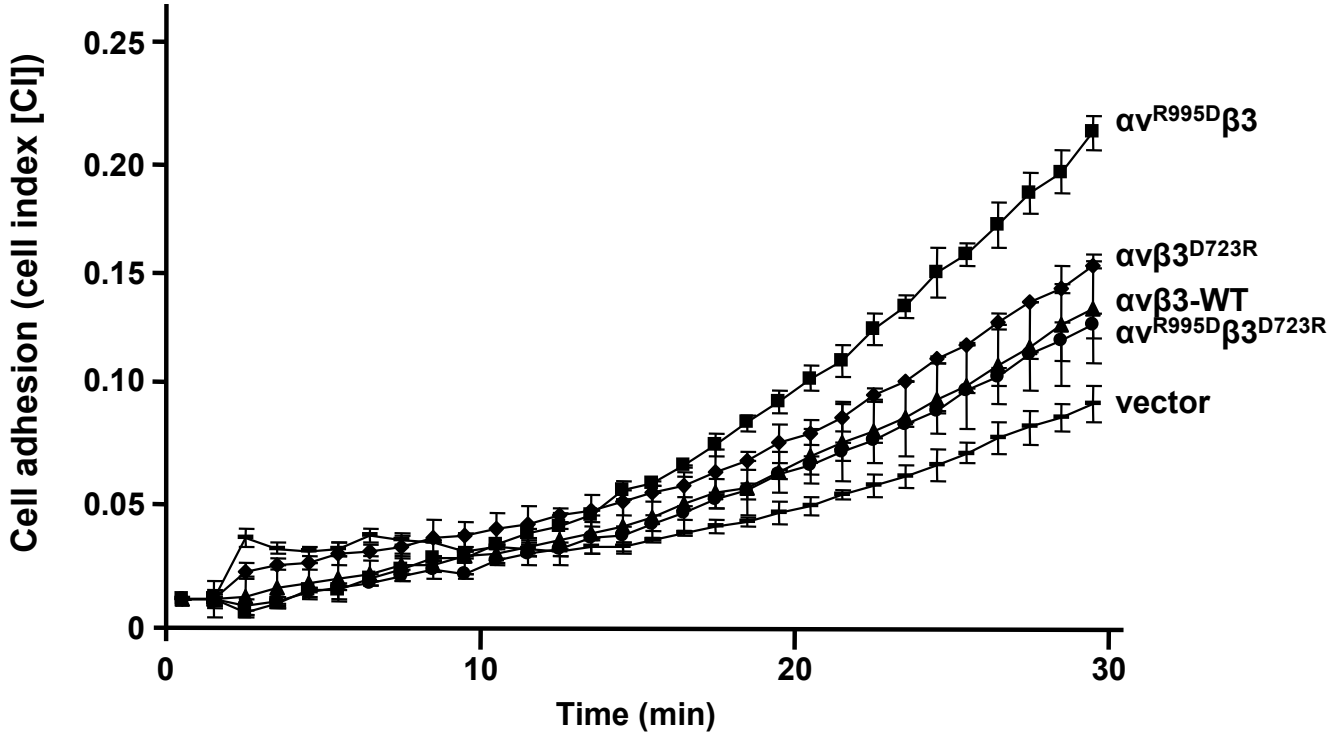

Fig. 48 Impact of integrin αvβ3 salt bridge formation on cellular adhesion

The adhesive strength of cells expressing integrin αvβ3-WT as well as the salt bridge mutants (αvβ3^{D723R}; αv^{R995D}β3; αv^{R995D}β3^{D723R}) was determined by use of the microelectronic real time-cell electronic sensor system *xCelligence system*^{TM}. For this, cells were seeded on VN coated E-plates and cell adhesion recorded over 30 min. Data are given as cell index (CI), representing relative changes in electrical impedance as measure of cell attachment and spreading (n=2, ±S.D.). One representative experiment out of three is depicted.

7 Discussion

7.1 Role of the integrin αvβ3 TMD sequence during integrin activation and signalling

7.1.1 Exchange of the integrin TMD by the TMD of glycophorin A causes conformational changes

Integrins are heterodimeric, transmembrane receptors, which transduce signals bidirectionally across the cell membrane. For the complete fulfilment of its functional features, the integrin receptor requires a special and flexible structure, passing through the cell membrane. The first crystal structures of the integrin αvβ3 ectodomain revealed in the low-affinity state a bent conformation (Xiong et al. 2001; Xiong et al. 2002). Moreover, over the last decade, a plethora of evidence had suggested that the process of integrin activation leads to conformational changes of the receptor (Adair et al. 2002; Takagi et al. 2002a; Luo et al. 2007; Zhu et al. 2008). These changes, leading to the high affinity state, imply extension of the whole, bent integrin receptor and a subunit separation in the transmembrane-cytoplasmic domains (Hantgan et al. 1999). Moreover, mutational studies and molecular modelling revealed that clasping and unclasping between integrin α- and β-TMD and cytoplasmic domains contribute to regulation of integrin activation.

Structures are known in both, active and inactive conformations for integrin extracellular ligand-binding fragments and cytoplasmic domains (Vinogradova et al. 2002; Luo et al. 2007). However, none of these structures include the integrin TMD and signal transmission by these domains across the cell membrane still remains elusive (Zhu et al. 2009). To date, our understanding of the functional mechanism how single protein-TMD associate and contribute to signal transduction through the cell membrane is confined to a limited number of experimental studies on isolated TMD (Zhu et al. 2009). To get further insight into TMD associations of integrins, Gottschalk and co-workers performed molecular dynamics simulation. Two models for the heterodimeric integrin TMD conformation were proposed. First, an integrin resting state, where the TMD interface has a distinct right-handed coiled-coil conformation (Gottschalk et al. 2002). Meanwhile, the proposed structure of the resting bent integrin conformation including its TMD has been confirmed by NMR (Lau et al. 2009) with a root mean square deviation (RMSD) of less than 1 Å between

the proposed computational model and the NMR structure. Second, Gottschalk predicted an activated intermediate integrin conformational state, occurring after inside-out and prior to outside-in signalling. Here, the integrin TMD adopt an energetically favoured transient GpA-like structure (Gottschalk 2005). Moreover, sequence analysis revealed that the integrin subunits and GpA encompass a similar binding motif in their TMD (Gottschalk et al. 2002). In case of GpA the GxxxG motif mediates strong homodimerisation (Lemmon et al. 1992a), whereas in the integrin binding motif the G residues are often substituted by A and S, which mediate specific, hydrophobic TMD interaction but to a much lesser extent (Langosch et al. 1996; Schneider et al. 2004b).

Despite the known fact that integrins adopt different conformations during activation, there is no direct evidence for an intermediate integrin conformation occurring prior to the high-affinity conformational state. The capture of transient conformational states is a major challenge in protein science. Therefore, frequently, model systems are used in order to gain mechanistic insights into such dynamic protein systems. These model systems aim at freezing intermediates by altering the protein sequence. In the present work, the intermediate integrin state is represented by an integrin chimera, expressing the complete TMD of GpA, which encompasses the TMD dimerisation motif GxxxG. Exchange of the integrin αvβ3-TMD by the TMD of homodimeric GpA is accompanied by conformational alterations. In the integrin chimera, the rotational orientation of the β-subunit has changed by approx. 100°, accompanied by an increase in the tilt angle between the two helical TMD (Fig. 49C). This leads to increased helix-helix interactions of the TMD. The TMD of GpA is known to mediate strong homodimerisation between the α-helical backbones of both subunits (Senes et al. 2004). This association is extremely stable and even occurs in the presence of harsh detergents under experimental conditions (Lemmon et al. 1992a; Senes et al. 2004). Consequently, integrin chimeras encompassing the TMD of GpA are hindered to separate their TMD and cytoplasmic regions and thus simulate a clasped TMD. In addition, the altered conformation and tilt angle between the two TMD causes a weakening of the membrane-proximal contacts N-terminal of the TMD (Fig. 49A-C). Those contacts in the leg region help stabilising the closed, low affinity conformation of the integrin. Weakening these contacts may therefore facilitate the transition from a closed, inactive conformation to an open, active conformation in the integrin ectodomains. Furthermore, to mimic a fully activated integrin, an I-mutation was introduced into the GxxxG dimerisation motif (GxxxI) of the GpA TMD, known to

abrogate TMD-clasping. Dissociation of this binding motif occurs because very subtle changes in the side-chain structure at certain sensitive positions disrupt the helix-helix association of the GxxxG dimerisation motif (Lemmon et al. 1992b).

In order to test the impact of the integrin αvβ3-TMD sequence on integrin activation and signal transduction, in the present study integrin chimeras (TMD-GpA; TMD-GpA-I) as well as integrin TMD-αvβ3 were expressed by stable transfection of human ovarian OV-MZ-6 cancer cells. Theoretically, in our model system, the TMD of integrin TMD-GpA is clasped because of the strong interaction of the α-helical backbone of the GxxxG binding motif. This integrin variant represents an intermediate conformation, occurring during integrin activation, whereas integrin TMD-GpA-I represents a fully activated integrin with a dissociated TMD.

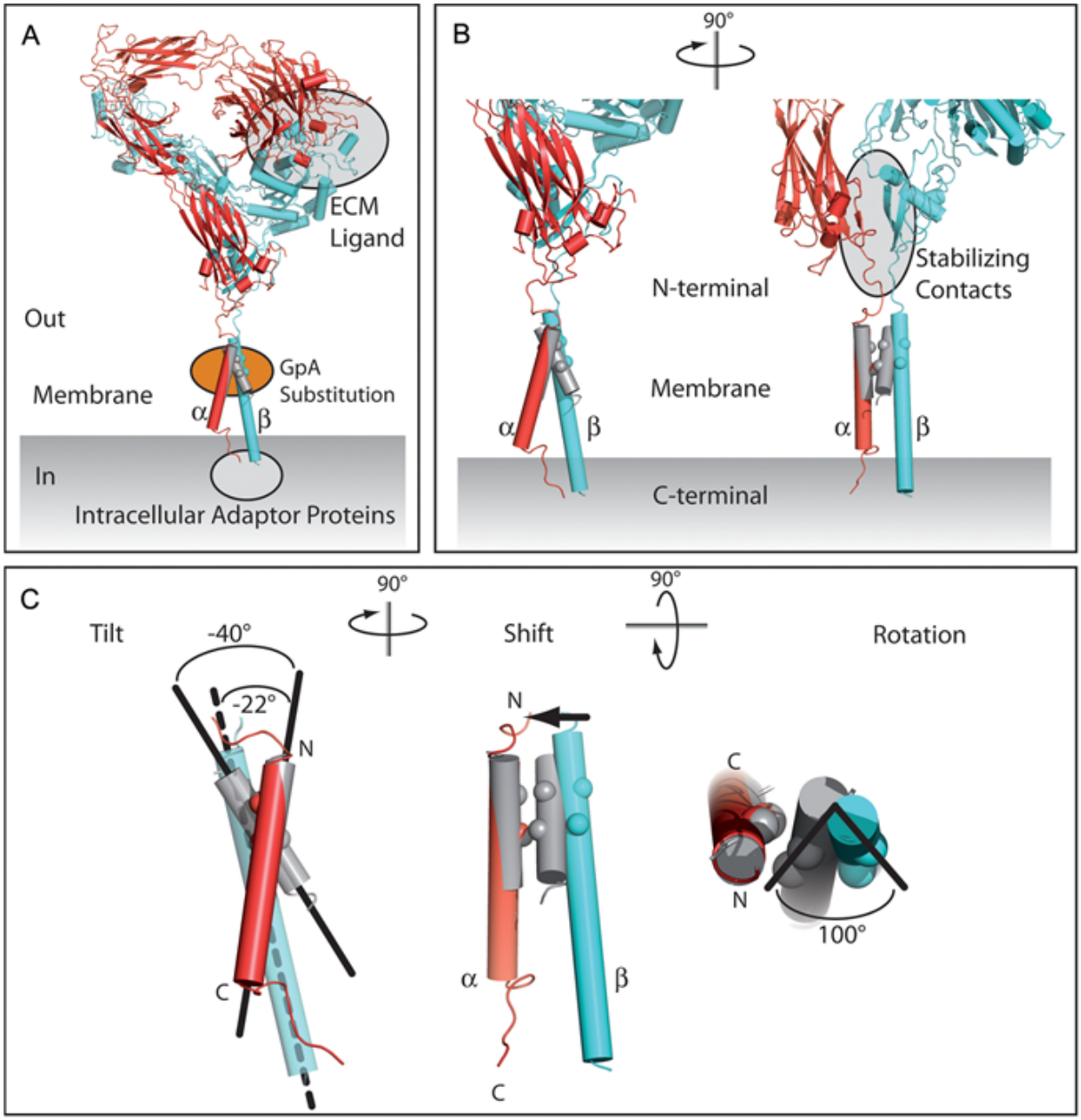

Fig. 49 Exchange of the integrin αvβ3 TMD with the TMD of GpA

A) A cartoon of a model of the full-length integrin is shown. Helices are drawn as cylinders. The α-subunit is depicted in red, the β-subunit in cyan. The ligand binding sites for ECM ligands as well as intracellular adaptor proteins are highlighted. The location of the sequence substitution is shown in orange. A TMD-GpA-conformation is superimposed on the integrin ground state conformation (grey). The superposition was based on the sequence substitution and the TMD-GpA structure was superimposed onto the α-subunit of the integrin. All ligand binding sites are spatially separated from the site of substitution. Any effect of the substitution is therefore an allosteric effect. **B)** Left: Zoom into the membrane-proximal region of A. Right: 90° rotation to the left of the zoom-in. Membrane-proximal contacts N-terminal of the TMD will be allosterically disturbed by the sequence substitution. **C)** Structural comparison of the TMD-GpA conformation (grey) and the integrin ground state TMD conformation. Left: side view; middle: front view; right: top view. The substitution will cause the TMD to be more tilted (left) and more closely packed (middle). Furthermore, the β-subunit will be rotated approximately 100° relative to the α-subunit (right) (Figure courtesy of K. Gottschalk 2011).

7.1.2 The integrin TMD sequence and its effect on outside-in signalling

It is thought that during integrin activation the TMD dissociate and also the cytoplasmic regions become separated. This allows binding of cytoskeletal proteins to the β integrin subunit. Thereby, an indirect link between the receptor and actin components of the cytoskeleton is provided (Calderwood et al. 1999; Brakebusch et al. 2003). This mechanical link is essential for cell migration. Integrins are the major components of focal adhesion sites, where they connect the cell with the underlying ECM. By providing a bond between the cytoskeleton and ECM proteins, integrins act as mechanosensors and serve as cellular traction sites during cell migration (Bershadsky et al. 2003; Puklin-Faucher et al. 2009).

According to our cell model system, engagement of talin and other components of the cytoskeleton with the integrin TMD-GpA cytoplasmic tails is prevented because of the clasped TMD, thereby blocking the respective binding sites. Indeed, immunocytochemical double staining of cells expressing integrin TMD-GpA and being adherent to VN revealed that these integrin αvβ3/GpA chimera and talin were not colocalised. Integrin TMD-GpA was predominantly localised on the cell surface, unlike talin, which was distributed all over the cytoskeleton. In contrast, integrin TMD-αvβ3 and TMD-GpA-I showed a different staining pattern, since both were obviously colocalised with talin on the cell surface. Another cytoskeletal component, whose linkage with integrin αvβ3 is important for integrin-mediated intracellular signalling, is paxillin. In response to integrin clustering paxillin is phosphorylated at position Y118. Thus, it is a marker for enhanced outside-in signalling and integrin clustering (Fuortes et al. 1994; Graham et al. 1994; Zhou et al. 2001). Colocalisation of the integrin αvβ3 TMD mutants and p-paxillin (Y118) was tested by immunocytochemical double staining as well as coimmunoprecipitation. Cells expressing integrin TMD-GpA showed, in the presence of VN, no linkage to p-paxillin (Y118) in contrast to cells displaying integrin TMD-αvβ3 and TMD-GpA-I, respectively. Moreover, the fact that integrin TMD-GpA-I was found to be in complex with p-paxillin, even in the absence of VN as shown by coimmunoprecipitation analysis, denoted a constitutively active integrin state, mimicked by this integrin variant. These results suggested that the integrin TMD-GpA chimera was not able to form complexes with intracellular adaptor proteins of the cytoskeleton. Thus, the ability to establish a linkage between the ECM via integrin αvβ3 to the cytoskeleton is lost upon TMD clasping, whereas TMD-GpA-I

provided a permanent linkage to cytoskeletal components, arising of its separated TMD and cytoplasmic regions.

As a result of integrin inside-out activation and the subsequent conformational rearrangements, including TMD separation, arising thereof, integrins regulate intracellular signalling cascades outside-in. Hence, FAK and other kinases like the MAPK erk$^{-1/-2}$ and PKB/Akt are activated. Integrin TMD-GpA lacks colocalisation with cytoskeletal protein talin. Thus, it was not surprising that, in all assays regarding integrin signalling, the integrin TMD-GpA chimera showed significantly lower phosphorylation and thus activation levels of the most important integrin-related signalling kinases compared to cells transfected with integrin TMD-αvβ3 and TMD-GpA-I, respectively. Hence, introduction of a clasped TMD led to a signalling-defective integrin αvβ3 TMD variant. In another study, performed by Zhu and coworkers (Zhu et al. 2007), integrin TMD clasping was experimentally provoked by introduction of an intersubunit disulfide bond. This approach led to similar results. Here, the generated integrin variant exhibited a profound defect in adhesion-induced outside-in signalling (Zhu et al. 2007). On the contrary, integrin TMD-GpA-I displayed a linkage to cytoskeletal proteins talin and p-paxillin in OV-MZ-6 cells. The unclasped TMD and resulting high affinity conformation of this integrin variant led to enhanced signal transduction outside-in, indicated by phosphorylation of relevant signalling kinases. In addition, the fact that integrin TMD-GpA-I displayed highest cellular signalling kinase phosphorylation levels, even in the absence of VN, argues for a constitutively active integrin αvβ3 TMD variant.

Integrin-mediated activation of intracellular signalling kinases strongly influences cellular processes like migration and proliferation (Giancotti et al. 1999; Howe et al. 2002). One effect of the restricted intracellular signalling in integrin TMD-GpA-transfected cells was the inhibition of their migratory capacity. Integrins act as cellular motors by connecting the cytoskeleton with proteins of the ECM. Our results strongly suggest that integrin TMD-GpA has a deficiency in coupling intracellular adapter proteins due to its clasped TMD. The resulting defect in activation of intracellular signalling cascades and the missing mechanical linkage prevented action of the cellular motors and inhibited cell migration. On the contrary, cells expressing integrin TMD-GpA-I showed the highest migratory capacity, even in the absence of VN. TMD-opening followed by connection to cytoskeletal adapter proteins and enhanced signal transduction of this integrin variant was also reflected by upregulated cell proliferation.

7.1.3 Impact of the clasped/unclasped integrin TMD on cellular adhesion

Integrins mediate cellular adhesion and contribute to cellular coherence by binding to different proteins of the ECM. Cellular adhesion is regulated by integrin inside-out signalling also termed integrin activation (Shattil et al. 2010). In principle, cellular adhesion can be divided in two steps: a) the initial attachment of a cell to a surface and b) the increase in the number of adhesive bonds following the initial attachment (Boettiger 2007). In this work, the adhesive capacity of integrin αvβ3 and its TMD mutants, with respect to its main ligand VN, was tested in three different experimental approaches. First, initial cellular adhesion was evaluated by impedance measurements. Second, cellular adhesion after short contacts with VN was measured by AFM. Third, cellular adhesion on longer time scales, which allow for cytoskeletal reorganisation and the formation of focal adhesions, was quantified by a spinning disc device.

For determination of initial cellular adhesive strength and spreading capacity, impedance measurements were performed. Interestingly, OV-MZ-6 cells transfected with integrin TMD-GpA-I and TMD-GpA showed an enhanced spreading capacity compared to cells transfected with integrin TMD-αvβ3. As expected, lowest adhesive capacity was observed for vector-transfected cells, which display low endogenous integrin αvβ3 levels. AFM measurements probed the cellular adhesive capacity under force, applied by the VN-coated cantilever towards a single cell. These studies revealed that cells expressing integrin TMD-GpA exhibited an increased adhesion rate towards VN and formed bonds more rapidly than those displaying integrin TMD-GpA-I. This might be caused by the clasped TMD of integrin TMD-GpA, which inhibits talin binding to the β3 cytoplasmic tail, as documented by the lack of colocalisation. Since talin is required to couple the integrin to the actin cytoskeleton, an inhibition of talin binding increases the lateral diffusion of the integrin TMD-GpA within the cell membrane. Therefore, the increased adhesion rate observed for cells expressing integrin TMD-GpA compared to both, TMD-GpA-I and TMD-αvβ3, can be explained by an increased lateral diffusion of this integrin construct within the cell membrane. Enhanced lateral diffusion may also favour increased cellular spreading capacity of cells expressing integrin TMD-GpA, as noticed during impedance measurements. Due to this lateral mobility in the cell membrane, this integrin mutant is able to bind rapidly to its ligand. In contrast, the observed higher spreading capacity of cells expressing integrin TMD-GpA-I compared to integrin TMD-αvβ3 more likely depends

on enhanced integrin clustering. Clustering of this integrin variant occurs because of the constitutively activated conformation. Thus, cells expressing integrin TMD-GpA-I are able to form focal adhesions and spread faster than cells displaying integrin TMD-αvβ3. Moreover, AFM measurements demonstrated that integrin TMD-GpA-I expressing cells rapidly disrupted from the VN-coated cantilever. Most interestingly, this was also accompanied by an increase in force needed for braking single tethers compared to integrin TMD-αvβ3. This combination indicates a constitutive linkage to the cytoskeleton, due to the separated TMD of the integrin TMD-GpA-I variant. An integrin coupled to the cytoskeleton is less flexible than an integrin that is freely diffusible within the membrane. This stiffness leads to faster disruptions of the integrin αvβ3/VN-interactions, but it also required the same high disruption force compared to integrin TMD-GpA. Additional to the rapid bond formation of integrin TMD-GpA with VN, the altered TMD sequence led to a strengthening of the integrin-ligand bond under force. When probed under external forces by performing AFM, integrin TMD-GpA showed an increase in force needed for breaking single tethers compared to integrin TMD-αvβ3. This demonstrated that integrin TMD-GpA-ligand bonds are better suited to withstand external forces than integrin TMD-αvβ3. Since the extracellular integrin domains, constituting the ligand binding site, were unaltered in the different integrin GpA TMD chimera, the observed effect argues for a conformational change.

AFM measurements of initial integrin-ligand bond formation demonstrated an increased adhesion rate for cells expressing integrin TMD-GpA compared to cells expressing TMD-GpA-I or TMD-αvβ3. Moreover, the defect of integrin TMD-GpA in coupling cytoskeletal proteins and the resulting increased lateral diffusion of this integrin variant within the cell membrane raised the question if the observed increase in force, needed for breaking single tethers of integrin TMD-GpA compared to integrin TMD-αvβ3, was an effect of enhanced affinity or avidity. Affinity describes the strength of a single receptor-ligand bond, whereas avidity is the combined strength of multiple bond interactions. Thus, to compare the measured adhesive strength, the present study aimed at distinguishing whether the observed strong adhesive capacity of integrin TMD-GpA was in fact due to enhanced affinity towards VN. To test this, the adhesive strength of the integrin TMD variants was additionally evaluated by usage of a spinning disc device. This method is well suited for quantification of adhesive integrin-ligand bonds, which assemble on longer time scales. The mean shear stress, which is required for cell detachment, is proportional to the number of

adhesive integrin-ligand bonds (Garcia et al. 1997; Boettiger et al. 2001; Shi et al. 2003). Hence, the number of integrin-ligand bonds measured by a spinning disc device is proportional to the affinity of the bond strength. Integrin TMD-GpA and TMD-GpA-I, respectively, exerted a higher and very similar adhesive strength compared to integrin TMD-αvβ3. This fact denoted for an increased affinity of both integrin variants towards VN. Yet, in the first 60 min of adhesion a more rapid bond formation of integrin TMD-GpA with VN was observed compared to integrin TMD-GpA-I. Taken together these data indicated that integrin TMD-GpA, when probed under force, is able to form bonds to VN with, at least, the same affinity as TMD-GpA-I. Surprisingly, data gained by all three methods revealed that cells expressing the signalling-deficient integrin αvβ3 variant TMD-GpA, with a clasped TMD, showed an increased capacity of cellular adhesion comparable to this seen in cells expressing the open, constitutively active integrin TMD-GpA-I variant. This is in apparent contrast to recent data by Springer and co-workers (Zhu et al. 2009). They showed that the affinity of integrin αIIbβ3 to FN decreased upon substitution of the integrin αIIbβ3 TMD by a GpA TMD sequence. Reasons for these conflicting results might arise from different experimental approaches for evaluating ligand binding. In the latter study, they measured binding of a soluble ligand, whereas in the present work, binding of integrin αvβ3 to VN was determined to a surface-immobilised ligand. This mirrors physiological conditions in which integrin ligands are firmly deposited into the surrounding ECM. It is a matter of fact that the kinetic of bond formation is drastically affected when reaction partners are retained to surfaces or membranes (Bell 1978). This is caused by a stiffer, more physiological environment, raising forces between cellular receptors and ligands. Integrins act as mechanosensors (Bershadsky et al. 2003; Puklin-Faucher et al. 2009). Thus, binding of immobilised VN enhances forces between receptor and ligand. The conformational basis for an adhesion functioning integrin with a clasped TMD is the higher tilt angle between both subunits of integrin TMD-GpA, arising of the strong dimerisation motif GxxxG (Fig. 49C). This causes a weakening of the membrane-proximal contacts N-terminal of the TMD. In the integrin legs, those contacts assist to stabilise the closed, low-affinity integrin conformation. Weakening of these contacts may therefore facilitate the transition from a closed, inactive conformation to an open, active integrin conformation, which is stimulated under force to bind a ligand. Interestingly, the strong TMD-dimerisation within the integrin TMD-GpA mutant inhibits proper control over the functional integrin states. Naturally, a flexible integrin structure is required that allows conformational changes,

necessary for integrin activation. Hence, TMD-dimerisation in a GpA-like conformation must be suboptimal for integrins compared to GpA itself. In most integrins, one of the G in the GxxxG motif is A or S, a residue small enough to allow dimerisation but thermodynamically less stable than the unmodified GxxxG motif in the GpA TMD (Senes et al. 2004). Such a modified interaction motif thermodynamically allows in integrins the transition between different TMD conformations of interacting TMD-helices and enables TMD dissociation. This sequence is therefore optimised for the conformational plasticity needed in integrins as opposed to GpA.

7.1.4 A flexible integrin TMD regulates inside-out and outside-in activation

For the present study, an integrin αvβ3 model system reflecting the different proposed conformational stages during integrin activation was created. It implies an intermediate integrin conformation with a clasped TMD, representing an integrin after inside-out and prior to outside-in signalling (TMD-GpA), and an integrin in its active conformation with an open TMD (TMD-GpA-I). Those here presented integrin αvβ3 cell transfectants - TMD-GpA or TMD-GpA-I - are models for two extremes: 1. activated clasped TMD-helices and 2. dissociated TMD-helices. The data of the present study demonstrated that a signalling- and migration-incapable integrin αvβ3-TMD-mutant with associated TMD (TMD-GpA) still supports strong and rapid cell adhesion. This chimera displays the characteristics of an intermediate integrin activation state, occurring right after inside-out signalling but prior to outside-in signalling (Fig. 50). The integrin TMD-GpA might represent a primed state, which is of low basal affinity in the absence of forces, but may form strong bonds in the presence of forces. Thus, this integrin variant is ideally suited to act as a force sensor. Hence, the integrin TMD-GpA mutant might represent a well-suited integrin model construct mimicking a so far still elusive signalling intermediate state.

In conclusion, by cellular expression of integrin chimera encompassing the TMD of GpA with unaltered intracellular and extracellular integrin domains, we were able to decouple outside-in from inside-out signalling. Here, we showed that outside-in signal transduction is not needed for strong integrin-mediated cell adhesion, it is, however, mandatory for cell migration. The WT integrin αvβ3 is flexible and able to adopt different states, whereas TMD-GpA arrests the integrin in an intermediate state and

TMD-GpA-I in a constitutively fully activated state (Fig. 50). This demonstrates that integrin function can be allosterically fine-tuned through the integrin TMD. Hence, the different TMD sequences in various integrins may be functionally important. Future studies will focus on two questions: a) is a GpA-like intermediate state physiologically existing; and b) do the differences in the integrin TMD variants reflect different requirements in signalling plasticity.

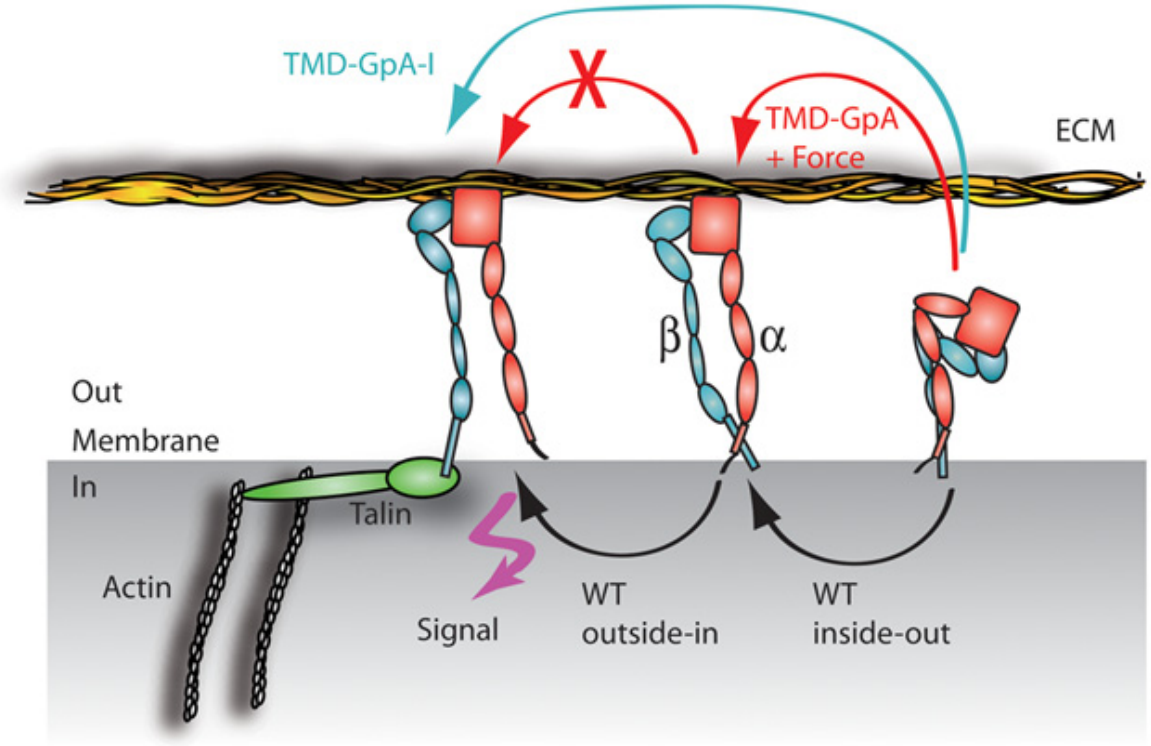

Fig. 50 Scheme of the proposed mechanism of integrin activation and signalling

The substitution of the integrin αvβ3 TMD by that of GpA causes a primed integrin state that is easily activated by force, but inhibits full activation due to strong TMD helix-helix interactions. Then again, the integrin TMD-GpA-I substitution causes a constitutively active integrin that is linked to intracellular adaptor proteins. These two model constructs may imitate different conformational stages during integrin αvβ3 signalling (Figure courtesy of K. Gottschalk 2011).

7.2 Functional role of the integrin αvβ3 cytoplasmic salt bridge during integrin activation and signalling

7.2.1 Disruption of the stabilising integrin αvβ3 cytoplasmic salt bridge

The cytoplasmic integrin domains play an important role in binding of intracellular proteins and in integrin activation. Membrane-proximal between the largely unstructured cytoplasmic tails, electrostatic interactions occur, including a salt bridge formed between amino acids of both integrin subunits (Hughes et al. 1996; Vinogradova et al. 2002; Lau et al. 2009). Salt bridges at the interface of two associating proteins contribute to stabilise dimerisation of certain domains (Donald et al. 2010). In the low affinity conformation, the integrin TMD are, at the transition to the cytoplasmic tails, in close proximity, which is inevitable for the formation of a salt bridge. Therefore, a plethora of evidence suggests that the low-affinity, bent integrin conformation is stabilised by a salt bridge formed between a positively (αv R995) and a negatively (β3D723) charged amino acid of the cytoplasmic tails (Hughes et al. 1996; Partridge et al. 2005; Ma et al. 2006; Lau et al. 2009). Support for the idea that an αv (R995)/ β3 (D723) salt bridge is an important constraint for the low-affinity state comes from NMR spectroscopical data. These revealed multiple hydrophobic and electrostatic contacts between the membrane-proximal helices of the integrin αIIb- and β3-cytoplasmic tails (Vinogradova et al. 2002). The salt bridge forming amino acids are located within highly conserved sequences of the αv- (GFFK**R**) and β3- (KLLITIH**D**) subunit (Hughes et al. 1996; Vinogradova et al. 2002; Lau et al. 2009). The conservation of this binding motif among the different integrins is a hint for the significance of the salt bridge.

In-vitro studies verified the importance of the stabilising integrin cytoplasmic salt bridge. It was shown that mutational disruption of the salt bridge in integrin αIIbβ3 or α5β1 promoted constitutive integrin signalling (O'Toole et al. 1994; Hughes et al. 1996). Furthermore, in a mouse model, it has been demonstrated that disruption of the integrin α4β7 salt bridge (α4 R/A^{GFFKR}) leads to changes of adhesion dynamics. Here, loss of the interaction destabilised the non-adhesive integrin conformation, thereby fostering integrin-mediated leukocyte adhesion and disturbing the properly balanced cycles of adhesion and de-adhesion required for efficient cell migration (Imai et al. 2008). However, the relevance of integrin cytoplasmic salt bridge formation for receptor activation is still a matter of debate. The group around

Campbell failed to detect significant interactions between both integrin tails by NMR studies (Ulmer et al. 2001). Moreover, Fässler and co-workers exchanged in an in-vivo mouse model the β1 salt bridge forming D into A (Czuchra et al. 2006). Despite this mutation of the salt bridge forming amino acids, the mice did not show any obvious phenotype. Primary keratinocytes, isolated form these mice, did not display any changes in adhesion, spreading, and migration compared to WT control cells. Therefore, it was suggested that the membrane-proximal salt bridge between α- and β1-cytoplasmic tails has no apparent function under physiological conditions in vivo (Czuchra et al. 2006).

Considering these contradictory results, it was reasonable to further elucidate the functional role of the integrin cytoplasmic salt bridge. Thus, in the present study, we focussed on the integrin αvβ3 cytoplasmic salt bridge and its role during integrin activation and signalling.

7.2.2 Integrin αvβ3 salt bridge disruption results in enhanced inside-out and outside-in signalling

Disruption of the integrin αvβ3 membrane-proximal salt bridge and its impact on integrin activation has not been shown before. To highlight its role, we disrupted the salt bridge by introduction of charge reversal mutations (αvR995D; β3D723R). First, the influence of these mutations on integrin-triggered intracellular signalling cascades outside-in was tested. For this, phosphorylation and thus activation of integrin-related signalling kinases FAK, MAPK/erk$^{-1/2}$, and PKB/Akt was determined as a measure of integrin-mediated intracellular signalling. The fact that cells expressing integrin αvβ3 with a disrupted salt bridge ($\alpha v^{R995D}\beta 3$) showed highest activation of intracellular signalling cascades, even in the absence of the ligand VN, denotes a constitutively active state of this integrin αvβ3 variant. Cells expressing integrin $\alpha v\beta 3^{D723R}$, also lacking salt bridge formation, also provoked higher activation levels of the studied signalling kinases compared to those expressing integrin αvβ3-WT. However, this occurred predominantly in the presence of VN or when activated with 5 mM Mn^{2+}. The charge reversal mutation integrin $\alpha v^{R995D}\beta 3^{D723R}$ initiated signalling kinase activation comparable to that displayed by cells expressing integrin αvβ3-WT. Moreover, both integrin variants with a disrupted salt bridge showed a more intense staining pattern of p-FAK at sites of focal adhesions than cells expressing integrin

αvβ3-WT or $\alpha v^{R995D}\beta 3^{D723R}$. Our data are in accordance with earlier results of Hughes and coworkers, who documented that the charge reversal mutation may restore the potential salt bridge between the α- and β-subunits (Hughes et al. 1996). Additionally, a constitutive linkage of integrin $\alpha v^{R995D}\beta 3$ with the cytoskeletal components talin and p-paxillin (Y118) was demonstrated by colocalisation studies in the absence of VN. This is an indication for integrin clustering and enhanced outside-in signalling. The other salt bridge abrogating mutant of integrin αvβ3 ($\alpha v\beta 3^{D723R}$) also demonstrated enhanced colocalisation with talin and p-paxillin. This denotes, in combination with the results of enhanced signalling in the presence of VN, for an intermediate activation of this integrin variant.

These results were also reflected by integrin αvβ3-mediated cell migratory and proliferative capacity. As a result of enhanced signal transduction, cells transfected with integrin $\alpha v^{R995D}\beta 3$ showed highest migratory capacity, even in the absence of VN. This demonstrated the constitutively activated nature of this integrin variant. Interestingly, cells expressing integrin $\alpha v\beta 3^{D723R}$ showed an enhanced migrative capacity only in the presence of VN. The results regarding cell migration are in contrast to the observations by Imai and coworkers (Imai et al. 2008). They observed strong integrin-mediated cell adhesion upon salt bridge disruption within the cytoplasmic domains of the leukocyte integrin α4β7. Thereby, the delicate balance of adhesion and de-adhesion, required for efficient and directed lymphocyte migration is disturbed. However, different to our experimental approach, they performed complex transendothelial migration assays with leukocytes. We performed wound scratch cell migration assays. Here, the constitutive linkage, predominantly observed for integrin $\alpha v^{R995D}\beta 3$, with cytoskeletal components like talin and paxillin enabled permanent triggering of integrin-regulated signalling kinases MAPK/$erk^{-1/-2}$. This in turn activated the MLCK, which led to enhanced cellular migration through activated myosin motors and their induction of the contraction of cellular actin bundles (Tanaka-Takiguchi et al. 2004).

The integrin cytoplasmic domains are strongly involved in integrin inside-out activation (O'Toole et al. 1994; Takagi et al. 2001). Thus, disruption of the stabilising salt bridge leads to enhanced integrin activation and inside-out signalling (Hughes et al. 1996; Imai et al. 2008). Indeed, we observed the highest capacity of initial cellular adhesion and spreading in cells expressing the active integrin $\alpha v^{R995D}\beta 3$. This was followed, by cells expressing the other salt bridge disrupting variant $\alpha v\beta 3^{D723R}$. Cells expressing integrin αvβ3-WT or $\alpha v^{R995D}\beta 3^{D723R}$ showed a comparable but lower

adhesive capacity. These results perfectly reflect the data gained by activation assays of Hughes and coworkers, regarding the platelet integrin αIIbβ3 (Hughes et al. 1996). After induction of integrin activation by ligand-induced binding site–6 antibody (LIBS6), they measured binding of the αIIbβ3 antibody (PAC1), which recognises integrin αIIbβ3 in the high-affinity conformation. Cells expressing integrin αIIb^{R995D}β3 and, to a lesser extent αIIbβ3^{D723R}, exhibited higher activation levels compared to WT integrin αIIbβ3. Moreover, Hughes and coworkers demonstrated that the charge reversal mutant αIIb^{R995D}β3^{D723R} complemented the activating effect of the individual mutations. They suggested that this double mutation may restore the potential salt bridge between the α- and the β-subunit, thus reforming the structural constraints that prevent the activation of the integrin.

7.2.3 The electrostatic/hydrophobic contacts of the integrin cytoplasmic interface

In the present study, we demonstrated the importance of the integrin αvβ3 cytoplasmic salt bridge for stabilising the transmembrane-cytoplasmic domain in the low-affinity conformation. Both, inside-out and outside-in integrin-mediated signalling were constitutively activated by mutational disruption of the salt bridge. All of the performed cell biological assays demonstrated that by restoring the integrin salt bridge through charge reversal amino acids, its stabilising effect was regained. In all assays, cells expressing integrin αv^{R995D}β3^{D723R} showed the same characteristics as cells expressing integrin αvβ3-WT. Thus, it can be assumed that via introduction of a charge reversal mutation on both integrin subunits, at least parts of the salt bridge forming contacts are restored, helping to stabilise the integrin in a non-active conformation.

Moreover, we observed that cells expressing integrin αv^{R995D}β3 with a disrupted salt bridge were fully activated and capable of complete signal transduction, even in the absence of VN. However, cells expressing αvβ3^{D723R} also displayed enhanced signalling levels and inside-out activation compared to cells expressing integrin αvβ3-WT but lower levels than cells expressing integrin αv^{R995D}β3. Moreover cells expressing integrin αvβ3^{D723R} required engagement by the ligand VN to be fully activated, other than the constitutively active cells expressing integrin αv^{R995D}β3. An NMR solution structure of integrin αIIbβ3 provides an explanation for this observed

intermediate activation. It gave insight into the hydrophobic and electrostatic interactions between the integrin cytoplasmic tails. Here, it was shown that the electrostatic interface of the cytoplasmic tails mainly involves one amino acid of the αIIb-subunit but more than one amino acid of the β3-cytoplasmic tail (Vinogradova et al. 2002) (Fig. 51). These hydrophobic and electrostatic interactions occur between: αIIb R995 (guanidyl group) + β3 D723 (carboxyl group); αIIb R995 (guanidyl group) + β3 E726 (carboxyl group); αIIb R995 (guanidyl group) + β3 H722 (imidazole group).

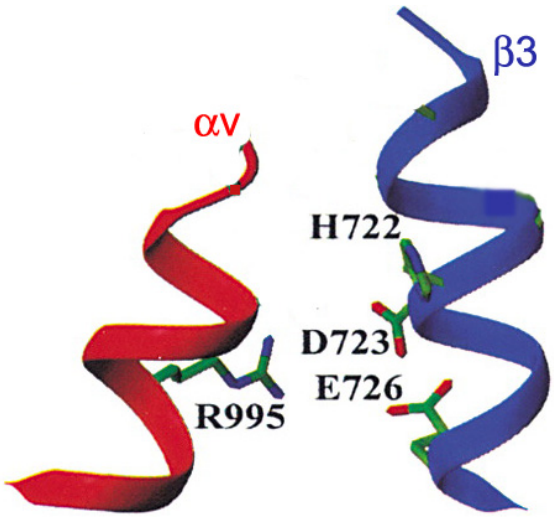

Fig. 51 Amino acids of the integrin αv- and β3-subunit that contribute to the electrostatic contacts of the cytoplasmic interface

The electrostatic contacts of the integrin cytoplasmic tails mainly involve side chains of the following pairs: αvR995 (guanidyl group)-β3H722 (imidazole group), αvR995 (guanidyl group)-β3D723 (carboxyl group), and αvR995 (guanidyl group)-β3E726 (carboxyl group) (Vinogradova et al. 2002) (Figure modified from Vinogradova et al. 2002).

Thus, in the present study, by mutation of αvR995 to D not only the main interaction with β3D723 but also the adjacent electrostatic interactions of the interface seem to be abrogated. Otherwise, when β3D723 is mutated to R, parts of the electrostatic interactions may be rescued by interaction of αvR995 with E726 and H722 of the β3-tail. Therefore, the cytoplasmic electrostatic contacts between the integrin αvR995D and β3 WT chain ($\alpha v^{R995D}\beta 3$) are more destabilised than in the $\alpha v\beta 3^{D723R}$ integrin mutant, leading to the observed effects.

The integrin $\alpha v\beta 3^{D723R}$ variant showed an intermediate state of activation. It constitutively bound talin in immunocytochemical colocalisation studies. However, in the absence of VN, activation of intracellular signalling cascades was not upregulated compared to integrin αvβ3-WT. Moreover, the adhesive strength and spreading

capacity of these cells was lower than that of cells expressing the fully activated integrin $\alpha v^{R995D}\beta 3$ but higher than that of those expressing the integrin αvβ3-WT. Our data are supported by data of Hughes and co-workers, who demonstrated that upon activation, cells expressing integrin $\alpha IIb^{R995D}\beta 3$ showed an approximately 2-fold enhanced binding of the activation specific antibody PAC1 directed to αIIbβ3, compared to those displaying $\alpha IIb\beta 3^{D723}$ (Hughes et al. 1996). Moreover, this partial integrin activation was also shown for the naturally occurring integrin mutations $\alpha IIb\beta 3^{D723H}$ and $\alpha IIb\beta 3^{D723A}$ (Schaffner-Reckinger et al. 2009). Both were found in patients with macrothrombocytopenia, an autosomal platelet disorder that is comprised of mild thrombocytopenia, platelet anisocytosis, and giant platelets. In this study, the intermediately activated integrin initiated an unexpected outside-in signalling, including a decrease in Ras homolog gene family member A (RhoA) activity, when expressed in non-megakaryocytic Chinese hamster ovary cells (CHO). This resulted in mimicking of megakaryocyte microtubule-driven pro-platelet formation. Schaffner-Reckinger and coworkers provided evidence that only partially activated integrin $\alpha IIb\beta 3^{D723H}$ and $\alpha IIb\beta 3^{D723A}$, but not a fully activated integrin αIIbβ3 mutant, were capable of initiating a signalling cascade in CHO cells causing a decrease in RhoA activity compared to αIIbβ3-WT (Schaffner-Reckinger et al. 2009). However, in a mouse model, disruption of the integrin α5β1 salt bridge, by mutation of the β1 cytoplasmic salt bridge forming amino acid, did not result in obvious impairment of the phenotype (Czuchra et al. 2006). As a consequence, the group around Fässler argued that the integrin cytoplasmic salt bridge has no apparent function in vivo. We also demonstrated in our study that the integrin $\alpha v\beta 3^{D723R}$ variant, which displays an intermediate state in integrin activation, does not necessarily result in constitutively activated integrin-mediated signalling. This is, because parts of the electrostatic interactions of the cytoplasmic tails are rescued by side interactions of αvR995D with E726 and H722 of the β3 tail. Comparing the amino acid sequences of αv(human)/α5(mouse) and β3(human)/β1(mouse) reveals that the parts coding for the integrin cytoplasmic tails are strongly conserved. In case of the αv/α5 subunits, both contain the GFFKR-motif, in case of β3/β5 both contain the KLLITIHDxxE-motif. Thus, the integrin cytoplasmic electrostatic interactions might also be rescued in the mouse integrin $\alpha 5\beta 1^{D759A}$ mutant. Consequently, this integrin variant did not result in a different phenotype in mice keratinocytes.

In summary, we propose that the interchain salt bridge in the integrin αvβ3 cytoplasmic domains is instrumental for the regulation of the adhesive strength and

the signalling state of integrin αvβ3. Our findings underline the functional role of the integrin cytoplasmic salt bridge in conformation-dependent integrin activation.

7.3 Conclusion- The integrin TMD and cytoplasmic contacts are essential for proper receptor activation and regulation

Integrins are allosterically regulated during the process of integrin activation. Binding of ECM ligands leads to conformational changes of the receptor, which then results in changes of intracellular signal transduction. In order to block αv-integrin-mediated cellular adhesion and signalling by engagement of the ligand binding site, a functional blocking mAb as well as an RGD-peptide were developed. However, in clinical trials, these attempts were not as effective as noticed in in-vitro studies. Thus, future works might focus on the development of allosteric inhibitors, capable of locking integrins in an inactivated state. For this, a detailed knowledge of the molecular mechanisms and conformational changes underlying integrin activation is mandatory. In this context, the present work dealt with the question what role a flexible regulation of the integrin TMD and cytoplasmic regions plays during integrin activation and signalling. One scientific aim was to provide evidence that the integrin intermediate conformational state exists during activation. In this work, it was demonstrated that integrins are allosterically fine-tuned through their TMD. An integrin with a clasped TMD (TMD-GpA) mediated strong adhesion to VN but prevented outside-in signalling. This chimera shows the characteristics of an intermediate integrin activation state occurring right after inside-out signalling but before outside-in signalling. In contrast, an unclasped integrin TMD (TMD-GpA-I) or disruption of the stabilising cytoplasmic contacts led to enhanced integrin inside-out activation and constitutive signal transduction outside-in of the cells. Thus, our data further underline the importance of the TMD conformation. In this context, we suggest that the varying sequences of different integrin TMD may have an influence on integrin activation. Moreover, the cytoplasmic electrostatic interactions were shown to be necessary for correct integrin regulation. Therefore, proper regulation of the complex processes of integrin activation and signalling is dependent on the stabilising, but flexible contacts of the transmembrane-cytoplasmic domains.

Aaboe, M., B.V. Offersen, A. Christensen and P.A. Andreasen PA (2003). “Vitronectin in human breast carcinomas.” Biochim Biophys Acta 1638(1): 72-82.

Adair, B. D. and M. Yeager (2002). "Three-dimensional model of the human platelet integrin alpha IIbbeta 3 based on electron cryomicroscopy and x-ray crystallography." Proc Natl Acad Sci U S A 99(22): 14059-64.

Alghisi, G. C., L. Ponsonnet and C. Ruegg (2009). "The integrin antagonist cilengitide activates alphaVbeta3, disrupts VE-cadherin localization at cell junctions and enhances permeability in endothelial cells." PLoS One 4(2): e4449.

Anthis, N. J., K. L. Wegener, F. Ye, C. Kim, B. T. Goult, E. D. Lowe, I. Vakonakis, N. Bate, D. R. Critchley, M. H. Ginsberg, et al. (2009). "The structure of an integrin/talin complex reveals the basis of inside-out signal transduction." Embo J 28(22): 3623-32.

Arnaout, M. A., B. Mahalingam and J. P. Xiong (2005). "Integrin structure, allostery, and bidirectional signaling." Annu Rev Cell Dev Biol 21: 381-410.

Bazzoni, G., D. T. Shih, C. A. Buck and M. E. Hemler (1995). "Monoclonal antibody 9EG7 defines a novel beta 1 integrin epitope induced by soluble ligand and manganese, but inhibited by calcium." J Biol Chem 270(43): 25570-7.

Beck, V., H. Herold, A. Benge, B. Luber, P. Hutzler, H. Tschesche, H. Kessler, M. Schmitt, H. G. Geppert and U. Reuning (2005). "ADAM15 decreases integrin alphavbeta3/vitronectin-mediated ovarian cancer cell adhesion and motility in an RGD-dependent fashion." Int J Biochem Cell Biol 37(3): 590-603.

Bell, G. I. (1978). "Models for the specific adhesion of cells to cells." Science 200(4342): 618-27.

Bershadsky, A. D., N. Q. Balaban and B. Geiger (2003). "Adhesion-dependent cell mechanosensitivity." Annu Rev Cell Dev Biol 19: 677-95.

Boettiger, D. (2007). "Quantitative measurements of integrin-mediated adhesion to extracellular matrix." Methods Enzymol 426: 1-25.

Boettiger, D., F. Huber, L. Lynch and S. Blystone (2001). "Activation of alpha(v)beta3-vitronectin binding is a multistage process in which increases in bond strength are dependent on Y747 and Y759 in the cytoplasmic domain of beta3." Mol Biol Cell 12(5): 1227-37.

Brakebusch, C. and R. Fassler (2003). "The integrin-actin connection, an eternal love affair." Embo J 22(10): 2324-33.

Brooks, P. C., A. M. Montgomery, M. Rosenfeld, R. A. Reisfeld, T. Hu, G. Klier and D. A. Cheresh (1994). "Integrin alpha v beta 3 antagonists promote tumor regression by inducing apoptosis of angiogenic blood vessels." Cell 79(7): 1157-64.

Brooks, P. C., S. Stromblad, R. Klemke, D. Visscher, F. H. Sarkar and D. A. Cheresh (1995). "Antiintegrin alpha v beta 3 blocks human breast cancer growth and angiogenesis in human skin." J Clin Invest 96(4): 1815-22.

Burnett, G. and E. P. Kennedy (1954). "The enzymatic phosphorylation of proteins." J Biol Chem 211(2): 969-80.

Cabodi, S., P. Di Stefano, P. Leal Mdel, A. Tinnirello, B. Bisaro, V. Morello, L. Damiano, S. Aramu, D. Repetto, G. Tornillo, et al. (2010). "Integrins and signal transduction." Adv Exp Med Biol 674: 43-54.

Cabodi, S., L. Moro, E. Bergatto, E. Boeri Erba, P. Di Stefano, E. Turco, G. Tarone and P. Defilippi (2004). "Integrin regulation of epidermal growth factor (EGF) receptor and of EGF-dependent responses." Biochem Soc Trans 32(Pt3): 438-42.

Calderwood, D. A., R. Zent, R. Grant, D. J. Rees, R. O. Hynes and M. H. Ginsberg (1999). "The Talin head domain binds to integrin beta subunit cytoplasmic tails and regulates integrin activation." J Biol Chem 274(40): 28071-4.

Carreiras, F., Y. Denoux, C. Staedel, M. Lehmann, F. Sichel and P. Gauduchon (1996). “Expression and localization of alpha v integrins and their ligand vitronectin in normal ovarian epithelium and in ovarian carcinoma.” Gynecol Oncol 62(2): 260-7.

Cary, L. A., D. C. Han, T. R. Polte, S. K. Hanks and J. L. Guan (1998). "Identification of p130Cas as a mediator of focal adhesion kinase-promoted cell migration." J Cell Biol 140(1): 211-21.

Chasis, J. A. and N. Mohandas (1992). "Red blood cell glycophorins." Blood 80(8): 1869-79.

Czuchra, A., H. Meyer, K. R. Legate, C. Brakebusch and R. Fassler (2006). "Genetic analysis of beta1 integrin "activation motifs" in mice." J Cell Biol 174(6): 889-99.

Dejana, E., S. Colella, G. Conforti, M. Abbadini, M. Gaboli and P. C. Marchisio (1988). "Fibronectin and vitronectin regulate the organization of their respective Arg-Gly-Asp adhesion receptors in cultured human endothelial cells." J Cell Biol 107(3): 1215-23.

Desgrosellier, J. S., L. A. Barnes, D. J. Shields, M. Huang, S. K. Lau, N. Prevost, D. Tarin, S. J. Shattil and D. A. Cheresh (2009). "An integrin alpha(v)beta(3)-c-Src oncogenic unit promotes anchorage-independence and tumor progression." Nat Med 15(10): 1163-9.

Desgrosellier, J. S. and D. A. Cheresh (2010). "Integrins in cancer: biological implications and therapeutic opportunities." Nat Rev Cancer 10(1): 9-22.

Devor, B. B., X. Zhang, S. K. Patel, T. R. Polte and S. K. Hanks (1993). "Chicken and mouse focal adhesion kinases are similar in structure at their amino termini." Biochem Biophys Res Commun 190(3): 1084-9.

Donald, J. E., D. W. Kulp and W. F. DeGrado (2010). "Salt bridges: geometrically specific, designable interactions." Proteins 79(3): 898-915.

D'Souza, S. E., M. H. Ginsberg and E. F. Plow (1991). “Arginyl-glycyl-aspartic acid (RGD): a cell adhesion motif.” Trends Biochem Sci 16(7): 246-50.

Engler, A. J., M. Chan, D. Boettiger and J. E. Schwarzbauer (2009). "A novel mode of cell detachment from fibrillar fibronectin matrix under shear." J Cell Sci 122(Pt 10): 1647-53.

Friedland, J. C., M. H. Lee and D. Boettiger (2009). "Mechanically activated integrin switch controls alpha5beta1 function." Science 323(5914): 642-4.

Fuortes, M., W. W. Jin and C. Nathan (1994). "Beta 2 integrin-dependent tyrosine phosphorylation of paxillin in human neutrophils treated with tumor necrosis factor." J Cell Biol 127(5): 1477-83.

García, A. J., P. Ducheyne and D. Boettiger (1997). "Quantification of cell adhesion using a spinning disc device and application to surface-reactive materials." Biomaterials 18(16): 1091-8.

García, A. J., F. Huber and D. Boettiger (1998). “Force required to break alpha5beta1 integrin-fibronectin bonds in intact adherent cells is sensitive to integrin activation state.” J Biol Chem 273(18): 10988-93.

Gasparini, G., P. C. Brooks, E. Biganzoli, P. B. Vermeulen, E. Bonoldi, L. Y. Dirix, G. Ranieri, R. Miceli and D. A. Cheresh (1998). "Vascular integrin alpha(v)beta3: a new prognostic indicator in breast cancer." Clin Cancer Res 4(11): 2625-34.

Geiger, B. (2006). "A role for p130Cas in mechanotransduction." Cell 127(5): 879-81.

Giancotti, F. G. and E. Ruoslahti (1999). "Integrin signaling." Science 285(5430): 1028-32.

Goodman, S. L., G. Holzemann, G. A. Sulyok and H. Kessler (2002). "Nanomolar small molecule inhibitors for alphav(beta)6, alphav(beta)5, and alphav(beta)3 integrins." J Med Chem 45(5): 1045-51.

Gottschalk, K. E. (2005). "A coiled-coil structure of the alphaIIbbeta3 integrin transmembrane and cytoplasmic domains in its resting state." Structure 13(5): 703-12.

Gottschalk, K. E., P. D. Adams, A. T. Brunger and H. Kessler (2002). "Transmembrane signal transduction of the alpha(IIb)beta(3) integrin." Protein Sci 11(7): 1800-12.

Graham, I. L., D. C. Anderson, V. M. Holers and E. J. Brown (1994). "Complement receptor 3 (CR3, Mac-1, integrin alpha M beta 2, CD11b/CD18) is required for tyrosine phosphorylation of paxillin in adherent and nonadherent neutrophils." J Cell Biol 127(4): 1139-47.

Hantgan, R. R., C. Paumi, M. Rocco and J. W. Weisel (1999). "Effects of ligand-mimetic peptides Arg-Gly-Asp-X (X = Phe, Trp, Ser) on alphaIIbbeta3 integrin conformation and oligomerization." Biochemistry 38(44): 14461-74.

Hapke, S., H. Kessler, N. Arroyo de Prada, A. Benge, M. Schmitt, E. Lengyel and U. Reuning (2001). "Integrin alpha(v)beta(3)/vitronectin interaction affects expression of the urokinase system in human ovarian cancer cells." J Biol Chem 276(28): 26340-8.

Hapke, S., H. Kessler, B. Luber, A. Benge, P. Hutzler, H. Hofler, M. Schmitt and U. Reuning (2003). "Ovarian cancer cell proliferation and motility is induced by engagement of integrin alpha(v)beta3/Vitronectin interaction." Biol Chem 384(7): 1073-83.

Helenius, J., C. P. Heisenberg, H. E. Gaub and D. J. Muller (2008). "Single-cell force spectroscopy." J Cell Sci 121(Pt 11): 1785-91.

Hersey, P., J. Sosman, S. O'Day, J. Richards, A. Bedikian, R. Gonzalez, W. Sharfman, R. Weber, T. Logan, M. Buzoianu, et al. (2010). "A randomized phase 2 study of etaracizumab, a monoclonal antibody against integrin alpha(v)beta(3), + or - dacarbazine in patients with stage IV metastatic melanoma." Cancer 116(6): 1526-34.

Hotchin, N. A. and A. Hall (1995). "The assembly of integrin adhesion complexes requires both extracellular matrix and intracellular rho/rac GTPases." J Cell Biol 131(6 Pt 2): 1857-65.

Howe, A. K., A. E. Aplin and R. L. Juliano (2002). "Anchorage-dependent ERK signaling--mechanisms and consequences." Curr Opin Genet Dev 12(1): 30-5.

Hughes, P. E., F. Diaz-Gonzalez, L. Leong, C. Wu, J. A. McDonald, S. J. Shattil and M. H. Ginsberg (1996). "Breaking the integrin hinge. A defined structural constraint regulates integrin signaling." J Biol Chem 271(12): 6571-4.

Humphries, J. D., A. Byron and M. J. Humphries (2006). "Integrin ligands at a glance." J Cell Sci 119(Pt 19): 3901-3.

Humphries, M. J. (1996). "Integrin activation: the link between ligand binding and signal transduction." Curr Opin Cell Biol 8(5): 632-40.

Hynes, R. O. (1992). "Integrins: versatility, modulation, and signaling in cell adhesion." Cell 69(1): 11-25.

Hynes, R. O. (2002). "Integrins: bidirectional, allosteric signaling machines." Cell 110(6): 673-87.

Imai, Y., E. J. Park, D. Peer, A. Peixoto, G. Cheng, U. H. von Andrian, C. V. Carman and M. Shimaoka (2008). "Genetic perturbation of the putative cytoplasmic membrane-proximal salt bridge aberrantly activates alpha(4) integrins." Blood 112(13): 5007-15.

Khwaja, A., P. Rodriguez-Viciana, S. Wennstrom, P. H. Warne and J. Downward (1997). "Matrix adhesion and Ras transformation both activate a phosphoinositide 3-OH kinase and protein kinase B/Akt cellular survival pathway." Embo J 16(10): 2783-93.

Kim, C., T. L. Lau, T. S. Ulmer and M. H. Ginsberg (2009). "Interactions of platelet integrin alphaIIb and beta3 transmembrane domains in mammalian cell membranes and their role in integrin activation." Blood 113(19): 4747-53.

Kim, M., C. V. Carman and T. A. Springer (2003). "Bidirectional transmembrane signaling by cytoplasmic domain separation in integrins." Science 301(5640): 1720-5.

Klemke, R. L., S. Cai, A. L. Giannini, P. J. Gallagher, P. de Lanerolle and D. A. Cheresh (1997). “Regulation of cell motility by mitogen-activated protein kinase.” J Cell Biol 137(2): 481-92.

Kong, F., A. J. Garcia, A. P. Mould, M. J. Humphries and C. Zhu (2009). "Demonstration of catch bonds between an integrin and its ligand." J Cell Biol 185(7): 1275-84.

Kucik, D. F. (2002). "Rearrangement of integrins in avidity regulation by leukocytes." Immunol Res 26(1-3): 199-206.

Langosch, D., B. Brosig, H. Kolmar and H. J. Fritz (1996). "Dimerisation of the glycophorin A transmembrane segment in membranes probed with the ToxR transcription activator." J Mol Biol 263(4): 525-30.

Lau, T. L., C. Kim, M. H. Ginsberg and T. S. Ulmer (2009). "The structure of the integrin alphaIIbbeta3 transmembrane complex explains integrin transmembrane signalling." Embo J 28(9): 1351-61.

Lawlor, M. A. and D. R. Alessi (2001). "PKB/Akt: a key mediator of cell proliferation, survival and insulin responses?" J Cell Sci 114(Pt 16): 2903-10.

Lemmon, M. A., J. M. Flanagan, J. F. Hunt, B. D. Adair, B. J. Bormann, C. E. Dempsey and D. M. Engelman (1992a). "Glycophorin A dimerization is driven by specific interactions between transmembrane alpha-helices." J Biol Chem 267(11): 7683-9.

Lemmon, M. A., J. M. Flanagan, H. R. Treutlein, J. Zhang and D. M. Engelman (1992b). "Sequence specificity in the dimerization of transmembrane alpha-helices." Biochemistry 31(51): 12719-25.

Li, R., N. Mitra, H. Gratkowski, G. Vilaire, R. Litvinov, C. Nagasami, J. W. Weisel, J. D. Lear, W. F. DeGrado and J. S. Bennett (2003). "Activation of integrin alphaIIbbeta3 by modulation of transmembrane helix associations." Science 300(5620): 795-8.

Liapis, H., L.M Adler, M.R. Wick and J.S. Rader (1997). “Expression of alpha(v)beta3 integrin is less frequent in ovarian epithelial tumors of low malignant potential in contrast to ovarian carcinomas.” Hum Pathol 28(4): 443-9.

Lössner, D., C. Abou-Ajram, A. Benge and U. Reuning (2008). "Integrin alphavbeta3 mediates upregulation of epidermal growth-factor receptor expression and activity in human ovarian cancer cells." Int J Biochem Cell Biol 40(12): 2746-61.

Lu, C., J. Takagi and T. A. Springer (2001). "Association of the membrane-proximal regions of the alpha and beta subunit cytoplasmic domains constrains an integrin in the inactive state." J Biol Chem 276(18): 14642-8.

Luo, B. H., C. V. Carman and T. A. Springer (2007). "Structural basis of integrin regulation and signaling." Annu Rev Immunol 25: 619-47.

Luo, B. H., T. A. Springer and J. Takagi (2004). "A specific interface between integrin transmembrane helices and affinity for ligand." PLoS Biol 2(6): e153.

Ma, Y. Q., J. Yang, M. M. Pesho, O. Vinogradova, J. Qin and E. F. Plow (2006). "Regulation of integrin alphaIIbbeta3 activation by distinct regions of its cytoplasmic tails." Biochemistry 45(21): 6656-62.

Miyamoto, S., H. Teramoto, O. A. Coso, J. S. Gutkind, P. D. Burbelo, S. K. Akiyama and K. M. Yamada (1995). "Integrin function: molecular hierarchies of cytoskeletal and signaling molecules." J Cell Biol 131(3): 791-805.

Möbus, V., C. D. Gerharz, U. Press, R. Moll, T. Beck, W. Mellin, K. Pollow, P. G. Knapstein and R. Kreienberg (1992). "Morphological, immunohistochemical and biochemical characterization of 6 newly established human ovarian carcinoma cell lines." Int J Cancer 52(1): 76-84.

Moser, M., K. R. Legate, R. Zent and R. Fassler (2009). "The tail of integrins, talin, and kindlins." Science 324(5929): 895-9.

Mosmann, T. (1983). "Rapid colorimetric assay for cellular growth and survival: application to proliferation and cytotoxicity assays." J Immunol Methods 65(1-2): 55-63.

Murphy, J. F., J. C. Bordet, B. Wyler, M. C. Rissoan, P. Chomarat, T. Defrance, P. Miossec and J. L. McGregor (1994). "The vitronectin receptor (alpha v beta 3) is implicated, in cooperation with P-selectin and platelet-activating factor, in the adhesion of monocytes to activated endothelial cells." Biochem J 304(Pt 2): 537-42.

Nguyen, D. H., A. D. Catling, D. J. Webb, M. Sankovic, L. A. Walker, A. V. Somlyo, M. J. Weber and S. L. Gonias (1999). “Myosin light chain kinase functions downstream of Ras/ERK to promote migration of urokinase-type plasminogen activator-stimulated cells in an integrin-selective manner.” J Cell Biol 146(1): 149-64.

O'Toole, T. E., Y. Katagiri, R. J. Faull, K. Peter, R. Tamura, V. Quaranta, J. C. Loftus, S. J. Shattil and M. H. Ginsberg (1994). "Integrin cytoplasmic domains mediate inside-out signal transduction." J Cell Biol 124(6): 1047-59.

Partridge, A. W., S. Liu, S. Kim, J. U. Bowie and M. H. Ginsberg (2005). "Transmembrane domain helix packing stabilizes integrin alphaIIbbeta3 in the low affinity state." J Biol Chem 280(8): 7294-300.

Pesho, M. M., K. Bledzka, L. Michalec, C. S. Cierniewski and E. F. Plow (2006). "The specificity and function of the metal-binding sites in the integrin beta3 A-domain." J Biol Chem 281(32): 23034-41.

Pierschbacher, M. D. and E. Ruoslahti (1984). "Cell attachment activity of fibronectin can be duplicated by small synthetic fragments of the molecule." Nature 309(5963): 30-3.

Preissner, K. T. and D. Seiffert (1998). "Role of vitronectin and its receptors in haemostasis and vascular remodeling." Thromb Res 89(1): 1-21.

Psachoulia, E., D. P. Marshall and M. S. Sansom (2010). "Molecular dynamics simulations of the dimerization of transmembrane alpha-helices." Acc Chem Res 43(3): 388-96.

Puklin-Faucher, E., M. Gao, K. Schulten and V. Vogel (2006). "How the headpiece hinge angle is opened: New insights into the dynamics of integrin activation." J Cell Biol 175(2): 349-60.

Puklin-Faucher, E. and M. P. Sheetz (2009). "The mechanical integrin cycle." J Cell Sci 122(Pt 2): 179-86.

Pytela, R., M. D. Pierschbacher and E. Ruoslahti (1985). "A 125/115-kDa cell surface receptor specific for vitronectin interacts with the argininee-glycine-aspartic acid adhesion sequence derived from fibronectin." Proc Natl Acad Sci U S A 82(17): 5766-70.

Reardon, D. A., K. L. Fink, T. Mikkelsen, T. F. Cloughesy, A. O'Neill, S. Plotkin, M. Glantz, P. Ravin, J. J. Raizer, K. M. Rich, et al. (2008). "Randomized phase II study of cilengitide, an integrin-targeting argininee-glycine-aspartic acid peptide, in recurrent glioblastoma multiforme." J Clin Oncol 26(34): 5610-7.

Reuning U. (2011). “Integrin αvβ3 promotes vitronectin gene expression in human ovarian cancer cells by implicating rel transcription factors.” J Cell Biochem 112(7): 1909-19.

Reuning, U., V. Magdolen, S. Hapke and M. Schmitt (2003). "Molecular and functional interdependence of the urokinase-type plasminogen activator system with integrins." Biol Chem 384(8): 1119-31.

Reynolds, A. R., I. R. Hart, A. R. Watson, J. C. Welti, R. G. Silva, S. D. Robinson, G. Da Violante, M. Gourlaouen, M. Salih, M. C. Jones, et al. (2009). "Stimulation of tumor growth and angiogenesis by low concentrations of RGD-mimetic integrin inhibitors." Nat Med 15(4): 392-400.

Rottem, S. and M. F. Barile (1993). "Beware of mycoplasmas." Trends Biotechnol 11(4): 143-51.

Ruoslahti, E. (1996). "RGD and other recognition sequences for integrins." Annu Rev Cell Dev Biol 12: 697-715.

Russ, W. P. and D. M. Engelman (2000). “The GxxxG motif: a framework for transmembrane helix-helix association.” J Mol Biol 296(3): 911-9.

Sambrook, J., E. F. Fritsch, and T. Maniatis (1989). “Molecular Cloning: A Laboratory Manual”, 2nd Ed., Cold Spring Harbor Laboratory, Cold Spring Harbor, NY

Schaffner-Reckinger, E., A. Salsmann, N. Debili, J. Bellis, J. De Mey, W. Vainchenker, W. H. Ouwehand and N. Kieffer (2009). "Overexpression of the partially activated alpha(IIb)beta3D723H integrin salt bridge mutant downregulates RhoA activity and induces microtubule-dependent proplatelet-like extensions in Chinese hamster ovary cells." J Thromb Haemost 7(7): 1207-17.

Schlaepfer, D. D., S. K. Hanks, T. Hunter and P. van der Geer (1994). "Integrin-mediated signal transduction linked to Ras pathway by GRB2 binding to focal adhesion kinase." Nature 372(6508): 786-91.

Schmitz, J., M. Benoit and K. E. Gottschalk (2008). "The viscoelasticity of membrane tethers and its importance for cell adhesion." Biophys J 95(3): 1448-59.

Schneider, D. and D. M. Engelman (2003). "GALLEX, a measurement of heterologous association of transmembrane helices in a biological membrane." J Biol Chem 278(5): 3105-11.

Schneider, D. and D. M. Engelman (2004a). "Involvement of transmembrane domain interactions in signal transduction by alpha/beta integrins." J Biol Chem 279(11): 9840-6.

Schneider, D. and D. M. Engelman (2004b). "Motifs of two small residues can assist but are not sufficient to mediate transmembrane helix interactions." J Mol Biol 343(4): 799-804.

Senes, A., D. E. Engel and W. F. DeGrado (2004). "Folding of helical membrane proteins: the role of polar, GxxxG-like and proline motifs." Curr Opin Struct Biol 14(4): 465-79.

Shattil, S. J., C. Kim and M. H. Ginsberg (2010). "The final steps of integrin activation: the end game." Nat Rev Mol Cell Biol 11(4): 288-300.

Shi, Q. and D. Boettiger (2003). "A novel mode for integrin-mediated signaling: tethering is required for phosphorylation of FAK Y397." Mol Biol Cell 14(10): 4306-15.

Shin, E. Y., J. Y. Lee, M. K. Park, Y. H. Chin, G. B. Jeong, S. Y. Kim, S. R. Kim and E. G. Kim (1999). "Overexpressed alpha3beta1 and constitutively activated extracellular signal-regulated kinase modulate the angiogenic properties of ECV304 cells." Mol Cells 9(2): 138-45.

Short, S. M., G. A. Talbott and R. L. Juliano (1998). "Integrin-mediated signaling events in human endothelial cells." Mol Biol Cell 9(8): 1969-80.

Sindelar, C. V., Z. S. Hendsch and B. Tidor (1998). "Effects of salt bridges on protein structure and design." Protein Sci 7(9): 1898-914.

Smith, H. W. and C. J. Marshall (2010). "Regulation of cell signalling by uPAR." Nat Rev Mol Cell Biol 11(1): 23-36.

Somanath, P. R., N. L. Malinin and T. V. Byzova (2009). "Cooperation between integrin alphavbeta3 and VEGFR2 in angiogenesis." Angiogenesis 12(2): 177-85.

Springer, T. A. (1997). "Folding of the N-terminal, ligand-binding region of integrin alpha-subunits into a beta-propeller domain." Proc Natl Acad Sci U S A 94(1): 65-72.

Tadokoro, S., S. J. Shattil, K. Eto, V. Tai, R. C. Liddington, J. M. de Pereda, M. H. Ginsberg and D. A. Calderwood (2003). "Talin binding to integrin beta tails: a final common step in integrin activation." Science 302(5642): 103-6.

Takagi, J., H. P. Erickson and T. A. Springer (2001). "C-terminal opening mimics 'inside-out' activation of integrin alpha5beta1." Nat Struct Biol 8(5): 412-6.

Takagi, J., B. M. Petre, T. Walz and T. A. Springer (2002a). "Global conformational rearrangements in integrin extracellular domains in outside-in and inside-out signaling." Cell 110(5): 599-11.

Takagi, J. and T. A. Springer (2002b). "Integrin activation and structural rearrangement." Immunol Rev 186: 141-63.

Tamkun, J. W., D. W. DeSimone, D. Fonda, R. S. Patel, C. Buck, A. F. Horwitz and R. O. Hynes (1986). "Structure of integrin, a glycoprotein involved in the transmembrane linkage between fibronectin and actin." Cell 46(2): 271-82.

Tanaka-Takiguchi, Y., T. Kakei, A. Tanimura, A. Takagi, M. Honda, H. Hotani and K. Takiguchi (2004). "The elongation and contraction of actin bundles are induced by double-headed myosins in a motor concentration-dependent manner." J Mol Biol 341(2): 467-76.

Truong, H. and E. H. Danen (2009). "Integrin switching modulates adhesion dynamics and cell migration." Cell Adh Migr 3(2): 179-81.

Ulmer, T. S., B. Yaspan, M. H. Ginsberg and I. D. Campbell (2001). "NMR analysis of structure and dynamics of the cytosolic tails of integrin alpha IIb beta 3 in aqueous solution." Biochemistry 40(25): 7498-508.

Vallar, L., C. Melchior, S. Plancon, H. Drobecq, G. Lippens, V. Regnault and N. Kieffer (1999). "Divalent cations differentially regulate integrin alphaIIb cytoplasmic tail binding to beta3 and to calcium- and integrin-binding protein." J Biol Chem 274(24): 17257-66.

Vinogradova, O., J. Vaynberg, X. Kong, T. A. Haas, E. F. Plow and J. Qin (2004). "Membrane-mediated structural transitions at the cytoplasmic face during integrin activation." Proc Natl Acad Sci U S A 101(12): 4094-9.

Vinogradova, O., A. Velyvis, A. Velyviene, B. Hu, T. Haas, E. Plow and J. Qin (2002). "A structural mechanism of integrin alpha(IIb)beta(3) "inside-out" activation as regulated by its cytoplasmic face." Cell 110(5): 587-97.

Wang, W., J. Zhu, T. A. Springer and B. H. Luo (2010). "Tests of integrin transmembrane domain homo-oligomerization during integrin ligand binding and signaling." J Biol Chem 286(3): 1860-7.

Weljie, A. M., P. M. Hwang and H. J. Vogel (2002). "Solution structures of the cytoplasmic tail complex from platelet integrin alpha IIb- and beta 3-subunits." Proc Natl Acad Sci U S A 99(9): 5878-83.

Whittaker, C. A. and R. O. Hynes (2002). "Distribution and evolution of von Willebrand/integrin A domains: widely dispersed domains with roles in cell adhesion and elsewhere." Mol Biol Cell 13(10): 3369-87.

Wong, N. C., B. M. Mueller, C. F. Barbas, P. Ruminski, V. Quaranta, E. C. Lin and J. W. Smith (1998). "Alphav integrins mediate adhesion and migration of breast carcinoma cell lines." Clin Exp Metastasis 16(1): 50-61.

Wu, H., G. Beuerlein, Y. Nie, H. Smith, B. A. Lee, M. Hensler, W. D. Huse and J. D. Watkins (1998). "Stepwise in vitro affinity maturation of Vitaxin, an alphav beta3-specific humanized mAb." Proc Natl Acad Sci U S A 95(11): 6037-42.

Xiao, T., J. Takagi, B. S. Coller, J. H. Wang and T. A. Springer (2004). "Structural basis for allostery in integrins and binding to fibrinogen-mimetic therapeutics." Nature 432(7013): 59-67.

Xiong, J. P., B. Mahalingham, J. L. Alonso, L. A. Borrelli, X. Rui, S. Anand, B. T. Hyman, T. Rysiok, D. Muller-Pompalla, S. L. Goodman, et al. (2009). "Crystal structure of the complete integrin alphaVbeta3 ectodomain plus an alpha/beta transmembrane fragment." J Cell Biol 186(4): 589-600.

Xiong, J. P., T. Stehle, B. Diefenbach, R. Zhang, R. Dunker, D. L. Scott, A. Joachimiak, S. L. Goodman and M. A. Arnaout (2001). "Crystal structure of the extracellular segment of integrin alpha Vbeta3." Science 294(5541): 339-45.

Xiong, J. P., T. Stehle, R. Zhang, A. Joachimiak, M. Frech, S. L. Goodman and M. A. Arnaout (2002). "Crystal structure of the extracellular segment of integrin alpha Vbeta3 in complex with an Arg-Gly-Asp ligand." Science 296(5565): 151-5.

Yang, J., Y. Q. Ma, R. C. Page, S. Misra, E. F. Plow and J. Qin (2009). "Structure of an integrin alphaIIb beta3 transmembrane-cytoplasmic heterocomplex provides insight into integrin activation." Proc Natl Acad Sci U S A 106(42): 17729-34.

Ye, F., G. Hu, D. Taylor, B. Ratnikov, A. A. Bobkov, M. A. McLean, S. G. Sligar, K. A. Taylor and M. H. Ginsberg (2010). "Recreation of the terminal events in physiological integrin activation." J Cell Biol 188(1): 157-73.

Zamir, E., B. Geiger (2001). “Molecular complexity and dynamics of cell-matrix adhesions.” J Cell Sci 114(Pt 20): 3583-90.

Zhao, J. and J. L. Guan (2009). "Signal transduction by focal adhesion kinase in cancer." Cancer Metastasis Rev 28(1-2): 35-49.

Zhou, X., J. Li and D. F. Kucik (2001). "The microtubule cytoskeleton participates in control of beta2 integrin avidity." J Biol Chem 276(48): 44762-9.

Zhu, J., C. V. Carman, M. Kim, M. Shimaoka, T. A. Springer and B. H. Luo (2007). "Requirement of alpha and beta subunit transmembrane helix separation for integrin outside-in signaling." Blood 110(7): 2475-83.

Zhu, J., B. H. Luo, P. Barth, J. Schonbrun, D. Baker and T. A. Springer (2009). "The structure of a receptor with two associating transmembrane domains on the cell surface: integrin alphaIIbbeta3." Mol Cell 34(2): 234-49.

Zhu, J., B. H. Luo, T. Xiao, C. Zhang, N. Nishida and T. A. Springer (2008). "Structure of a complete integrin ectodomain in a physiologic resting state and activation and deactivation by applied forces." Mol Cell 32(6): 849-61.

Danksagung

Ich möchte mich ganz herzlich bedanken bei:

Prof. Dr. Ute Reuning, für die intensive Betreuung meiner Arbeit, Ihre beständige Unterstützung und fachlichen Ratschläge, die gute Zusammenarbeit und das mir entgegengebrachte Vertrauen, sowie die Korrektur meiner Dissertationsschrift.

Prof. Dr. Horst Kessler, der es mir ermöglicht hat diese, DFG geförderte Arbeit, durchzuführen, sowie für die Vertretung meiner Doktorarbeit an der Fakultät für Chemie der Technischen Universität München.

Prof. Dr. Manfred Schmitt dafür, dass ich in der Klinischen Forschergruppe der Frauenklinik, Klinikum rechts der Isar, meine Arbeit durchführen durfte, seine nützlichen Ratschläge, die finanzielle Unterstützung während meines Stipendiums, sowie die Hilfe beim FACSen.

Prof. Dr. Kay-E. Gottschalk, der mit seiner Forschung die Basis für meine Arbeit gelegt hat, immer voll guter Ideen bzw. Erklärungen steckt und mir die Durchführung der AFM-Experimente am Lehrstuhl für Angewandte Physik der Ludwigs-Maximillian Universität ermöglicht hat.

Anke Benge, für die gute und schnelle praktische Einarbeitung, alle Hilfe und Unterstützung im Labor, die kollegiale Zusammenarbeit und dafür, dass ich oft etwas zum Lachen hatte, danke Anke!

Jan Opfer, für die gute Zusammenarbeit und Hilfe bei der Durchführung der AFM Experimente, v.a. bei der Auswertung der riesigen AFM-Datenmengen mit Hilfe seines selbst entwickelten Computerprogramms.

Prof. David Boettiger, PhD, von der University of Pennsylvania, der mir in seiner Zeit am Max-Planck-Institut für Biochemie, Abteilung Molekulare Medizin, den Spinning-disc-assay gezeigt und seine Apparatur zur Verfügung gestellt hat.

Lilli Volkhart und Leonora Brunie, die mir die αv- und β3-Plasmide zur Verfügung gestellt haben, die sie während ihrer Zeit in der KliFo der Frauenklinik mit vielen Mutagenese-PCRs generiert bzw. verändert haben.

Allen Mitarbeitern der Klinischen Forschung der Frauenklinik, Klinikum rechts der Isar, für jegliche Hilfe und die schöne Zeit!

Prof. Dr. Marion Kiechle, für die finanzielle Unterstützung, als mein Stipendium ausgelaufen war.

Prof. Dr. Axel Walch dafür, dass ich den AxioImager am Institut für Pathologie, Helmholtz Zentrum München, so oft benutzen durfte und Dr. Isabel Winkelmann, die mir die Bedienung der Software gezeigt hat.

Der TUM für das Stipendium „Chancengleichheit für Frauen in Forschung und Lehre“, ohne das die Finanzierung meiner Arbeit am Schluss nicht möglich gewesen wäre.

Andreas Raschke, der immer für mich da ist und mich während meiner Dissertationszeit sehr unterstützt hat!